HINDERED ROTATION AND HETEROGENIETY IN GAS-SOLID INTERACTIONS: 1. NON-SPHERICAL POTENTIAL FUNCTIONS FOR THE ADSORPTION OF N_2 AND CO_2 ON GRAPHITIZED CARBON P33 (2700°); 2. TWO-SURFACE VIRIAL ANALYSIS FOR THE ADSORPTION OF Ar, Kr AND Xe ON HEXAGONAL BORON NITRIDE

A THESIS

Presented to

The Faculty of the Division

of Graduate Studies

by

Alvin Charles Levy

In Partial Fulfillment

of the Requirements for the Degree

Doctor of Philosophy

in the School of Chemistry

Georgia Institute of Technology

April, 1976

HINDERED ROTATION AND HETEROGENIETY IN GAS-SOLID INTERACTIONS:

1. NON-SPHERICAL POTENTIAL FUNCTIONS FOR THE ADSORPTION OF N_2 AND CO_2 ON GRAPHITIZED CARBON P33 (2700°); 2. TWO-SURFACE VIRIAL ANALYSIS FOR THE ADSORPTION OF Ar, Kr AND Xe ON HEXAGONAL BORON NITRIDE

Approved:

Robert A. Pierotti, Chairman

G. A. Miller

W. T. Ziegler

Date approved by Chairman: 30 April 76

ACKNOWLEDGMENTS

The author wishes to express his sincere appreciation to all those who assisted in making this investigation possible.

Thanks are due to the author's thesis advisor, Dr. Robert A. Pierotti, for his assistance and direction throughout the investigation. The author also appreciates assistance on various aspects of the project given by Drs. Howard E. Thomas, Reginald N. Ramsey and Albert Liabastre and Messrs. Stephen L. Parrot, C. C. Yang, Rand H. Childs and Gerald O'Brien.

Special thanks are also due Dr. Reginald N. Ramsey for providing several of the figures published in this dissertation.

TABLE OF CONTENTS

	Page
ACKNOWLEDGMENTS	ii
LIST OF TABLES	v
LIST OF ILLUSTRATIONS	vii
SUMMARY	ix
Chapter	
I. INTRODUCTION	1
Statement of Problem	1
Historical Background	3
II. APPLICATION OF THE VIRIAL TREATMENT TO LOW COVERAGE SURFACE ADSORPTION	8
Introduction	8
The Spherical Potential Function	10
The Non-Spherical Potential Function for Linear Molecules: Nitrogen and Carbon Dioxide	14
The Non-Spherical Potential Function for Planar Molecules: Benzene	19
The Third Gas-Solid Virial Coefficient and Two Dimensional Gas Treatment	20
Two Surface Virial Treatment of Adsorption	25
The Thermodynamic Properties from Virial Coefficients	27
III. APPARATUS-CONSTRUCTION AND OPERATION	31
Introduction	31
Gas Transfer System	31
Pressure Measurement System	37
Sample Cell	43
Cryostat	46
Materials	47
IV. DATA TREATMENT	53
Isotherm Calculation	53
Determination of z_o	60

Chapter Page

V. ADSORPTION OF N_2 AND CO_2 ON P33 (2700°). 63

B_{2s}, B_{3s} and B_{2D} Parameters. 63
Virial Analysis by Spherical Potential Models. . 66
Thermodynamic Treatment of Virial Data 70
Non-Spherical Potential Model for CO_2 and N_2 Adsorption on P33. 76
Non-Spherical Potential Model for Benzene Adsorption on P33. 85
Lattice Summation Technique of Kiselev for Non-Spherical Molecules. 89

VI. ADSORPTION OF RARE GASES ON HEXAGONAL BORON NITRIDE. 95

VII. CONCLUSIONS. 106

Assessment of Results. 106
Recommendations for Further Study. 108

Appendices

A. ADDITIONAL LITERATURE REVIEW 110

B. DERIVATION OF THE VIRIAL TREATMENT OF LOW COVERAGE SURFACE ADSORPTION. 113

C. TWO DIMENSIONAL VIRIAL DERIVATION. 121

D. ERROR ANALYSIS 123

E. ISOTHERM DATA. 127

BIBLIOGRAPHY. 136

VITA. 140

LIST OF TABLES

Table		Page
1.	Apparatus Volume, Pressure and Temperature Specifications.	35
2.	Values of z_o, Gas Phase σ and ε_{12}^*/k for Various Gas-Boron Nitride and Gas-P33 (2700°) Systems . .	62
3.	Values of B_{2s}, B_{3s} and B_{2D} for the N_2-P33 (2700°) System.	64
4.	Values of B_{2s}, B_{3s} and B_{2D} for the CO_2-P33 (2700°) System.	65
5.	Surface Parameters for Various Gas-P33 (2700°) Systems Using the Spherical (9,3) Potential Model for the B_{2s} Analysis and a (12,6) Potential for the B_{2D} Analysis.	67
6.	B_{2s} Values for the Adsorption of Benzene on Graphitized Carbon P33.	69
7.	Thermodynamic Properties of the N_2-P33 (2700°) and CO_2-P33 (2700°) Systems	71
8.	Decrease in Rotational Entropy for the Adsorption of Various Substrates on P33.	74
9.	Principal Polarizabilities of Nitrogen, Carbon Dioxide and Benzene	78
10.	Parallel and Perpendicular Distance of N_2 and CO_2 Centers from the P33 (2700°) Surface at Zero Potential.	81
11.	B_{2s} Surface Parameters for the N_2-P33 (2700°) and CO_2-P33 (2700°) Systems Using the Non-Spherical (9,3) Potential Model	82
12.	Analysis of B_{2s} Data for the Adsorption of Benzene on P33 Using the (9,3) Non-Spherical Potential Model	87

Table		Page
13.	Comparison of ε^*_{1s}/k, Z^* and V_0/k for N_2-P33 and Benzene-P33 Systems by Equation (38) and Lattice Summation.	92
14.	Best Fit Value of B_{2s} for the Adsorption of Xe, Kr and Ar on Hexagonal Boron Nitride	96
15.	Parameter for the Adsorption of Xe, Kr and Ar on Hexagonal Boron Nitride from B_{3s} Data	97
16.	Best-Fit Parameters for the Adsorption of Xe, Kr and Ar on Hexagonal BN from B_{2s} Data.	98
17.	Various Values of ε^{*b}_{1s}/k (°K) for the Adsorption of Inert Gases on the Basal Plane of Boron Nitride.	104
18.	N_2-P33 (2700°) Adsorption Data	128
19.	N_2-P33 (2700°) Adsorption Data	129
20.	CO_2-P33 (2700°) Adsorption Data.	130
21.	N_2-P33 (2700°) BET Plot Data	131
22.	Ar-P33 (2700°) and Ar-BN Adsorption Data at the Ice Point.	132
23.	Ar-BN Adsorption Data.	133
24.	Kr-BN Adsorption Data.	134
25.	Xe-BN Adsorption Data.	135

LIST OF ILLUSTRATIONS

Figure		Page
1.	Lennard-Jones (12,6) Potential for Two Molecules.	11
2.	Linear Molecules Adsorbed on a Homogeneous Surface	15
3.	Benzene Adsorbed on a Homogeneous Surface	21
4.	Diagram of Adsorption Apparatus	32
5.	Diagram of Gas Transfer System.	33
6.	Manometer and Cathetometer Arrangement.	38
7.	Cryostat.	47
8.	Graphite and Hexagonal BN Structures.	50
9.	Adsorption Isotherms for Argon on BN and P33 (2700°) at 273.150°K.	54
10.	Adsorption Isotherms for Nitrogen on Graphitized Carbon P33 (2700°).	55
11.	Adsorption Isotherms for Carbon Dioxide on Graphitized Carbon P33 (2700°).	56
12.	Adsorption Isotherms for Argon on Hexagonal Boron Nitride	57
13.	Adsorption Isotherms for Krypton on Hexagonal Boron Nitride	58
14.	Adsorption Isotherms for Xenon on Hexagonal Boron Nitride	59
15.	Kihara Model for a Linear Molecule.	79
16.	Angle Averaged Non-Spherical Potential Function at Various Temperatures: N_2-P33.	83
17.	Angle Averaged Non-Spherical Function at Various Temperatures: CO_2-P33.	84

Figure Page

18. Angle Averaged Non-Spherical Potential Function at Various Temperatures: Benzene-P33. 88

19. Plot of $\varepsilon^{*e}_{1s}/\varepsilon^{*b}_{1s}$ Versus Area for Ar, Kr and Xe Adsorbed on BN Containing 3.25% Edge Sites . . . 102

SUMMARY

A high precision adsorption apparatus previously constructed by Ramsey was used to measure the adsorption of the linear molecules N_2 and CO_2 on graphitized carbon black P33 (2700°) and the adsorption of Ar, Kr and Xe on hexagonal boron nitride. The BET areas of the P33 and BN samples were 11.84 and 4.98 m^2/g, respectively. The virial approach to adsorption was used to analyze the experimental data.

In the treatment of the second gas-solid virial coefficients, B_{2s}, for the N_2-P33 and CO_2-P33 systems, a Lennard-Jones (9,3) spherical potential function was first used. The values of the surface area, A, were found to be 7.88 and 5.80 m^2/g for N_2-P33 and CO_2-P33, respectively. The surface area determined from the Ar-P33 data of Sams, Constabaris and Halsey on this identical sample by a similar analysis was 8.45 m^2/g. The apparent depression of A was attributed to hindered rotation of the adsorbed N_2 and CO_2.

To account for the hindered rotation, a non-spherical (9,3) potential function was proposed. It treated the polarizability of the adsorbate and the hard-sphere interaction separation, z_o, as a function of the angle the symmetry axis of the adsorbate made with a normal to the surface plane.

The surface areas obtained for N_2-P33 and CO_2-P33 by

the non-spherical model were 8.41 m^2/g and 8.51 m^2/g, respectively. This is consistent with the Ar-P33 value.

The results of the treatment of B_{2s} data by both potential models is summarized in the table below.

Depth of Potential Wells (°K) from the Analysis of B_{2s} Data by Spherical and Non-Spherical Potential Functions

Adsorbate	Spherical Potential	Non-Spherical Potential Configuration	
		Parallel	Perpendicular
N_2	1143	1201	1261
CO_2	1702	1841	1215

Application of the non-spherical potential to the benzene-P33 data of Smallwood gave a more realistic value of A than obtained from the spherical potential, but was still low by a factor of four.

The third gas-solid virial coefficients, B_{3s}, for the N_2-P33 and CO_2-P33 systems were analyzed by first determining the corresponding two-dimensional gas virial coefficients, B_{2D}. Analysis of the B_{2D} data using a spherical Lennard-Jones (12,6) potential function gave a value for the minimum in the potential well, ε^*_{12}/k, of 75°K for N_2-P33 versus the gas phase value of 95.05°K. This supports the theory of Sinanoğlu and Pitzer which predicts a decrease in the net pair interaction due to a perturbation by the surface field. A similar observation was made by Sams, Constabaris and

Halsey for the Ar-P33 system. The value of ε^*_{12}/k for CO_2-P33 in the presence of the surface was found to be 215°K versus the gas phase value of 189°K.

The rare gas-BN data was treated by a two-surface virial approach since it was known to have both basal plane and edge sites, the edge being the higher energy surface. The B_{2s} data was fit with the restraints that the percent edge sites, total surface area and ratio of the potential minima of the edge to basal plane interactions be the same for all three systems. Improvement in the fit to the B_{2s} data was obtained in each case. The results are listed in the table below.

Depth of Potential Wells (°K) for the Inert Gas-BN Systems Containing 3.25% Edge Sites

Gas	High Energy Surface	Low Energy Surface
Ar	1735	1038
Kr	2200	1305
Xe	2810	1650

A two-surface approach was also developed to treat the rare gas-BN B_{3s} data. Depressions of ε^*_{12}/k relative to the gas phase values were obtained in each case.

CHAPTER I

INTRODUCTION

Statement of Problem

The purpose of the research described herein is to obtain a better understanding of the nature of the physical forces which exist between molecules. The investigative technique includes measurements and analysis of data obtained on a number of gas-solid adsorption systems. These include rare gas-boron nitride and nitrogen and carbon dioxide-graphitized carbon P33(2700°) studies.

The understanding of surface phenomena is in itself of great practical importance. Industrial applications include catalysis, adhesion, textile processing and dyeing and removal of oil from shale to name a few. This work is not directed to any one application but to the basic understanding of intermolecular physical interactions.

A large number of gas phase, single component systems have been studied in detail with respect to intermolecular interactions. The gas-solid adsorption system is more complicated in that it is a two component system. However, since one of the components, the solid adsorbent, is fixed, the system is still relatively simple and can be reasonably handled from a mathematical standpoint by examining the

perturbing effect of the adsorbent on the adsorbate in the neighborhood of the phase interface.

In both the boron nitride and graphite studies, a high precision adsorption apparatus constructed by Ramsey[1] is used. In the first, the interaction of the rare gases, argon, krypton and xenon with hexagonal boron nitride is explored. Prior studies on these systems[1-4] have shown that boron nitride consists of both basal plane and edge surfaces, the relative amount of each being dependent on the particle size of the platelets. In reference 3, the effects of the two surfaces on the experimental second gas-solid virial coefficient, B_{2s}, is separated by attributing the isotherm curvature to the higher energy edge, fitting the curvature to a Langmuir model, and then subtracting the edge effect out to predict the basal plane B_{2s}^{b}. The Langmuir approach is required since the isotherms do not contain the very low pressure, low coverage data necessary for the precise determination of B_{2s}^{b} by a two-surface virial separation treatment. In this work, the isotherms are measured in the low coverage regions and a two surface virial treatment is used without further assumption to obtain the molecular interaction parameters for the two surfaces.

In the second part of this work, the adsorbent is graphitized carbon black P33(2700°) and is the identical sample used by Halsey and coworkers[5-8] in their pioneering determination of Ar-P33 interaction parameters via the virial

analysis. This presents the opportunity to do research with a previously well defined adsorbent. The adsorbates are nitrogen and carbon dioxide. The use of N_2 and CO_2 introduces an additional effect not obtained with rare gases; that being the effect of orientation of a non-spherical molecule with the surface. The problem here is to formulate a model for a non-spherical potential function which adequately explains the experimental data. Previously, Pierotti[9] explained the adsorption of benzene on graphite with a harmonic approximation to a Lennard-Jones type potential. This path is not chosen in this case since the depth of the potential well for N_2 and CO_2 is not nearly as large as for benzene thereby making the harmonic approximation not as appropriate.

Historical Background

Monolayer Adsorption

One of the first completely theoretical treatments of monolayer adsorption was given by Langmuir[10] in 1916. Langmuir assumed that the rate of adsorption was proportional to the pressure of the gas above the solid and the fraction of the surface not covered, $1-\theta$. The rate of desorption was assumed proportional to the fraction of surface covered, θ. At equilibrium the rates of adsorption and desorption were equal and the resultant isotherm equation was

$$P = K_L\theta/(1-\theta) \tag{1}$$

where K_L was a proportionality constant.

The weaknesses of the Langmuir approach are that it assumes localized adsorption with no lateral interaction between adsorbate molecules, ideal gas phase behavior, and only monolayer adsorption.

The physical meaning of the Langmuir K_L can be found using statistical thermodynamic considerations giving

$$K_L = \frac{kT\ e^{-U_o/kT}}{\Lambda^3 q_x q_y q_z} \tag{2}$$

where q_x, q_y and q_z are molecular vibrational partition functions of the adsorbed molecule, U_o is the potential energy of an adsorbate molecule in the field of the surface and Λ is the thermal de Broglie wavelength of the adsorbed molecule in the gas phase defined by

$$\Lambda = \left[\frac{h^2}{2\pi mkT}\right]^{1/2} . \tag{3}$$

A second localized model was proposed by Fowler and Guggenheim[11] which allowed for lateral interaction. The resultant isotherm equation was

$$P = K_{FG}\theta/(1-\theta)\exp(-CW\theta/kT) \tag{4}$$

where W was defined as the interaction energy per pair of nearest neighbors at their equilibrium distance of separation, C was related to the coordination number of the lattice and K_{FG} was equal to K_L as previously defined.

A model frequently used to describe mobile adsorption is the two-dimensional van der Waals equation of state[12]

$$(\pi + \alpha/\sigma^2)\ (\sigma-\beta) = kT \tag{5}$$

and the corresponding isotherm equation

$$P = K_{VDW}\theta/(1-\theta)\exp[\theta/(1-\theta) - 2\alpha\theta/(kT\beta)]$$

where α and β are the two dimensional gas phase parameters corresponding to the three-dimensional van der Waals a and b, σ is a two-dimensional area analogous to the volume and π is the two dimensional spreading pressure.

Here,

$$K_{VDW} = (kT/\Lambda q_z\beta)\exp(-U_o/kT) \tag{6}$$

where U_o is the potential energy parameter of the adsorbate in the external field, q_z is vibration partition function normal to the surface and Λ is as previously defined.

More recent approaches by McAlpin and Pierotti[13,14] involve a statistical treatment of monolayer adsorption based on the significant structure theory of liquids.[15]

The technique of analysis for this work is based on the virial treatment of imperfect gases as extended to adsorption.[16] This method based on the grand canonical partition function has the advantage of giving physical meaning to the forces existing between the adsorbate molecule singly, in pairs, etc., and the solid surface whereas the previously discussed methods based on the canonical ensemble gives only the average forces of a field of molecules in the presence of the surface. The virial approach is discussed in detail in Chapter II.

Multilayer Adsorption

The concept of multilayer adsorption was proposed to explain the step-like nature of isotherms observed as P/P_o approached unity. P_o is the saturated vapor-pressure of liquid adsorbate at the isotherm temperature. The best known of the multilayer equations was proposed by Brunauer, Emmett and Teller[17] in 1938 and is essentially an extension of the Langmuir equation to multilayer adsorption in one of the following two forms:

$$\theta = \frac{CP}{(P_o/P)\ (1+(C-1)P/P_o)} \tag{7}$$

or

$$\frac{P}{N_a(P_o-P)} = \frac{1}{N_m C} + \frac{(C-1)P}{N_m C P_o} \tag{8}$$

where

C = constant

N_a = number of moles of gas adsorbed

N_m = number of moles of gas in a monolayer

and the other terms are previously defined.

The BET plot has long been a standard for determining the surface area of solids.

As can be seen from equation (8), a plot of P/P_o versus $P/P_o/(1-P/P_o)$ will give a slope and intercept such that

$$N_m = 1/(\text{slope} + \text{intercept}). \tag{9}$$

With N_m and the area of a molecule, the surface area, A, can then be obtained.

A discussion of some of the more recent literature concerning work generally related to this area of study, but not to the specific cases experimentally investigated, is given in Appendix A.

CHAPTER II

APPLICATION OF THE VIRIAL TREATMENT TO LOW COVERAGE SURFACE ADSORPTION

Introduction

The virial equation for surface adsorption is expressed in the form

$$N_a = \sum_{i \geq 1}^{\infty} C_{i+1,s} \, (P/RT)^i \tag{10}$$

where

$$C_{2s} = B_{2s}, \tag{11a}$$

$$C_{3s} = B_{3s} + B_{2s}B_2 \quad \text{and} \tag{11b}$$

$$C_{4s} = B_{4s} + 2B_{3s}B_2 + \frac{1}{2} B_{2s} \, (B_3 + B_2^2). \tag{11c}$$

The B's refer to the virial coefficients for the gas-solid system (s subscripted) and the gas-gas system where the virial equation is expressed as a power series in fugacity rather than pressure. The details of the derivation of this equation can be found in Appendix B.

The virial coefficients are in turn defined by the

configurational integral, Z, of the canonical partition function, Q, such that

$$B_{2s} = (Z_1 - Z_1^o) \tag{12}$$

and

$$B_{3s} = (Z_2 - Z_2^o - Z_1^2 + Z_1^{o2}) \tag{13}$$

where Z_1 and Z_1^o are the configuration integrals for one adsorbate molecule in the presence and absence of the surface respectively. Z_2 and Z_2^o are similarly defined.

The configuration integral Z_1 is given by

$$Z_1 = \int_v e^{-U_{1s}/kT} dv \tag{14}$$

where U_{1s} is the potential of interaction of a gas molecule with the surface. Likewise

$$Z_1^o = \int_v e^{-U_1^o/kT} dv \tag{15}$$

Since for only one adsorbate molecule, $U_1^o = 0$, B_{2s} is given by

$$B_{2s} = \int_v (e^{-U_{1s}/kT} - 1) dv. \tag{16}$$

The next problem is then to determine the form of U_{1s}.

The Spherical Potential Function

The nature of the forces involved in the gas-solid systems explored here are mainly London[18] type dispersion attractive forces, induced dipole-induced dipole, and some form of repulsive force. For spherical molecules the most widely used function incorporating both of these features is the Lennard-Jones[19] (n,m) potential which is generally written in the form

$$U\{r\} = Br^{-n} - Cr^{-m} \tag{17}$$

where n and m are positive integers with n > m to reflect the shorter range nature of the repulsive term. C and B are the respective attractive and repulsive constants for the system involved.

Reference to Figure 1 shows that for this potential function the following observations can be made:

$$U = 0 \quad \text{at} \quad r = r_o, \tag{18a}$$

$$\left(\frac{\partial U}{\partial r}\right)_{r=r^*} = 0 \quad \text{and} \tag{18b}$$

$$U\{r^*\} = -\varepsilon^*. \tag{18c}$$

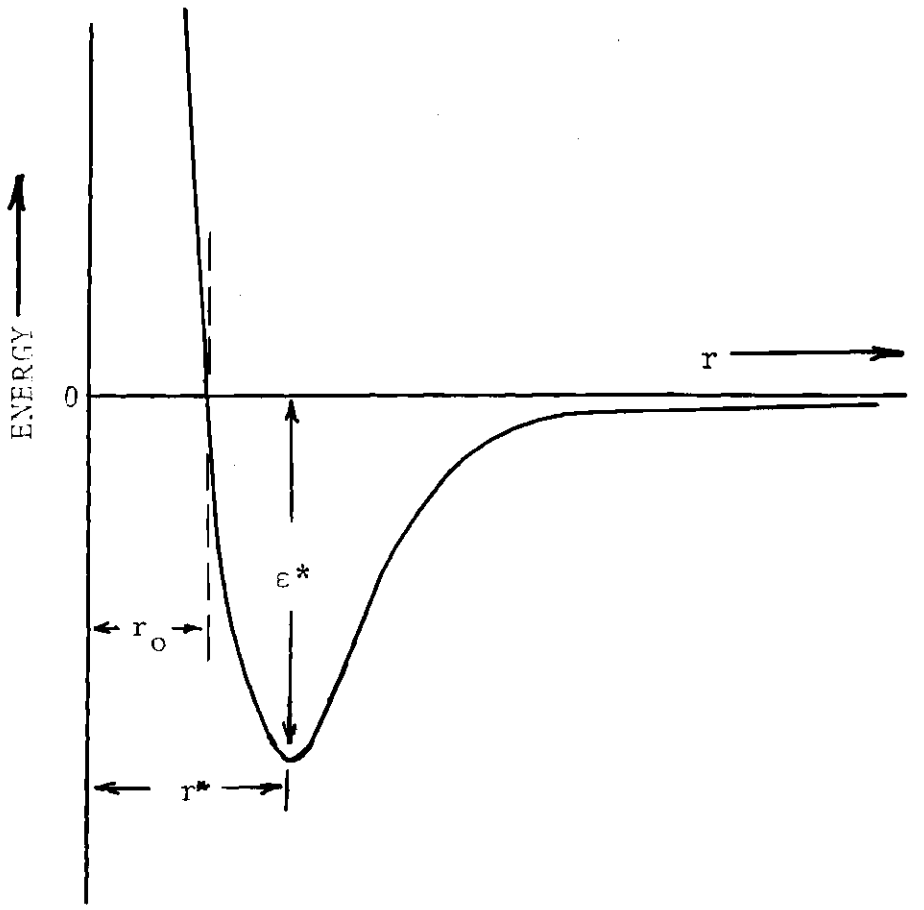

Figure 1. Lennard-Jones (12,6) Potential for Two Molecules

The above conditions lead to the relationships

$$r_o^{(n-m)} = B/C \quad \text{and} \tag{19}$$

$$B = Cr_o^{(n-m)}$$

or

$$r^{*(n-m)} = \frac{n}{m}\frac{B}{C} = \frac{n}{m} r_o^{(n-m)} , \tag{20}$$

$$C = \left(\frac{n}{n-m}\right)\left(\frac{n}{m}\right)^{\frac{m}{n-m}} \varepsilon^* \; r_o^{m} \quad \text{and} \tag{21}$$

$$\varepsilon^* = \left(\frac{n-m}{n}\right)\left(\frac{m}{n}\right)^{\frac{m}{m-n}} C/r_o^{m} \quad . \tag{22}$$

Combination of equation (17) through (22) then gives the desired result

$$U\{r\} = \left[\frac{n}{n-m}\right]\left[\frac{n}{m}\right]^{\frac{m}{n-m}} \varepsilon^*[(r_o/r)^n - (r_o/r)^m] \tag{23}$$

For dispersion type forces m is equal to six. The value of n is taken here as twelve since this appears to adequately represent the repulsive nature of many physical systems. This gives for the Lennard-Jones (12,6) potential

$$U\{r\} = 4\varepsilon^* \; [(r_o/r)^{12} - (r_o/r)^6] \quad . \tag{24}$$

For the interaction of a gas with a solid adsorbent the total potential of interaction of a gas molecule with the adsorbent is given by a summation over all adsorbent molecules or

$$U_{1s} = \sum_{\substack{i \text{ adsorbent} \\ \text{molecules}}} U\{r_i\}. \tag{25}$$

However, in order to get a more analytic form for U_{1s}, the summation can be replaced by an integration over the surface without loss of rigor in the treatment. This integration has the effect of reducing the values of n and m by three such that a (12,6) potential becomes a (9,3) potential thereby giving for a spherical adsorbate molecule

$$U_{1s}\{z\} = \frac{3}{2}\sqrt{3}\,\varepsilon^*_{1s}[(z_o/z)^9 - (z_o/z)^3] \tag{26}$$

where z is now the perpendicular distance of the center of the adsorbate molecule from the plane containing the centers of the surface adsorbent atoms, z_o is the value of z at $U_{1s} = 0$ and $-\varepsilon^*_{1s}$ is the value of U_{1s} at the potential minimum.

Substitution of equation (26) into (16) and integration gives for a general (n,m) potential

$$B_{2s} = Az_o \sum_{i\geq 0}^{\infty} (1/i!)(1/n)E^{((n-m)i+1)/n}\Gamma((mi-1)/n) \tag{27}$$

where $n > m$,

$$E = \left(\frac{n}{n-m}\right) \left(\frac{n}{m}\right)^{\frac{m}{n-m}} \varepsilon^*_{1s}/kT \tag{28}$$

and $\Gamma((mi-1)/n)$ is the gamma function.

The details of this derivation can be found in Appendix A of reference 1.

For the specific case of the (9,3) potential

$$\frac{B_{2s}}{Az_o} = \sum_{i\geq 0}^{\infty} (1/i!)(1/9)\left(\frac{3\sqrt{3}}{2}\,\frac{\varepsilon^*_{1s}}{kT}\right)^{\frac{6i+1}{9}} \Gamma\left(\frac{3i-1}{9}\right) \tag{29}$$

$$= I(\varepsilon^*_{1s},T)$$

where $I(\varepsilon^*_{1s},T)$ represents the sum in the right side of equation (29).

The Non-Spherical Potential Function for Linear Molecules: Nitrogen and Carbon Dioxide

For a non-spherical linear molecule, the potential depends not only on the distance of the molecular center of mass from the surface, but also on the angle of orientation, θ, of the adsorbed molecule with respect to the surface as shown in Figure 2. If the Lennard-Jones (n,m) form is preserved then

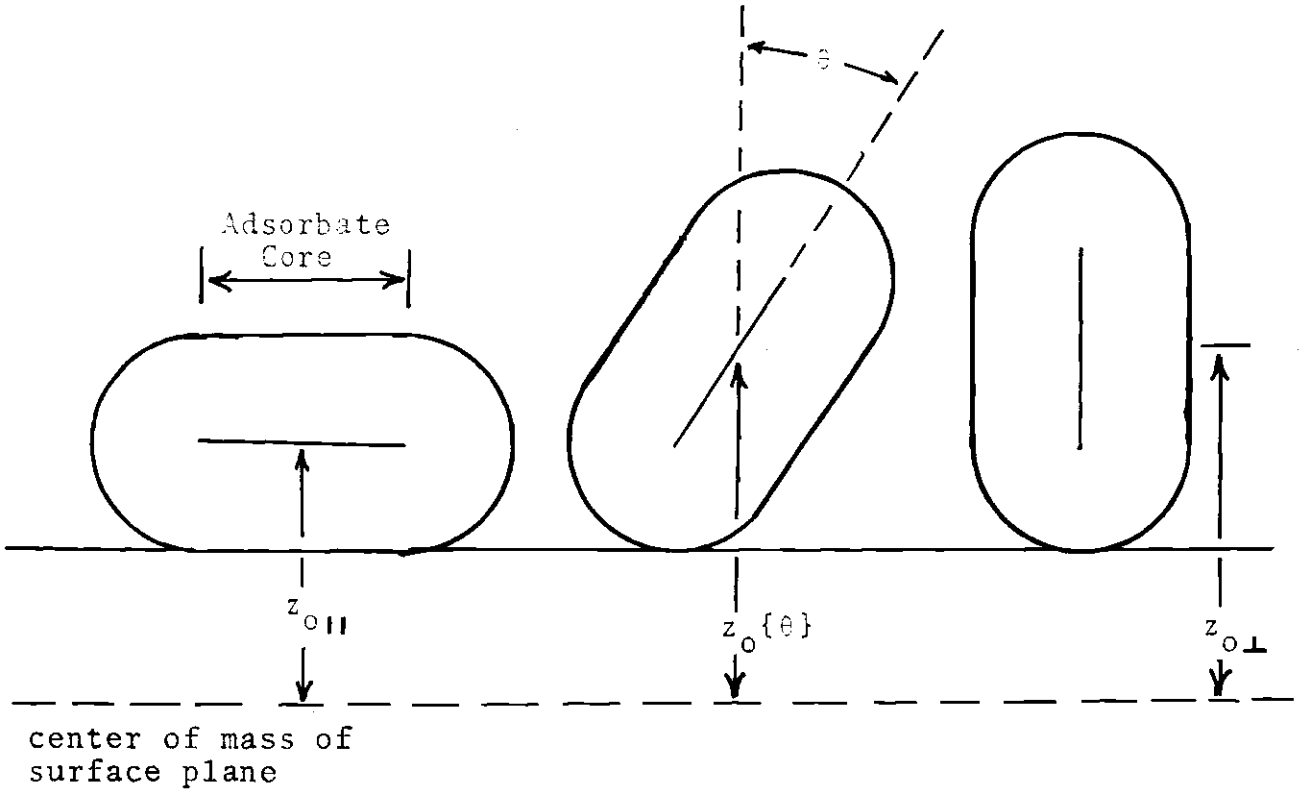

Figure 2. Linear Molecules Adsorbed on a Homogeneous Surface

$$U_{1s}\{z,\theta\} = B\{\theta\}z^{-n} - C\{\theta\}z^{-m} \tag{30}$$

For London forces,[18]

$$C_L = \frac{3}{2}\left[\frac{I_1 I_2}{I_1+I_2}\right]\alpha_1\alpha_2 \tag{31}$$

where the I's and α's refer to the ionization potentials and polarizabilities respectively of the adsorbent and adsorbate in the case of adsorption.

Now if α_2 is for a linear adsorbate molecule, then α_2 is in fact $\alpha_2\{\theta\}$.

In the presence of an external field such as a surface, the polarizability of the linear molecule as seen from the direction of the field is[20]

$$\alpha_2\{\theta\} = \alpha_\perp\cos^2\theta + \alpha_\parallel\sin^2\theta \tag{32}$$

where $\alpha_\perp$ and $\alpha_\parallel$ are the polarizabilities for the perpendicular and parallel orientation of the molecular axis with respect to the surface. The angle θ is taken as zero in the perpendicular orientation. This is illustrated in Figure 2.

Substitution of equation (32) into (31) then gives

$$C\{\theta\} = \frac{3}{2}\left[\frac{I_1 I_2}{I_1+I_2}\right]\alpha_1(\alpha_\perp\cos^2\theta + \alpha_\parallel\sin^2\theta)$$

which can be arranged in the form

$$C\{\theta\} = \frac{3}{2}\left[\frac{I_1 I_2}{I_1+I_2}\right]\alpha_1\alpha_{\parallel}\left[1+\cos^2\theta \quad \left(\frac{\alpha_{\perp}}{\alpha_{\parallel}} - 1\right)\right] \tag{33}$$

Note that

$$C\{\theta\} = C_{\parallel}\,(1+A'\cos^2\theta) \tag{34a}$$

where $C_{\parallel}$ is the value of C with the molecule parallel to the surface and

$$A' = \frac{\alpha_{\perp}}{\alpha_{\parallel}} - 1. \tag{34b}$$

Recall from equation (21) that for the spherical case

$$C = \left(\frac{n}{n-m}\right)\left(\frac{n}{m}\right)^{\frac{m}{n-m}} \varepsilon^* r_o{}^m.$$

It then follows that for the linear molecule that

$$C\{\theta\} = \left(\frac{n}{n-m}\right)\left(\frac{n}{m}\right)^{\frac{m}{n-m}} \varepsilon^*_{1s\parallel}\, z^m_{o\parallel}\,(1+A'\cos^2\theta) \tag{35}$$

where $\varepsilon^*_{1s\parallel}$ is the negative of the potential minimum for the linear molecule in the parallel orientation and $z_{o\parallel}$ is the value of z where the potential is zero for the parallel orientation.

It also follows from equation (19) that

$$B\{\theta\} = C\{\theta\}(z_o\{\theta\})^{(n-m)} \tag{36}$$

Reference to Figure 2 shows that

$$z_o\{\theta\} = z_{o\parallel}(1+B'\cos\theta) \tag{37a}$$

where

$$B' = \frac{z_{o\perp} - z_{o\parallel}}{z_{o\parallel}} = \frac{z_{o\perp}}{z_{o\parallel}} - 1 \tag{37b}$$

Finally, substitution of equation (35) through (37a) into (30) gives the desired result,

$$U_{1s}\{z,\theta\} = \left(\frac{n}{n-m}\right)\left(\frac{n}{m}\right)^{\frac{m}{n-m}} \varepsilon^*_{1s\parallel}$$

$$\cdot\ (1+A'\cos^2\theta)\left[\left(\frac{z_{o\parallel}}{z}\right)^n (1+B'\cos\theta)^{n-m} - \left(\frac{z_{o\parallel}}{z}\right)^m\right] \tag{38}$$

Unfortunately, substitution of equation (38) into (17) does not give a function which we could integrate to yield an analytic function for B_{2s}. However, it can be evaluated by computer techniques which involve getting an effective potential value, U_{1seff}, averaged over all θ for a

given value of z such that

$$U_{1seff}\{z\} = \frac{\sum_{0°\leq\theta\leq 90°} U\{\theta,z\}e^{-U\{\theta,z\}/RT}}{\sum_{0°\leq\theta\leq 90°} e^{-U\{\theta,z\}/RT}} . \qquad (39)$$

The increment of θ required such that B_{2s}/Az_o does not change appreciably by doubling the increment is dependent on $\varepsilon^*_{1s_{||}}$, A' and B'. The increment in z of 0.02 z_o as applied to the spherical treatment of CO_2 data was found to give a best fit value of Az_o which differed from that obtained via equation (29) by only 0.6%. $\sigma \ln Az_o$ was unchanged. The above calculation requires a considerable number of calculations making the availability of a computer such as the CDC Cyber 74 necessary.

The Non-Spherical Potential Function for Planar Molecules: Benzene

The potential function for linear molecules described by equation (38) can be modified to represent planar benzene. Here, the angle θ is taken to represent the angle the plane of the ring makes with the perpendicular surface. An angle of 0° represents the ring standing on end perpendicular to the surface. A second angle, ψ, allows for rotation of benzene about the axis-perpendicular to the plane of the ring. The reference point of this rotation is taken as th

center of mass of the C-H bond closest to the surface with ψ equal to 0° when the C-H bond axis makes the angle θ with the surface. It is obvious from the symmetry of the molecule that ψ can only take on the values 0° through 30°. This is illustrated in Figure 3.

Now, the polarizability of the molecule perpendicular to the surface is dependent on θ in the same manner as described by equation (32), but is independent of ψ. However, the distance of the center of mass of benzene from the surface at zero potential, is now a function of θ and ψ. This is given by an equation analogous to (37),

$$z_o\{\theta,\psi\} = z_{o\parallel} \quad (1+B'\cos\theta\cos\psi) \tag{37a}$$

where B' is as previously defined with $z_{o\parallel}$ being the value in the perpendicular position with ψ equal to 0°.

From the above, the potential function takes the form

$$U_{1s}\{z,\theta,\psi\} = \left(\frac{n}{n-m}\right) \left(\frac{n}{m}\right)^{\frac{m}{n-m}} \varepsilon^*_{1s\parallel} \quad (1+A'\cos^2\theta)$$

$$\bullet\,[(z_{o\parallel}/z)^n(1+B'\cos\theta\cos\psi)^{n-m}-(z_{o\parallel}/z)^m]. \tag{38a}$$

The Third Gas-Solid Virial Coefficient and Two Dimensional Gas Treatment

The third gas-solid virial coefficient, B_{3s}, reflects

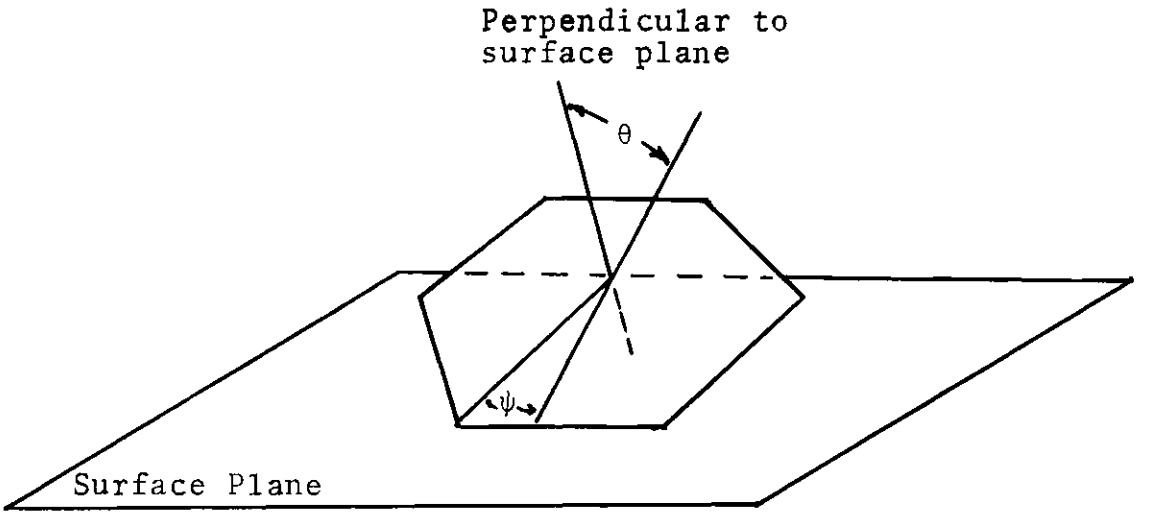

Figure 3. Benzene Adsorbed on a Homogeneous Surface

the interaction of an adsorbate molecular pair with the surface. Experimentally, it can be determined from the coefficient of the $(P/kT)^2$ term, C_{3s}, which has been previously defined by equation (12b),

$$C_{3s} = B_{3s} + B_{2s}B_2. \tag{12b}$$

In Appendix C it is shown how B_{3s} is related to the second virial coefficient for an imperfect two-dimensional gas. The form of the relationship is

$$-\frac{B_{2D}}{A} = \frac{B_{3s}}{2B_{2s}^{2}} \tag{40}$$

If some independent means of determining the surface area, A, is available, then B_{2D} can be evaluated and related to the two-dimensional pair potential, U_{12}, by

$$B_{2D} = -\frac{1}{2}\int_A [e^{(-U_{12}\{r\}/kT)} - 1]dA$$

$$= -\frac{1}{2}\int_0^\infty [e^{(-U_{12}\{r\}/kT} - 1]\pi r dr. \tag{41}$$

The Lennard-Jones (n,m) pair potential for U_{12} is given by[8]

$$U_{12}\{r\} = \left(\frac{n}{n-m}\right) \left(\frac{n}{m}\right)^{(m/n-m)} \varepsilon^*_{12} \left[(\sigma/r)^n - (\sigma/r)^m\right] \qquad (42)$$

where ε^*_{12} is the value of U_{12} at the potential minimum and σ is the value of r at $U_{12} = 0$.

Substitution of equation (42) into (41) and subsequent integration yields

$$\frac{B_{2D}}{\pi\sigma^2} = - \sum_{i\geq o}^{\infty} \frac{1}{ni!} E^{[(n-m)i+2]/n} \Gamma\left(\frac{mi-2}{n}\right) \qquad (43)$$

where

$$E = \left[\frac{n}{n-m}\right] \left(\frac{n}{m}\right)^{m/n-m} \varepsilon^*_{12}/kT$$

For the special case of the (12,6) potential

$$B_{2D} = - \pi\sigma^2 \sum_{i\geq o}^{\infty} \frac{(4\varepsilon^*_{12}/kT)^{((6i+2)/12)}}{12i!} \Gamma\left(\frac{6i-2}{12}\right) \qquad (44)$$

The values of σ and ε^*_{12}/k obtained in this manner can then be compared with that obtained from three-dimensional gas phase data.

One very important point should be made about the previous discussion. B_{2D} as given in equation (40) is a

two-dimensional quantity defined in terms of three-dimensional virial coefficients. As such, it neglects the effect of non-planarity in B_{2D} and the possible perturbing effect of the surface on the pair interaction as a function of z.

A more precise form of equation (42) which takes into account the above has been proposed by Sinanoğlu and Pitzer[21] and is given by

$$U\{r_{12},z_m\} = 4\varepsilon^*_{12}[(r_o/r_{12})^{12} - (r_o/r_{12})^6] + S(z_m)/r^3_{12} - 3S\{z_m\}\cos^2\theta/r^3_{12} \qquad (42a)$$

where z_m is the distance of the center of mass of the pair from the surface, θ is the angle between r_{12} and z_m and $S\{z_m\}$ is a function dependent on $U_{1s}\{z\}$ and the excitation energies of the adsorbent and the interacting molecules. The quantities r_o and r_{12} are as previously defined.

Examination of equation (42a) leads to the conclusion that the last term on the right hand side is a correction for non-planarity and the second term corrects for the perturbation of the pair interaction by the surface. Also, the two terms are opposite in sign since $\cos^2\theta$ cannot be negative. The sign of $S\{z_m\}$ is positive such that for $\theta>55°$ the effective value of ε^*_{12} is reduced and for $\theta<55°$, it is increased. Since the majority of the adsorption occurs between z_o and $2z_o$ (>95% at $\varepsilon^*_{1s}/kT = 4$), the net effect of

the above should be an ε^*_{12} which is reduced relative to the gas phase value.

Based on the above, Pierotti and Thomas,[22] have shown that a more correct form of equation (40) is

$$(B'_{2D}-\alpha)/A = -\ (B_{3s}+4B_{2s}B_2)/2B^2_{2s} \qquad (40a)$$

where B'_{2D} is the average value in the presence of the field assuming planarity and α is the correction for non-planarity.

Since $B_{2s}B_2$ is small compared to B_{3s} except very close to the two-dimensional Boyle temperature and the correction for non-planarity is also small relative to B'_{2D} except near the two-dimensional Boyle temperature, equation (40) is used in the subsequent analysis of B_{3s} data.

The Two-Surface Virial Treatment of Adsorption

For an adsorbent such as BN which has both basal plane and edge sites associated with the platelets, a two surface virial treatment can be applied. In this case the first two experimental coefficients of the virial equation are

$$C_{2s} = B^e_{2s} + B^b_{2s} \qquad (45)$$

and

$$C_{3s} = (B^b_{3s} + B_2\ B^b_{2s}) + (B^e_{3s} + B_2\ B^e_{2s}) \tag{46}$$

where the superscripts b and e refer to the basal plane and edge surface respectively. If X is the fraction of edge surface defined by

$$X = \frac{A^e}{A^b + A^e}$$

and z_o is taken the same for both surfaces, the equation analogous to (29) is

$$\frac{C_{2s}}{Az_o} = (1-X)\ I\ (\varepsilon^{*b}_{1s}, T) + X\ I(\varepsilon^{*e}_{1s}, T) \tag{47}$$

After determination of B^b_{2s} and B^e_{2s}, B_{2D} can be determined if it is assumed that

$$B^{eff}_{3s} = B_{3s}^{\ b} + B_{3s}^{\ e} \tag{48}$$

and that the values of B_{2D} are the same on the basal plane and edge. This gives

$$-\frac{B_{2d}}{A^b} = \frac{B_{3s}^{\ b}}{2(B^b_{2s})^2} \tag{49a}$$

and

$$-\frac{B_{2D}}{A^e} = \frac{B_{2s}^e}{2(B_{2s}^e)^2} \quad . \tag{49b}$$

Substitution of equation (49a) and (49b) into (48) gives

$$-B_{2D} = \frac{1}{2} \frac{B_{3s}^{eff}}{\frac{(B_{2s}^b)^2}{A_b} + \frac{(B_{2s}^e)^2}{A^e}} \tag{50}$$

The values of ε_{12}^*/k and σ can then be determined in the usual manner from the temperature dependence of B_{2D}.

<u>Thermodynamic Properties from Virial Coefficients</u>

The isosteric heat of adsorption is defined as

$$q_{st} = RT^2 \left(\frac{\partial \ln P}{\partial T}\right)_{N_{ads}} . \tag{51}$$

If equation (10) is inverted and substituted into equation (51) then

$$q_{st} = RT - RT^2 \left[\frac{d\ln B_{2s}}{dT}\right] - RT^2 \left[\frac{d[B_{3s} + B_{2s}\ B_2)/B_{2s}^2]}{dT}\right] N_{ads} + \ldots \tag{52}$$

At zero coverage

$$q_{st}^{o} = \lim_{N_{ads}\to 0} q_{st} = RT - RT^2 \left[\frac{d\ln B_{2s}}{dT}\right]. \tag{52a}$$

The isosteric Gibb's free energy change at zero coverage is defined as

$$\overline{\Delta G}_{st}^{o} = \lim_{N_{ads}\to 0} RT\ln(f/N_{ads}) = RT\ln(RT/B_{2s}). \tag{53}$$

Combining equations (52) and (53) gives for the isosteric entropy change at zero coverage

$$\overline{\Delta S}_{st}^{o} = R\ln(B_{2s}/RTe) + RT(d\ln B_{2s}/dT). \tag{54}$$

where e is the base of the natural logarithm, 2.71828.

For a gaseous adsorbate, the molar equilibrium enthalpy change is given by

$$\overline{\Delta H}_{ads} = -RT^2 \left[\partial\ln f/\partial T\right]_{\pi}. \tag{55}$$

To obtain a relationship between the two dimensional spreading pressure, π, and the fugacity, the two-dimensional virial equation for adsorption

$$\frac{\pi A}{RT} = B_{2s}\ (f/RT) + \frac{1}{2} B_{3s}\ (f/RT)^2 + \frac{1}{3} B_{4s}\ (f/RT)^3 + \ldots \tag{56}$$

is inverted and substituted into equation (55) to give

$$\overline{\Delta H}_{ads} = RT^2 \left(\frac{d\ln B_{2s}}{dT}\right) + \pi A \left[\frac{B_{3s}}{2B_{2s}^{\ 2}} - T \left(\frac{d(B_{3s}/2B_{2s}^{\ 2})}{dT} \right) \right] + . \quad (57)$$

In terms of B_{2s} and N_{ads},

$$\overline{\Delta H}_{ads} = RT^2 \left(\frac{d\ln B_{2s}}{dT}\right) + \frac{RT}{A} \left[\frac{dB_{2D}}{dT} - B_{2D}\right] N_{ads} + \ldots \quad (58)$$

which when extrapolated to zero coverage gives

$$\overline{\Delta H}^{o}_{ads} = RT - q^{o}_{st}. \quad (59)$$

Definition of the molar Gibbs free energy change of adsorption at infinite dilution, $\overline{\Delta G}^{o}_{ads}$, involves the specification of a hypothetical standard state spreading pressure, π_o, where the molecules have the properties they would have at infinite dilution. The standard state for the gas phase is unit fugacity,

$$\overline{\Delta G}^{o}_{ads} = \lim_{N_{ads} \to 0} RT\ln(f/\pi) = RT\ln \left[\frac{\pi_o A}{B_{2s}}\right]. \quad (60)$$

Combination of equation (59) and (60) give the molar entropy change at zero coverage

$$\overline{\Delta S}^{o}_{ads} = R\ln\left[\frac{B_{2s}}{\pi_o A}\right] + RT\,\frac{d\ln B_{2s}}{dT} \quad . \tag{61}$$

CHAPTER III

APPARATUS-CONSTRUCTION AND OPERATION

Introduction

The apparatus, with minor modification, is that constructed by Ramsey to measure the adsorption of the inert gases on BN. Construction details may be obtained from reference 1.

The basic apparatus consisted of four sections:

Gas Transfer System

Pressure Measurement System

Sample Cell

Cryostat

A generalized diagram of the apparatus is shown in Figure 4. A description of these sub-systems and their operation follows.

Gas Transfer System

A detailed diagram of the gas transfer system is shown in Figure 5. The main element is five gas pipets ranging in volume from ten to 160 cm^3. The pipets are contained in an insulated box, BB, which acts as the container for an ice bath. Each gas pipet has fuducial marks, FM1 and FM2, on the small bore tubing extending out of the insulated box. The pipet volumes were previously determined in the box by

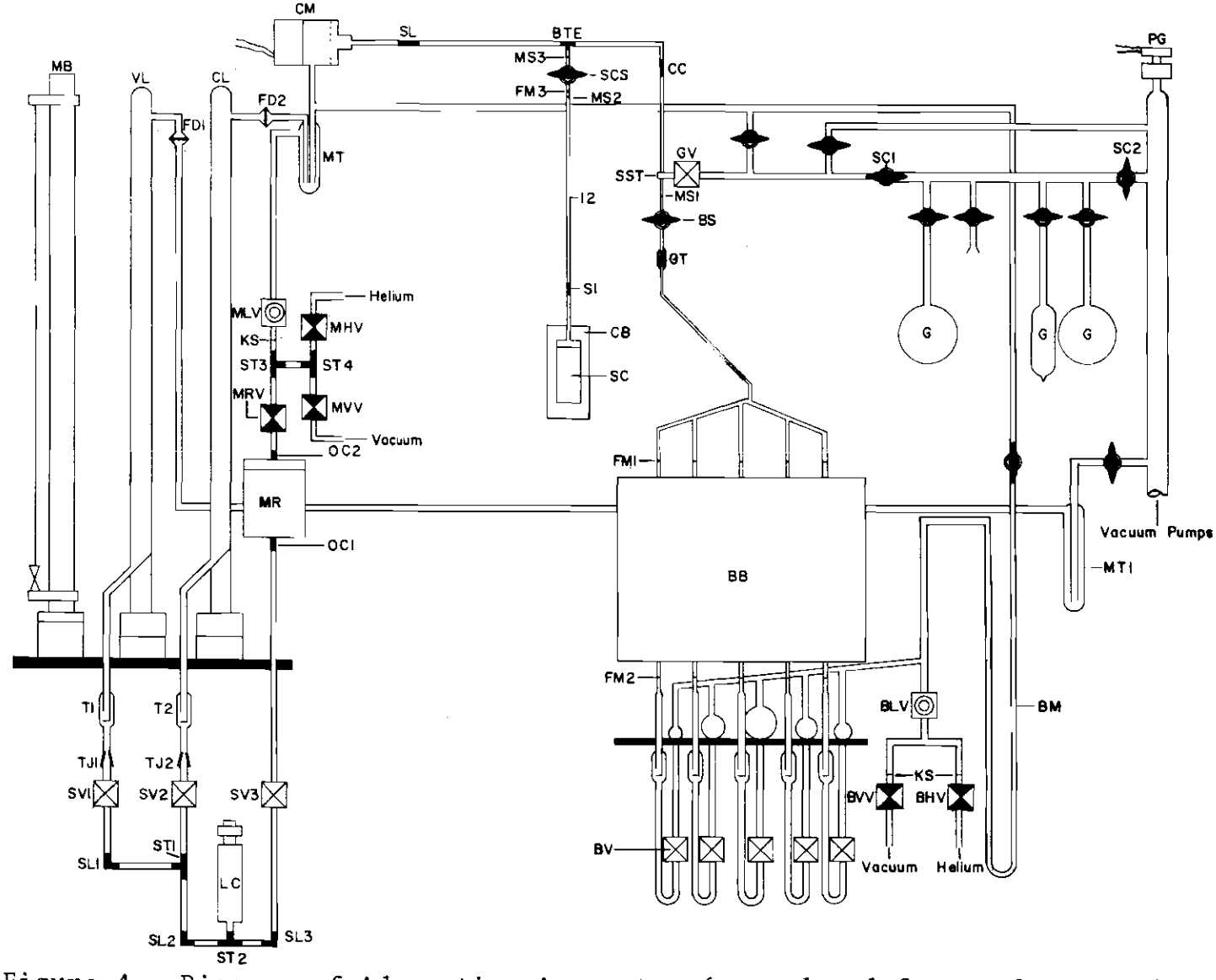

Figure 4. Diagram of Adsorption Apparatus (reproduced from reference 1)

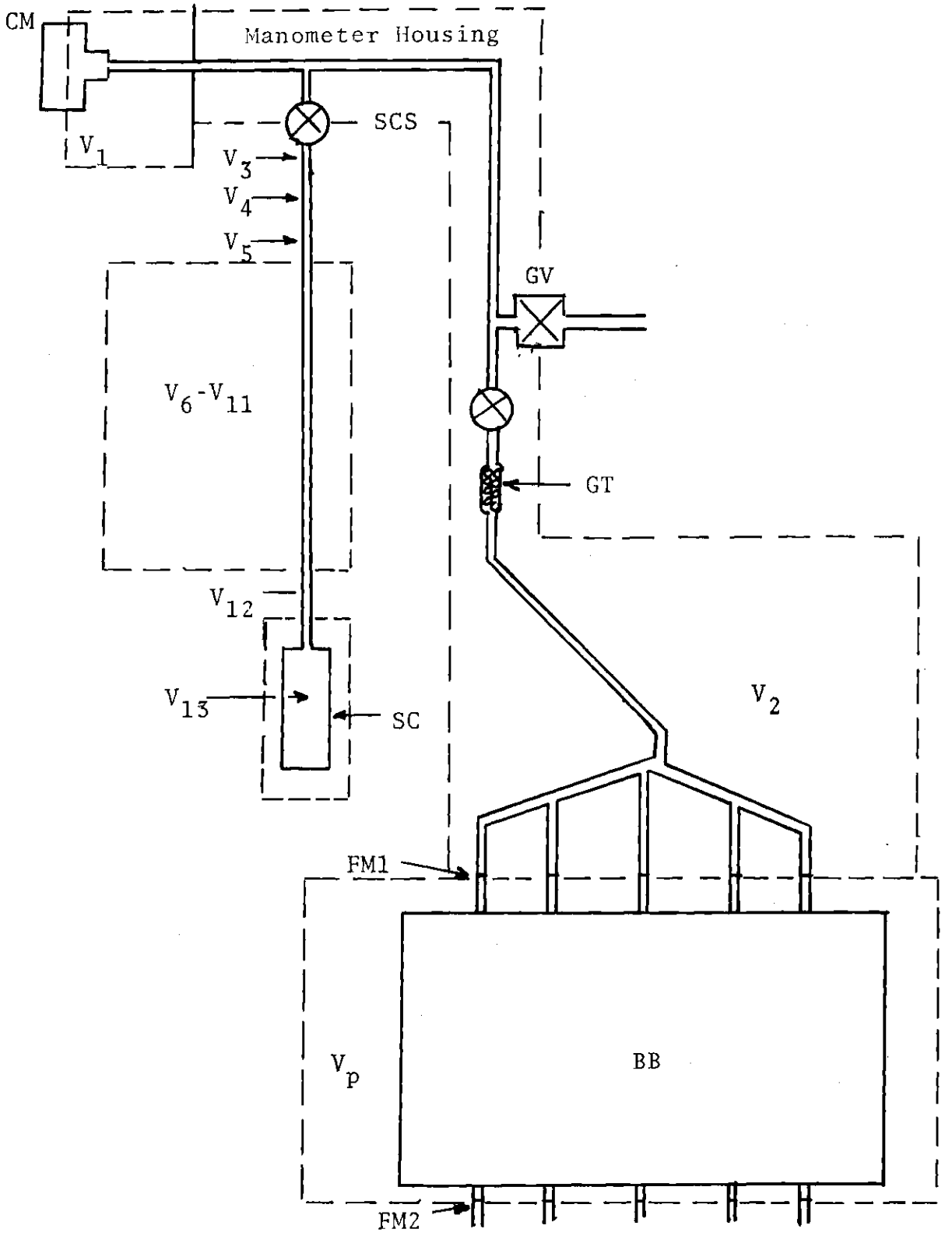

Figure 5. Diagram of Gas Transfer System

mercury displacement. Volumes of the pipets are given in Table 1. Although total dose volumes, V_p, of from ten to 310 cm^3 can be obtained, it was found desirable to limit the dose volume to a maximum of 150 cm^3. This limited the volume over which the experimental pressure error applied which will be further discussed in the section on error analysis, Appendix D.

The pipets are connected to a gas supply, G, by the valve, GV, and to the sample cell through the one mm bore stopcock, SCS. The pipets are interfaced to the pressure measurement system through the capacitance manometer, CM. A small trap containing gold beads, GT, is placed between CM and V_p to trap mercury vapor which might otherwise contaminate CM.

The volumes of CM and the associated tubing inside the thermostated manometer enclosure, V_1, are determined from physical dimensions. The temperature of V_1 is measured by a thermocouple, TC14, attached to the head of CM. The remaining volume of the dose system between V_1 and V_p, V_2, is determined by a series of expansion and compression measurements using the available pipet volumes. The temperature of V_2 is taken as the average of two thermocouples, TC15 and TC16, placed along V_2. Values of V_1 and V_2 are given in Table 1.

The experimental procedure is first to insure that valves SCS and GV are closed and that the system pressure as

Table 1. Apparatus Volume, Pressure and Temperature Specifications

Section Designation	Volume cm^3	Temperature	Pressure
Gas Pipets (V_p)			
10	11.0971±0.0004	273.150°K	P_p
20	21.3714±0.0005	273.150°K	P_p
40	40.5536±0.0013	273.150°K	P_p
60	63.8411±0.0009	273.150°K	P_p
150	150.7375±0.0007	273.150°K	P_p
V_1	2.931	TC14	h_c
V_2	1.766 ±0.006	AV(TC15-TC16)	h_c
V_3	0.252	AV(TC15-TC16)	h_c
V_4	0.0349	AV(TC1-$T_{at}V_2$)	h_c
V_5 thru V_{10}	0.0744 ea.	TC1-TC7 in prs.	h_c
V_{11}	0.0592	AV(TC7-TC8)	h_c
V_{12}	0.0592	AV(TC8-PRT)	h_c
V_{13}(BN)	40.705 ±0.010	273.150°K	P_{13}
	Eq. (69)	Other than 273.150°K	P_{13}
V_{13}(P33)	62.803 ±0.007	273.150°K	P_{13}
	62.637 ±0.003	205.188°K	
	62.974 ±0.004	318.992°K	
	Eq. (70)	Above 273.150°K	
	Eq. (71)	Below 273.150°K	

indicated by the Phillips Gauge, PG, is in the range 10^{-6} to 10^{-7} Torr. The box, BB, is then packed with ice which has been equilibrated in distilled water. The pipet volume is then adjusted to the desired value by filling with mercury through valves BV. To insure that the mercury is not brought up so fast as to be blown through the system, an auxillary mercury manometer, BM, is installed in the system. One end is connected to the mercury reservoir used to fill the pipet and the other to the mercury manometer side of CM. The pressure in BM is controlled through valves, BVV, BHV, and BLV. Since CM is used as a null device, a calibration mark can be placed on the auxillary manometer representing the head of mercury required to fill a given pipet. Therefore, even though the mercury level can not be seen in the pipet, the level can be controlled by reference to the auxillary manometer. This procedure is particularly necessary when changing the pipet volume after the dose has been introduced into the sample cell, SC.

After adjusting V_p, the gas supply value, GV, is opened until a small deflection of the capacitance manometer on its least sensitive scale is obtained. This is then balanced by introducing helium on the other side of the capacitance manometer. Gas is then simultaneously fed into both the dosage system and mercury manometer systems at approximately zero capacitance manometer deflection until the desired pressure is obtained. The initial dose is allowed to

equilibrate for approximately two hours. The insulated box is repacked with equilibrated ice at half hour intervals and approximately fifteen minutes prior to a pressure reading.

Pressure Measurement System

Whereas the critical system volumes and temperatures are, in general, determined to six significant figures, great care is necessary to determine the pressure to 0.001 cm. Diagrams of this system are shown in Figures 4 and 6.

A precision bore (one inch diameter) mercury U tube manometer is used to indicate the pressure. The manometer is interfaced to the constant volume portion of the apparatus by a capacitance manometer, CM, connected to the right manometer tube, CL. The pressure in CL is maintained the same as on the sample cell side of CM by introducing or removing helium through the valves MLV, MHV and MVV. This arm is maintained at a constant level at all pressures by adjustment of a piston-cylinder control, LC. The position of the CL meniscus is set by viewing through a bifilar microscope, MC, which is illuminated from behind CL by a lamp, C1. The left hand side of the manometer, VL, is connected to the main pump system so that the gas pressure in VL is always 10^{-6} to 10^{-7} Torr. The mercury level in this side is dependent on the system pressure. The meniscus of VL is illuminated from behind by a lamp, V1, which is mounted

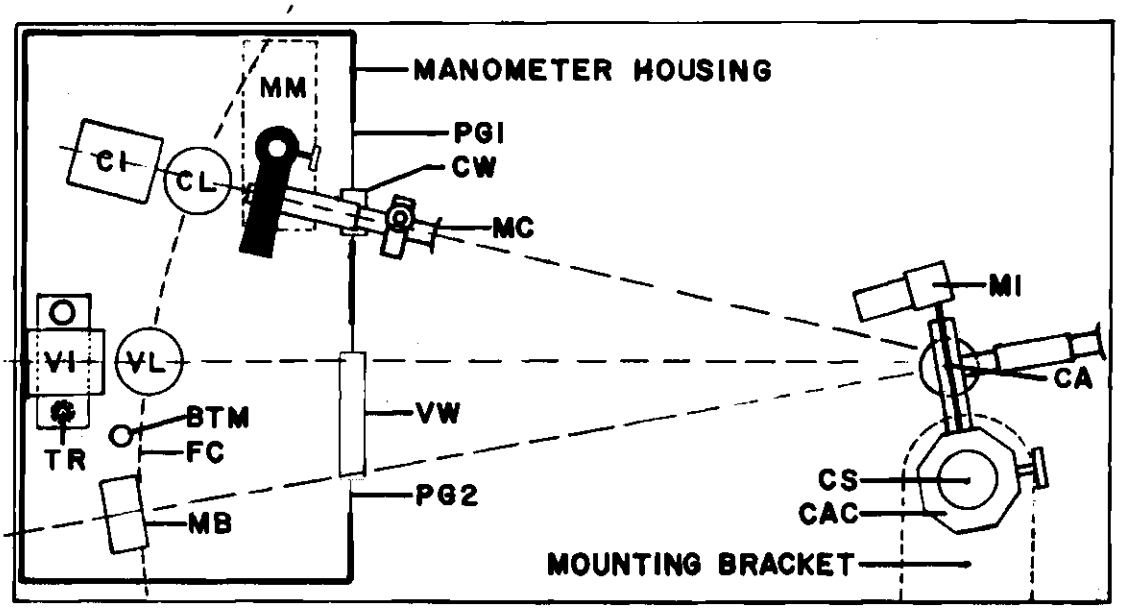

Figure 6. Manometer and Cathetometer Arrangement (reproduced from reference 1)

on a threaded rod, TR. The rod is coupled to a motor which when activated drives the lamp up or down as desired.

The mercury level in VL is viewed by a cathetometer, CA, which is mounted on a micrometer slide whose level can be set on a finished steel rod, CS. The slide is referenced to a standard meter bar, MB, positioned to the left of VL. MB is illuminated by an L & N galvamometer light. The level in CL is also referenced to MB so that the difference in the apparent head of mercury, h_a, between CL and VL can be determined to a precision of 0.0010 cm.

The previously described pressure system, except for the cathetometer-slide section, is enclosed in a large thermostated box with a plexiglass front, PG, having slit cut outs, VW, for viewing the meter bar and U-tube manometer.

The temperature in the box is maintained by a Sargent Thermonitor whose probe is positioned in the center front of the box. It is used to activate two one hundred watt light bulbs contained in a small enclosure within the top rear of the box and a twenty-five watt bulb in the top of the box. Air is supplied from the outside through the heating enclosure by a small fan. An auxiliary fan is also mounted on the left inside wall of the box for air circulation. The temperature of the meter bar and the mercury in the manometer, t_{mb}, is taken as the average of a thermometer placed in the bottom level of the box and the thermocouple, TC13, in the center of the box. Temperature fluctuation over

the period of an experimental run are generally ± .03°C. However, occasionally a temperature upset in the building during a run would result in a fluctuation of up to 0.10°C.

Prior to an experimental run the meniscus in CL is set and then measured as done for VL. This is done before each run in case changes in temperature or slight shifts of the apparatus might have changed the position of the VL meniscus relative to the meter bar. This was found to change by approximately .004 cm over the entire experimental period. Prior to the reading of any mercury height, a rubber hammer is used to tap the meniscus to insure that the true equilibrium position is attained.

After the apparent height of the mercury head, h_a, is attained, it first has to be corrected for expansion of the meter bar to give the true height. The meter bar calibration certificate showed that MB is 1000.004 millimeters at 20°C with a thermal expansion coefficient of 9.9×10^{-6} per degree centigrade. The true height is then

$$h = h_a \ (1.0000004)(1+((t_{mb}-20)9.9 \times 10^{-6}/°C)) \qquad (62)$$

This height then has to be converted to an equivalent height of mercury at 0°C and acceleration due to gravity, g, of 980.655 cm/sec^2.

This height is given by

$$h_1 = h(g/g_1)(d/d_1) \tag{63}$$

where the values with the subscript 1 refer to the values at 0°C and the unsubscripted values to the experimental conditions.

The value of g at the approximate position of the apparatus on the Georgia Tech campus was determined to be 979.529 cm/sec^2. The ratio of the densities of a fluid at two different temperatures is just the inverse of the ratio of the volumes. The volume of a mass of mercury around room temperature has been shown to be adequately represented by[23]

$$V = V_o\ (1 + 1.818 \times 10^{-4}\ t) \tag{64}$$

where V_o is the volume of the mass at 0°C.

Therefore,

$$d/d_1 = 1/(1 + 1.818 \times 10^{-4}\ t_{mb}) \tag{65}$$

Substitution of the appropriate values into equation (63) gives

$$h_1 = h_a\ \frac{(.998842)(1+(t_{mb}-20) \times 9.9 \times 10^{-6}/°C))}{(1 + 1.818 \times 10^{-4}\ t_{mb})}\ . \tag{66}$$

A second correction which has to be made is for any deviation, C, of the capacitance manometer from the zero null condition. This is given by

$$h_c = h_1 + C. \tag{67}$$

The final correction arises from the use of a capacitance manometer. This comes about since

- the mercury level in CL and the sample cell were at different vertical heights from CM,
- the gas in the sample cell and VL were at different temperatures, and
- different gases were in the sample cell and CL.

The magnitude of this correction is in general small. The expression for the pressure, P, where the balancing gas in CL is helium is given by

$$P = h_c \ (0.99986 + (M_{wgas} \times h_{gas}/T_{gas})(1.18 \times 10^{-6})) \tag{68}$$

where

M_w = the molecular weight of the adsorbate

T_{gas} = the temperature of the gas in either the sample cell or V_p depending on which P is being calculated.

h_{gas} = distance of the center of the sample cell or V_p from CM. This was 350 mm in each case.

For the formal derivation of equation (68), see reference 1.

Sample Cell

The sample cell, SC, is connected to the gas transfer system through the one mm stopcock, SCS. Between SC and SCS is a length of monel tubing which is divided into a number of volumes for calculation purposes. This is required due to the temperature gradient between SC and SCS. The section of the monel tubing between the entrance to the top of the cryostat and SCS is designated V_3 with the temperature being the same as for V_2. The remaining length of tubing is divided into nine sections, V_4 through V_{12}, with eight thermocouples, TC1 through TC8 placed along its length for temperature determination. The sizes of these volumes were determined from the dimension of the tubing and are given in Table 1 along with a listing of the thermocouples used for temperature measurement.

The sample cell, SC, is constructed of nickel and has a well in the bottom for insertion of a platinum resistance thermometer, RT, which is used for temperature determination of SC at all temperatures other than the ice point. At the ice point, SC is immersed in a one gallon dewar ice bath to a depth of at least one inch above the top of SC.

For systems using BN as the adsorbent, the volume of SC accessible to the gas phase, V_{13}, is determined at the ice

point using helium as the calibrating gas. It is assumed that B_{2s} for the adsorption of helium on BN is zero at 0°C. The volume of V_{13} at other temperatures is determined using the coefficient of linear expansion of BN, β,[24] and polycrystalline nickel, α.[25] The resultant equation is

$$V_{13}(t) = V_{sc}(0°C) + 3\alpha t\ V_{SC}(0°C) - (1+\beta t)\ V_{BN}(0°C) \qquad (69)$$

where

$\alpha = (12.54 \times 10^{-6} + 8.75 \times 10^{-9}\ t - 7.5 \times 10^{-12}\ t^2 + 6.25 \times 10^{-15}\ t^3)/°C$

$\beta = 41.15 \times 10^{-6}/°C$

$V_s(0°C)$ = Volume of empty SC = $V_{BN}(0°C) + V_{13}(0°C)$

$V_{BN}(0°C) = 36.77\ cm^3$ (volume of BN at 0°C)

and t is the temperature in °C.

Determination of V_{13} when graphite is used as the adsorbent and N_2 is the adsorbate presented a problem at high temperature. Since B_{2s} is very small under this condition, small errors in volume introduced in using coefficients of thermal expansion to determine the volume at other than the base temperature might be large relative to B_{2s}.

In order to avoid this source of error, V_{13} is determined at a higher temperature as well as the ice point and the expansion coefficient is assumed to be linear between these points. The resultant equation for V_{13} is given below

$$V_{13}(t) = (62.803 + 3.730 \times 10^{-3} t)\ cm^3 \qquad (70)$$

In fact, at 318.992°K where V_{13} is determined with helium, the actual volume is found to differ from that calculated from expansion coefficients by several hundredths of a cm^3. This would have introduced a significant error in B_{2s} for the N_2- graphite system at this temperature. Determination of V_{13} with helium at 205.188°K gives a value of the volume which essentially agrees with the thermal expansion technique when corrections are made for adsorption of helium at this temperature. Also, at the lower temperature, B_{2s} for N_2- graphite is large enough so that small errors in V_{13} are also small compared to B_{2s}. The resultant expansion equation used below 0°C is

$$V_{13}(t) = V_{13}(0°C) + 3\alpha t\ V_{SC}(0°C) - (1+\beta' t)\ V_c(0°C). \qquad (71)$$

where α is as previously defined and β' is the cubic expansion coefficient determined from the variation in interplanar spacing of graphite with temperature, d[26]

$$\beta' = 2.825 \times 10^{-5}/°C$$

$$V_{SC} = 73.190\ cm^3$$

$$V_C(0°C) = \text{volume of graphite sample} = 10.387\ cm^3$$

Cryostat

Construction

The cryostat is diagramed in Figure 7. The main element of the system is a cylindrical copper block, CB, which fits around SC. Centered in the bottom of CB is a platinum resistance thermometer, RT, (L & N Model 8164, Serial No. 1593183) which also fits into the well of SC. After CB is inserted over SC, a split copper block, CB1, is inserted over SC in the remaining opening of CB.

CB is wrapped with two coils of constantan wire to form two heaters, J1 and J2; each of about 140 ohms resistance. The heaters are powered by a twin dc power supply (Power Design type TW 5005). A third heater, J3, is used to heat the inlet tube and is powered by an HP model 6125A power supply. Also implanted in CB are four thermocouples, TC9 through TC12. Two are placed in the side and one each on the top and bottom. The external wire connections enter the system through the brass tube, BT, which is attached to the main cryostat supported by an I beam. A smaller support plate, SP, is attached to the bottom of BT. A brass cannister, BVC, can be inserted over CB and fastened to SP by means of a Woods Metal seal. The final part of the insulating system is a dewar contained in a cannister, DSC, which can be raised to enclose BVC and provide a vacuum seal by means of an oring at CSP. Both BVC and DSC can be separately evacuated for insulating purposes. At temperatures below the ice point,

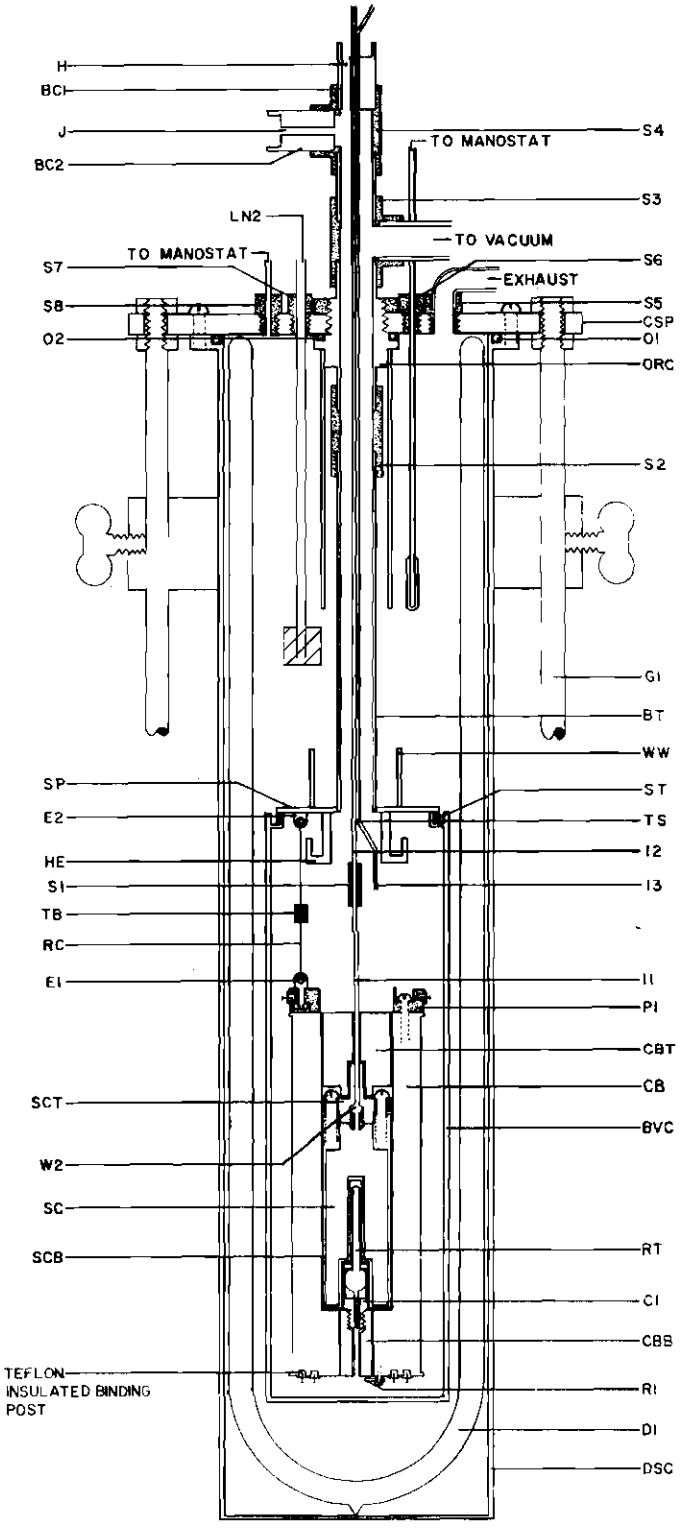

Figure 7. Cryostat (reproduced from reference 1)

BVC is evacuated and DSC is filled with either a dry ice-acetone mixture or liquid nitrogen. The liquid level controller, LN2 is used in the latter case.

At temperatures above 0°C and up to ~100°C, the system is operated by one of two methods; evacuation of DSC without BVC attached or evacuation of BVC with an air bath in DSC. Both methods are satisfactory.

More specific construction details may be found in reference 1.

Operation

The first step in the cryostat operation when measuring isotherms below 0° is to fill DSC with the appropriate coolant to bring the temperature to the general range desired before evacuating BVC. When operating above 0°C, evacuation is completed before heating as this allows the block to come to temperature quicker. The temperature of V_{13} is measured by RT in accordance with the 1968 IPTS scale.

The resistance of RT is measured with a temperature controlled Mueller Bridge (L & N No. 8069B, Serial No. 1551895) powered by an L & N 099034 constant current power supply. Bridge balance is indicated by a guarded dc null meter, NM (L & N type 9834).

To maintain the desired temperature, heater J1 is adjusted so as nearly balance the heat loss. The heater J2 is then manual on-off operated so that the temperature fluctuation as indicated by NM is not greater than ± .002°C.

The thermocouples TC9-12 are used as an indication of whether or not SC is at thermal equilibrium. In general, equilibrium was maintained at least one hour before the first point was measured.

Materials

The gases used were all research grade contained in Pyrex containers supplied by Air Reduction Sales, Inc., and Matheson, Co.

All except for CO_2 were certified to have 90 PPM impurities or less. The CO_2 had 0.1 mole percent N_2 impurity. However, the difference between adsorptive potentials of CO_2 and N_2 on P33(2700°) is not great enough to warrant a correction for the 0.1% N_2 impurity in CO_2. Also the expected average percent error in B_{2s} for CO_2-P33 as calculated in Appendix D is 0.23% which is greater than the N_2 impurity in CO_2.

Two adsorbents were used in the experimentation, the hexagonal modification of boron nitride and graphitized carbon P-33 (2700°). Diagrams of the structure of each are shown in Figure 8. The cell constants are

	BN[27]	Graphite[24]
a	0.2504 nm	0.2456 nm
b	0.6662 nm	0.6696 nm
bond length	0.1446 nm	0.142 nm

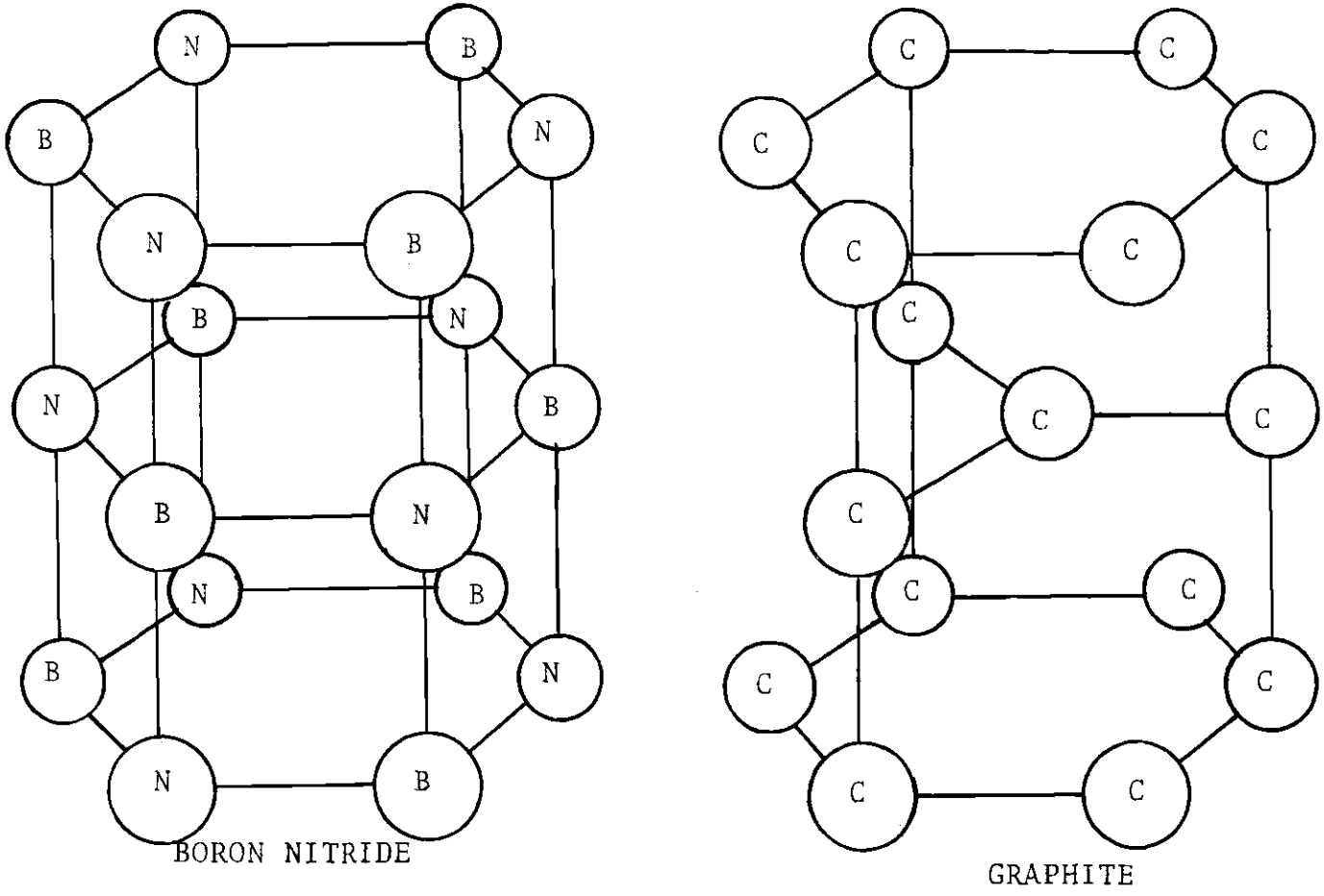

Figure 8. Graphite and Hexagonal BN Structures

The values for the various coefficients of expansion have been previously given.

Details of the make-up of the BN sample can be obtained from reference 1. Briefly, the sample was determined to be made up of flat crystals with thin edges. Estimates of the fraction edge area from electron micrographs varied from five to ten percent. The BET area of this sample as determined with argon by Ramsey[1] was 4.98 m^2/g.

The other adsorbent used was graphitized P-33. P-33 is normally made up of spherical aggregates of parallel layer groups.[28] Upon treatment at 2700°-3000°C in the absence of air the layers attain the graphite configuration and the particles are no longer spherical. Instead, the individual particles are doubly truncated hexagonal and octagonal bipyramids.[29] The faces of these particles present an almost completely homogeneous surface for adsorption studies. Graham[30] has estimated that the surface area of P-33 (2700°) contains approximately 0.1% high energy sites. More recently Putman and Fort[31] have estimated 0.5% high energy sites on their sample of Sterling FT-D5 (2700-3700°) when using the two surface separation technique described in reference 2 and 0.25% when using the technique of Graham. It is, however, evident from previous work done on this sample[5-8] and from this work that the P-33 (2700°) used here is completely homogeneous for purposes of the virial analysis over the experimental temperature range explored. If, as

stated by Graham,[30] the interaction with the high energy sites is twice as great as for the balance of the surface, then any high energy sites in excess of 0.03% should be easily detectable.

As stated in Chapter I, this particular P33(2700°) sample is the identical one used by Halsey and co-workers[5-8] in their Ar-P33 studies. As such, any results of this work can properly be compared with those of references 5 through 8.

A BET analysis of N_2 adsorption on the P33(2700°) sample gives a surface area of 11.86 m^2/g. This compares favorably with reported values in the range 11.4 - 12.5 m^2/g. The data for the BET Plot is given in Appendix E.

CHAPTER IV

DATA TREATMENT

Isotherm Calculation

The number of moles of gas adsorbed, N_a, at a given temperature and pressure is calculated in the usual manner. First, the total number of moles in the dose system, N_T, is calculated and then the number of moles remaining in the gas phase after interaction with the surface is subtracted. The number of moles in any volume, V_i, of the system is given by

$$N_i = \frac{P_i V_i}{RT_i + B_i P_i}$$

where B_i is the second gas virial coefficient at T_i. The values of and/or method of calculation of V_i, T_i and P_i are given in Table 1.

As a check of the system, Ramsey's[1] ice point isotherm of Ar-BN and Constabaris'[32] ice point isotherm of Ar-P33 (2700°) were duplicated. Agreement was well within the accuracy of the experiment. These data along with all other experimental adsorption data may be found in Appendix E. Plots of the isotherms are shown in Figures 9 through 14.

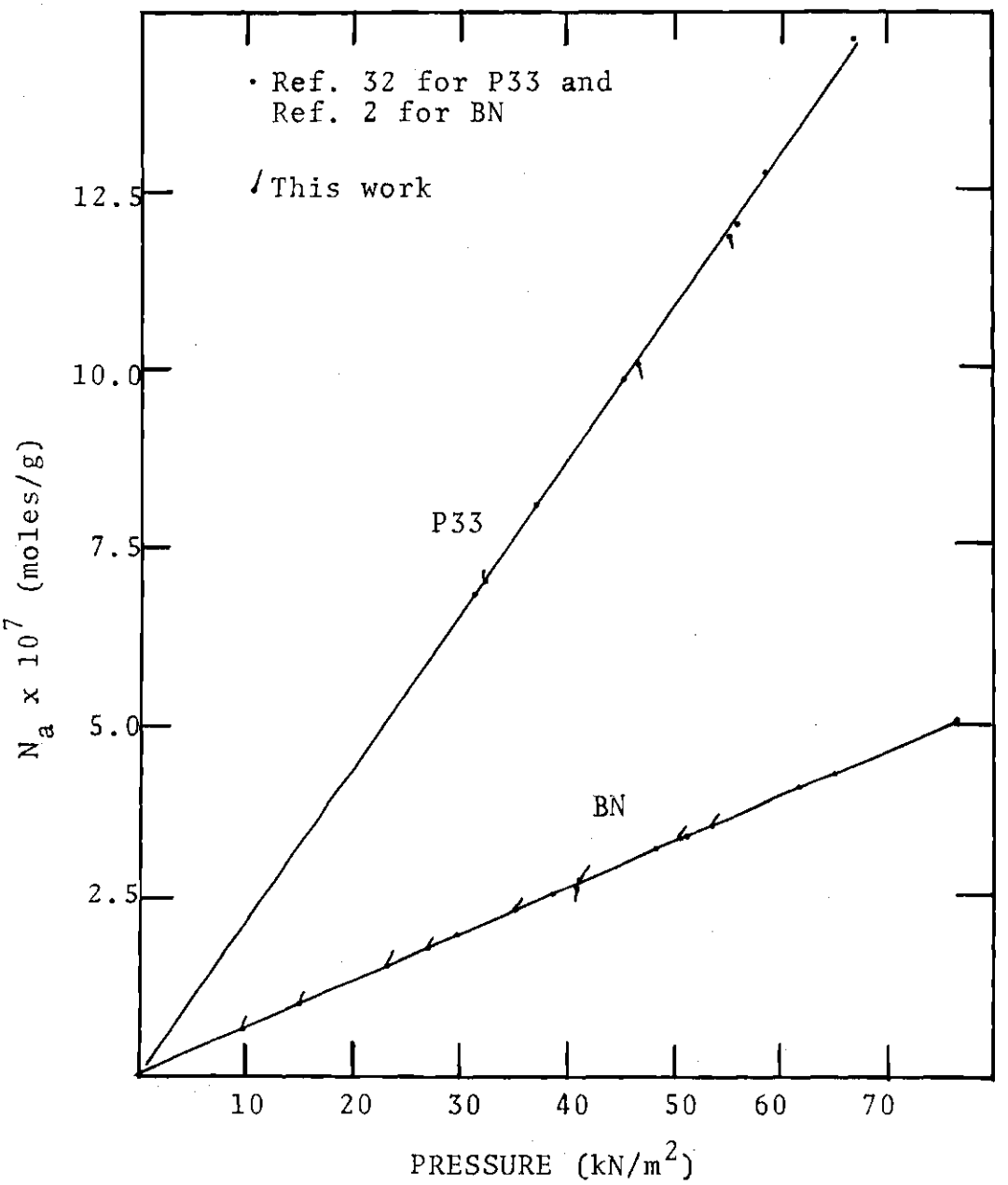

Figure 9. Adsorption Isotherms for Argon on BN and P33 (2700°) at 273.150°K

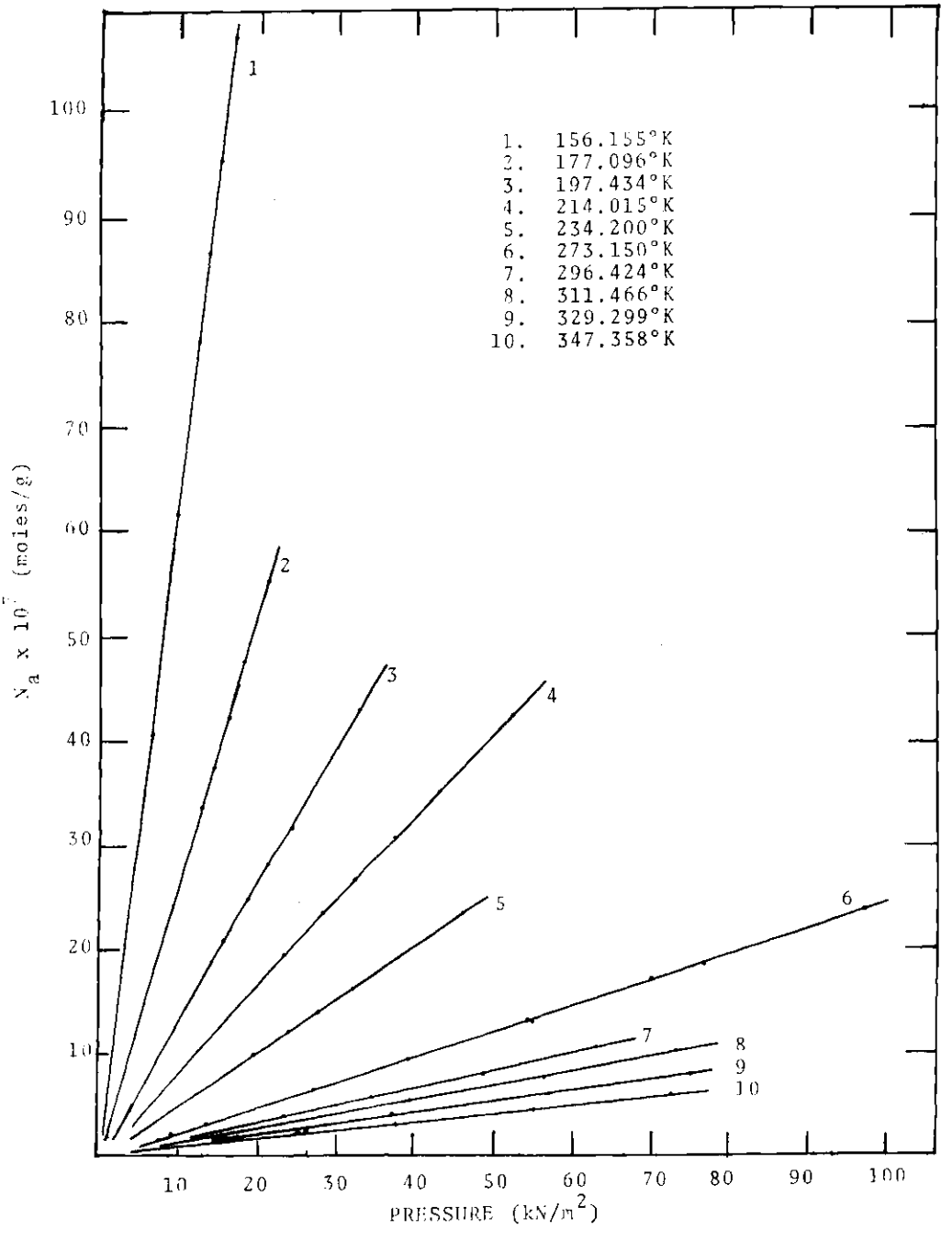

Figure 10. Adsorption Isotherms for Nitrogen on Graphitized Carbon P33 (2700°)

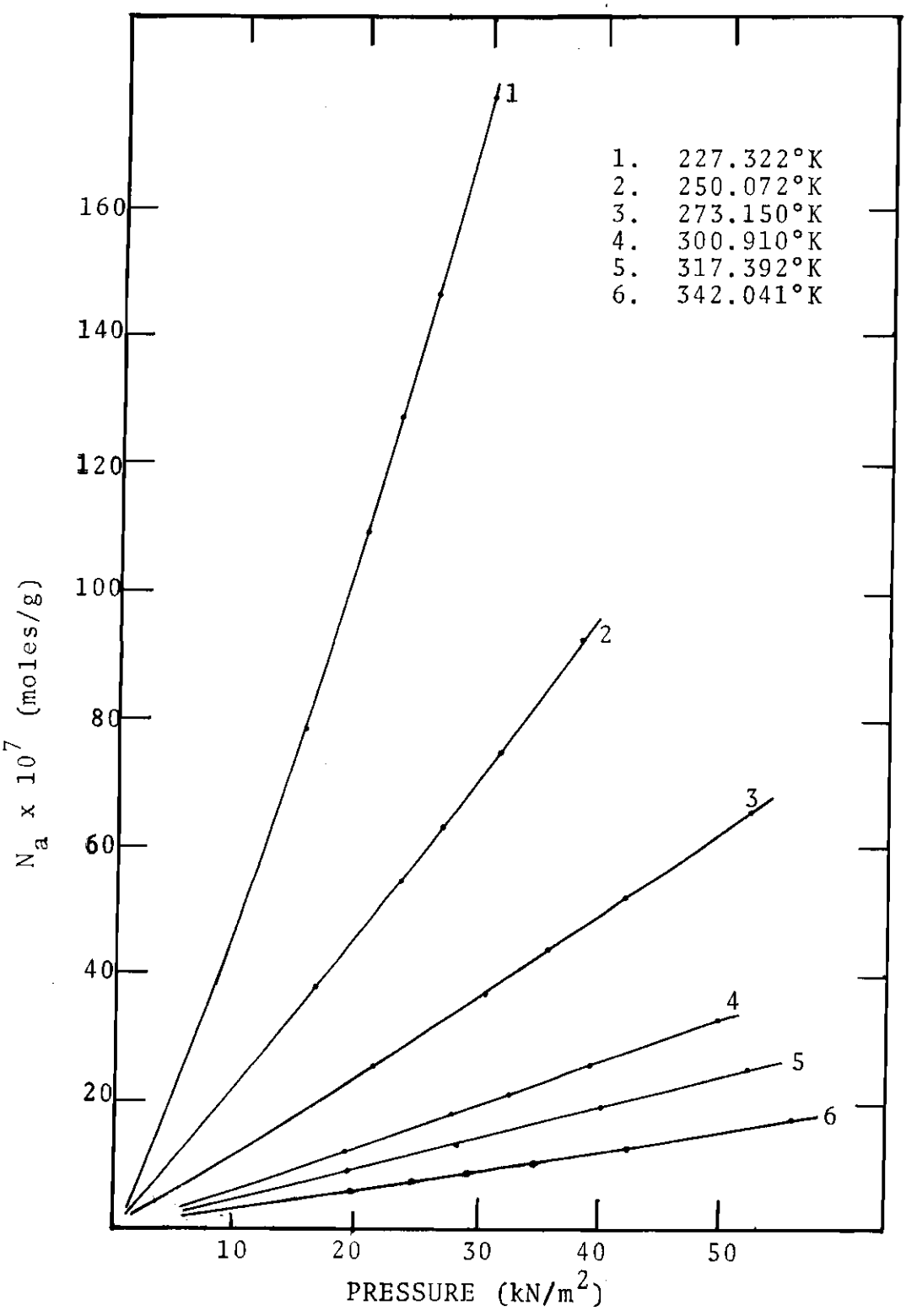

Figure 11. Adsorption Isotherms for Carbon Dioxide on Graphitized Carbon P33 (2700°)

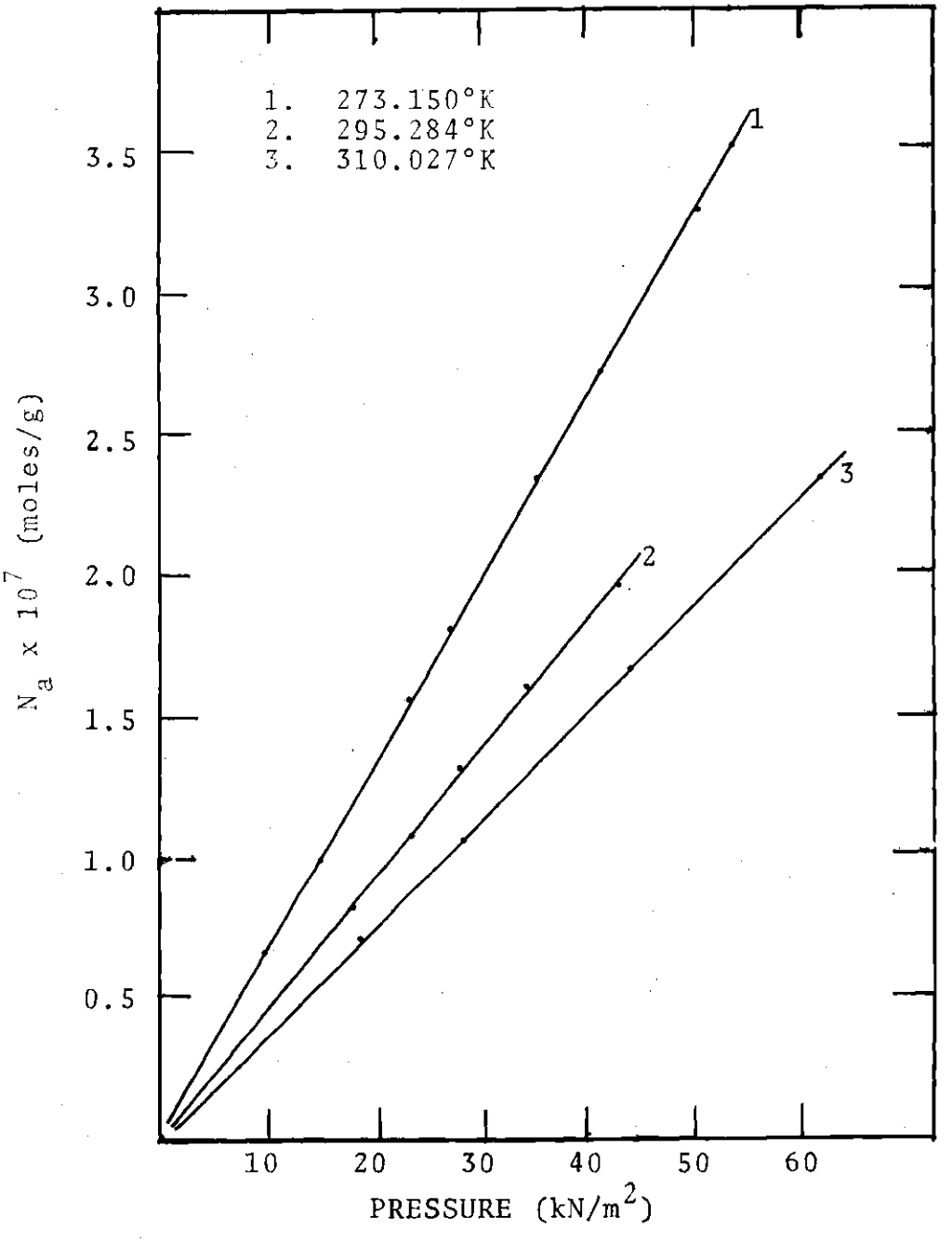

Figure 12. Adsorption Isotherms for Argon on Hexagonal Boron Nitride

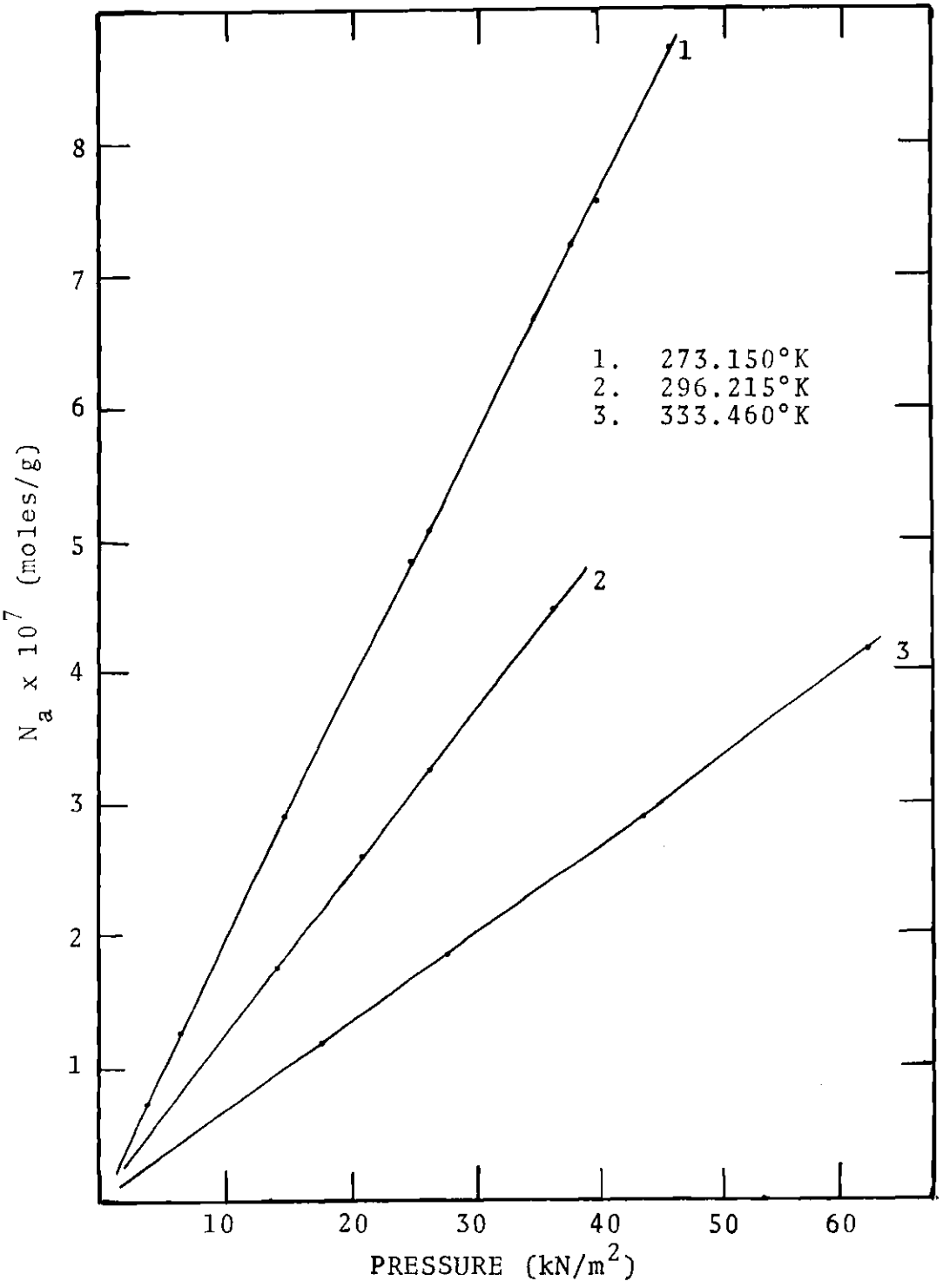

Figure 13. Adsorption Isotherms for Krypton on Hexagonal Boron Nitride

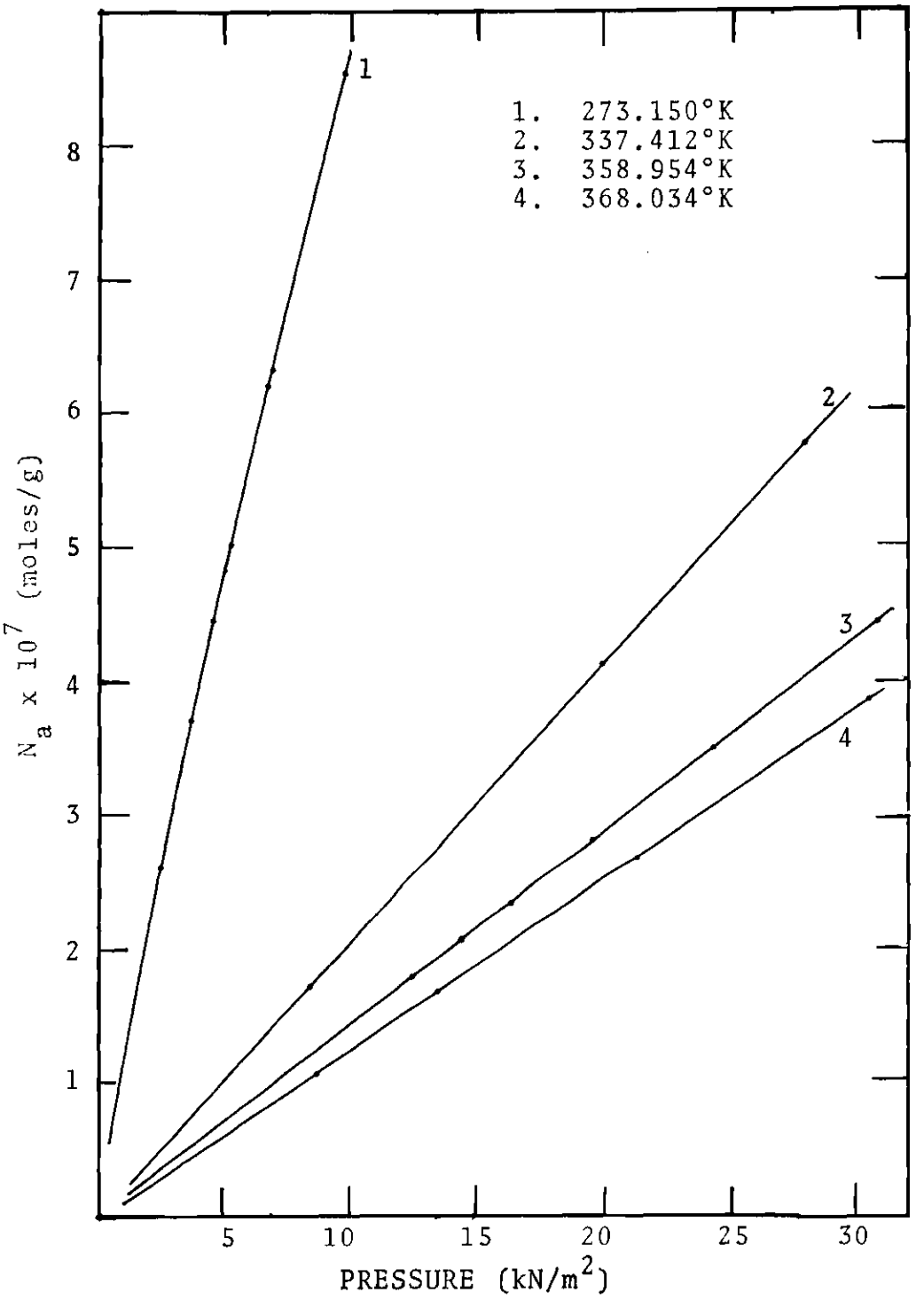

Figure 14. Adsorption Isotherms for Xenon on Hexagonal Boron Nitride

Determination of z_o

The result of the analysis of B_{2s} by the methods described in Chapter II gives values of Az_o and ε^*_{1s}/k for the spherical model and $Az_{o\,||}$ and $\varepsilon^*_{1s\,||}/k$ for the non-spherical model. In order to determine the value of A some determination of z_o or $z_{o\,||}$ must be made. One method is to take the distance between centers of two different hard spheres as

$$\sigma_{AB} = \frac{1}{2}(\sigma_A + \sigma_B) \tag{72}$$

where σ_A and σ_B are the hard sphere diameters of molecules type A and B respectively.

If this is carried over to surface adsorption, then the distance of an adsorbate center from the plane passing through the center of surface adsorbent molecules at zero potential is given by

$$z_{oAp} = \frac{1}{2}(\sigma_A + \sigma_p) \tag{73}$$

where σ_A is the gas phase hard sphere diameter of the adsorbate molecule and σ_p is the "effective" hard sphere diameter of the surface plane. This is referred to as an "effective" hard sphere diameter since the plane may contain different atoms as in the case of BN as well as having adsorption sites

over planar atoms or at points in between.

Now, if z_{oAp} can be determined for one gas-solid system, then σ_p can be computed from

$$\sigma_p = 2z_{oAp} - \sigma_A \ . \tag{74}$$

With this value of σ_p, the value of z_{oAp} for any other system employing the same adsorbent can be determined from tables of gas phase hard sphere diameters of the adsorbate.

By a lattice summation technique, Crowell and Steele[33] and Crowell and Chang[34] have estimated the equilibrium distance of Ar from the graphite and BN surfaces to be 0.340 nm and 0.338 nm respectively. For a Lennard-Jones (9,3) potential, one has

$$z_o = z^*/3^{1/6} \tag{75}$$

Therefore, by using the value of σ_{Ar}[35] given in Table 2, the values of σ_{P33} and σ_{BN} can be calculated. This then permits z_o for any gas P-33 or gas-BN system to be calculated. Values of z_o for the system investigated in this work and calculated in the above manner are given in Table 2.

Table 2. Values of z_o, Gas Phase σ and ε_{12}^*/k for Various Gas-Boron Nitride and Gas-P33 (2700°) Systems[a]

	z_o (nm)	σ (nm)	ε_{12}^*/k (°K)
P33 Systems			
Ar	0.2831	0.341	119
N_2	0.2975	0.3698	95.05
CO_2	0.3369	0.4486	189
C_6H_6	0.4586	0.692	308
P33	--	0.2252	--
BN Systems			
Ar	0.283	0.341	119
Kr	0.296	0.3679	166.7
Xe	0.317	0.4100	221
BN	--	0.224	--

[a]Reference 35.

CHAPTER V

ADSORPTION OF N_2 AND CO_2 ON P33(2700°)

B_{2s}, B_{3s} and B_{2D} Parameters

The values of B_{2s} and C_{3s}, where applicable, were computed for N_2 and CO_2 adsorption on P-33 (2700°) from the adsorption data given in Appendix E. The values of B_{3s} were then computed in equation (11b) where C_{3s} data was available.

The two-dimensional second virial coefficient, B_{2D}, was then computed via equation (40). The value of the surface area, A, used was 8.96 m^2/g; the value determined by Sams, Contabaris and Halsey[8] from B_{2D} data for Ar adsorption on this sample. The values of B_{2s}, B_{3s} and B_{2D} are given in Tables 3 and 4. The absence of B_{3s} and B_{2D} data at some temperatures indicates that the values of C_{3s} were too small to be computed with any accuracy. In these cases experimental error would have dominated C_{3s}. Also note that in Tables 3 and 4 the highest temperature B_{2s} value for both N_2 and CO_2 adsorption is designated not to be used in subsequent analysis. This is due to high relative error which the uncertainty in sample cell volume might contribute to B_{2s} at these temperatures. See the sample cell section of Chapter III for a more detailed explanation.

Table 3. Values of B_{2s}, B_{3s} and B_{2D} for the N_2-P33 (2700°) System

T (°K)	B_{2s} (cm^3/g)	B_{3s} (cm^6/g-mole)	$B_{2D} \times 10^{-7}$ [a] (cm^2/mole)
156.155	0.87907[b]	-3889.6	22.55
177.096	0.39989[b]	-1012.2	28.36
197.434	0.22312[b]	- 400.5	36.04
214.015	0.15058[b]	- 190.7	37.68
234.200	0.10059[b]	- 11.8[e]	31.79[e]
273.150	0.05477[c]	--	--
296.424	0.04105[c]	--	--
311.466	0.03506[c]	--	--
329.299	0.02916[c]	--	--
347.355	0.02391[c,d]	--	--

[a]Based on A = 8.96 m^2/g from Reference 8.

[b]Isotherm fit to $N_a = a_0+a_1P+a_2P^2$ with (0,0) weighted by a factor of ten.

[c]Isotherm fit to $N_a = a_0+a_1P$ with (0,0) weighted by a factor of ten.

[d]Not used in ε^*_{1s}/k, Az_o analysis due to uncertainty in V_{13} at this temperature.

[e]Not used in ε^*_{12}/k, σ_{12} fit due to large relative uncertainty in B_{3s} at this temperature.

Table 4. Values of B_{2s}, B_{3s} and B_{2D}[a] for the CO_2-P33 (2700°) System

T (°K)	B_{2s} (cm^3/g)	B_{3s} (cm^6/g-mole)	$B_{2D} x10^{-7}$ (cm^2/mole)
227.322	0.85534	15,593	-95.48
250.072	0.45890	2712	-57.70
273.150	0.27166	659.1	-40.01
300.910	0.16595	119.8	-19.48
317.392	0.12816	--	--
342.041	0.09077[b]	- 20.1[c]	+ 8.21[c]

[a]Based on A = 8.96 m^2/g from Reference 8.

[b]Not used in ε^*_{1s}/k, Az_o fit due to uncertainty in V_{13} at this temperature.

[c]Not used in ε^*_{12}/k, σ_{12} fit due to large relative uncertainty in B_{3s} at this temperature.

Virial Analysis by Spherical Potential Models

The B_{2s} and B_{2D} data given in Tables 3 and 4 were then fit using the (9,3) and (12,6) spherical potential models respectively in equations (29) and (44). Values of ε^*_{1s}/k and Az_o were optimized by minimization of the standard deviaition in $\ln Az_o$, $\sigma \ln Az_o$. Likewise, the fit in equation (44) to obtain ε^*_{12}/k and σ_{12} was adjusted to give a minimum in the standard deviation of σ_{12}.

The results of this analysis of N_2-P33 and CO_2-P33 adsorption is given in Table 5 along with the Ar-P33 results of Sams, Constabaris and Halsey[6-8] and the benzene-P33 data assembled by Pierotti.[9] Note that the value of ε^*_{1s}/k obtained using the (9,3) model on the CO_2-P33 (2800°C) data of Myers and Prausnitz[36] is essentially the same as for this work. However, the values of Az_o are different. This may be simply due to different adsorbent surface areas. No B_{2D} analysis was carried out on this data since the scatter in the available data was too great to give meaningful values of C_{3s} and no isotherms below the ice point were obtained.

Also note that two sets of results are given for benzene adsorption. The data in parenthesis is that of Pierotti[9] on B_{2s} data assembled from several sources. The other set is from an analysis of the data of Smallwood[37] by the author. These data are included in the Pierotti analysis. However, Pierotti obtained slightly different values of B_{2s} from Smallwood's data. All B_{2s} values are included in

Table 5. Surface Parameters for Various Gas-P33 (2700°) Systems Using the Spherical (9,3) Potential Model for the B_{2s} Analysis and a (12,6) Potential for the B_{2D} Analysis

Adsorbate	Ar[a]	N_2[b]	CO_2		C_6H_6	
			b	c	d	e
B_{2s} Analysis						
ε^*_{1s}/k (°K)	1107	1143	1702	1701	5060	5390
$Az_o x10^3$ (cm^3/g)	2.393	2.344	1.955	1.743	0.143	0.052
$\sigma \ln Az_o$	0.0030	0.0032	0.0070	0.0116	0.068	0.087
z_o (nm)	0.2831	0.2975	0.3369		0.4586	
A (m^2/g)	8.45	7.88	5.80	5.17	0.31	0.11
BET Area (m^2/g)	--	11.84	--		--	
B_{2D} Analysis						
ε^*_{12}/k (°K)	96	75	215	--	--	
A (m^2/g)	8.96	8.96	8.96	--	--	
σ_{12} (nm)	0.340	0.305	0.406	--	--	
$\sigma(\sigma_{12})$	--	0.05	0.12	--	--	
2D Boyle Temp. (°K)	153.6	117	335	--	--	

[a]Data from Reference 8.

[b]This work.

[c](9,3) analysis of B_{2s} data from Reference 36.

[d]Analysis of B_{2s} data, Column 3, Table 6.

[e]Analysis of B_{2s} data, Column 2, Table 6.

Table 6.

Smallwood's data are separated out from the first analysis for separate treatment since it is the most complete benzene data available and since the use of data from one source eliminates the problem of differing adsorbent surface areas which may exist from sample to sample.

An important point to note from both analyses is that $\sigma \ln Az_o$ is extremely large as compared with Ar, N_2 and CO_2 results. There are two possible explanations for this. The first is that there is considerable uncertainty in B_{2s} values obtained from the adsorption data. Unfortunately, the very low coverage points necessary are not available so that extrapolations must be done from data containing curvature. The possible error varies from 5% in the high temperature values to 10% and greater for the low temperature B_{2s} data. The second possibility for the large $\sigma \ln Az_o$ is that the (9,3) spherical model is simply not applicable since benzene in no way approximates spherical behavior.

Reference to the values of A extracted from Az_o by dividing by z_o for each of the adsorbates point out the effect of hindered rotation. The Ar-P33 data gives a value of 8.45 m^2/g. Then as the molecules become increasingly non-spherical the value of A decreases with increasing rapidity. If A is too small, then so is Az_o. In a thermodynamic sense, a decrease in the capacity factor, Az_o, corresponds to a loss of entropy. This entropy loss comes

Table 6. B_{2s} Values for the Adsorption of Benzene on Graphitized Carbon P33

Temperature (°K)	$B_{2s} x10^{-2}$ cm^3/g Ref. 9	Analysis of Ref. 37
250	149	
273.16	27.72	22.97
273.2	18.35	
288.16	10.10	9.92
293.	8	
298.16	4.88	4.89
303.16	3.54	3.63
308.2	3.07	
322.6	1.54	
323.16	1.52	1.52

from the restriction of the rotation of the molecule by the surface plane. Further discussion of the entropy loss due to hindered rotation is discussed with the thermodynamic analysis of the B_{2s} and B_{3s} data.

Table 5 also contains the results of the two-dimensional analysis via equation (44). The best fit values for the hard sphere diameter, σ_{12}, of N_2 and CO_2 are smaller than the corresponding literature values listed in Table 2. As with Az_o, this is also a possible indication of hindered rotation. The value of ε^*_{12}/k for N_2 is somewhat lower than the literature value based on gas phase analysis as in the case of the Ar-P33 system.[8] The reduction is due to the perturbing effect of the solid.[21] On the other hand, ε^*_{12}/k for CO_2-P33 is slightly larger than the gas phase value. An explanation for this is given in the discussion of the thermodynamic data.

Thermodynamic Treatment of Virial Data

Table 7 contains the thermodynamic data for the N_2-P33 and CO_2-P33 systems based on analysis of virial coefficients by equations (51) through (61). The contention of a rotational contribution to entropy loss on adsorption can be supported by evaluation of the $-\overline{\Delta S}^o_{ads}/R$ at the ice point. But, first a more detailed analysis of the various components of $\overline{\Delta S}^o_{ads}$ is in order.

For the adsorption process

Table 7. Thermodynamic Properties of the N_2-P33 (2700°) and CO_2-P33 (2700°) Systems

T (°K)	$(q^o_{st}/R)x10^{-3}$ (°K)	$((dq_{st}/dN_a)/R)x10^{-6}$ (°K)	$-(\overline{\Delta H}^o_{ads}/R)x10^{-3}$ (°K)	$-\overline{\Delta S}^o_{ads}/R$ [b]
N_2-P33				
156.155	1.274	2.14(2.17) [c]	1.027	3.14
177.096	1.196	2.14(2.06) [c]	1.019	3.11
197.434	1.211	2.14(2.00) [c]	1.012	3.06
214.015	1.221	2.14(1.92) [c]	1.008	3.03
234.200	1.237	a	1.003	3.01
273.150	1.269	a	0.996	2.98
296.424	1.289	a	0.992	2.97
311.466	1.302	a	0.990	2.96
329.299	1.318	a	0.988	2.97
	$\overline{\Delta H}^o_{ads}/R(0°K) = -1.056°Kx10^3$		$\Delta C_p/R = 0.213$	
CO_2-P33				
227.322	1.856	21.9(15.5) [c]	1.588	3.57
250.072	1.795	17.4(14.6) [c]	1.545	3.39
273.150	1.781	13.6(13.9) [c]	1.507	3.25
300.910	1.771	9.9(13.2) [c]	1.470	3.11
317.392	1.768	a	1.451	3.05
	$\overline{\Delta H}^o_{ads}/R(0°K) = -1.927°Kx10^3$		$\Delta C_p/R = 1.514$	

[a] B_{3s} data either not available or not precise enough for determination.

[b] Adsorption from gas phase at unit fugacity to adsorbed phase at 0.338 dynes/cm spreading pressure, A = 8.41 m^2/g.

[c] Computed using Eq. (81b) and ε^*_{12}/k and σ_{12} from Table 5 in Reference 39 tables.

$$\overline{\Delta S}^{o}_{ads} = \overline{\Delta S}^{o}_{tr} + S^{vib} + \overline{\Delta S}_{rot} \ . \tag{76}$$

For mobile adsorption,[38]

$$\overline{\Delta S}_{tr} = \frac{R}{2} \ln M + \frac{R}{2} \ln T + 2.30 \tag{77}$$

and

$$S_{vib} = \frac{R(\frac{h\nu}{kT})}{(e^{h\nu/kT}-1)} - R \ln (1-e^{-h\nu/kT}) \tag{78}$$

where ν is the vibrational frequency of the adsorbate normal to the surface and M is the molecular weight of the adsorbate.

Here $\overline{\Delta S}_{tr}$ is the entropy change due to the loss of one degree of transtational entropy, S^{vib} is the vibrational entropy of the adsorbed molecule perpendicular to the surface and $\overline{\Delta S}_{rot}$ is the rotational entropy loss on adsorption. If $\overline{\Delta S}_{tr}$ and S^{vib} can be calculated and $\overline{\Delta S}^{o}_{ads}$ measured experimentally, $\overline{\Delta S}_{rot}$ can be back calculated. The problem is to get a reliable value for ν. Myers and Prausnitz[36] adopted a method for determining ν as follows.

The experimental values of $\overline{\Delta S}^{o}_{ads}$ for the rare gases adsorbed on P33 were determined as previously described. Since $\overline{\Delta S}_{rot}$ must be zero for the rare gases, S^{vib} could be calculated by subtracting $\overline{\Delta S}_{tr}$ from $\overline{\Delta S}^{o}_{ads}$. From equation (78), ν for each system was calculated and finally the force

constant k_z determined from the harmonic oscillator model,

$$k_z = 4\pi^2 \nu^2 m \tag{79}$$

where m is the mass of one molecule.

A plot of k_z versus $\sqrt{T_c}$, where T_c is the critical temperature of the adsorbate, was made. This plot proved to be linear. The force constants for all other substances adsorbed on P33 could then be taken off this graph if T_c was known and S^{vib} calculated via equation (78). This allowed $\overline{\Delta S}_{rot}$ to be calculated as previously described.

To evaluate the ice point data for N_2-P33 and CO_2-P33 by this method, the values reported in Table 7 must be first put on a 12 m^2/g basis since this is the basis for the plot of k_z vs. $\sqrt{T_c}$ from reference 36. The results of the analysis are shown in Table 8 along with the rare gas data used to determine the k_z vs. $\sqrt{T_c}$ graph. A rotational entropy loss is indeed found with the trend being in the proper direction for the relative degrees of hindered rotation expected. Note that the value of $\overline{\Delta S}_{rot}$ for CO_2 is larger for the Myers and Prausnitz[36] data. This is a result of the larger value of B_{2s} at the ice point obtained in this work and possibly the differences in the sample surface areas. See equation (61).

The isosteric heats and enthalpies of adsorption at zero coverage given in Table 7 are also consistent with

Table 8. Decrease in Rotational Entropy for the Adsorption of Various Substrates on P33

Adsorbate	T (°K)	$-\overline{\Delta S}^{o}_{ads}/R$ (°K)	$-\overline{\Delta S}^{o}_{tr}/R$ (°K)	S^{vib}/R (°K)	$-\overline{\Delta S}^{o}_{rot}/R$ (°K)	k_z Dynes/cm
N_2	273.150	3.28	5.63	2.45	0.10	3295
CO_2	273.150	3.45(3.71)[a]	5.84	2.46	0.16(0.33)[a]	5060
C_6H_6[a]	293.15	7.38	6.17	2.66	3.88	6870
Ne[a]	78.61	3.42	4.83	1.41	0	1620
Ar[a]	158.08	3.48	5.52	2.04	0	3600
Kr[a]	279.47	3.28	6.18	2.89	0	4210
Xe[a]	295.05	3.34	6.43	3.09	0	4950

[a]Reference 36.

ε^*_{1s}/k. The fact that they are slightly temperature dependent indicates that ΔC_p is non-zero, where

$$\overline{\Delta H}^o_{ads} = \overline{\Delta H}^o_{ads}(0°K) + \int_0^T \Delta C_P dT \ . \tag{80}$$

The change in q_{st} as a function of coverage as indicated by dq_{st}/dN_a is temperature dependent for CO_2-P33 but not for N_2-P33. By equation (52),

$$dq_{st}/dN_a = -RT^2 \left[\frac{d(B_{2s} + B_{2s}B_2)/B_{2s}^2}{dT} \right] \tag{81a}$$

which can be approximated as

$$-dq_{st}/dN_a \simeq \frac{2R}{A} dB_{2D}/d(\tfrac{1}{T}) \ . \tag{81b}$$

The object then is to determine the temperature dependence of $dB_{2D}/d(1/T)$. This is done using the tables of Morrison and Ross[39] for $T^*(dB^*_{2D}/dT^*)$ using the best fit values of ε^*_{12}/k and σ_{12} given in Table 5. The results are listed in Table 7.

The calculated and experimental values for N_2 given in Table 7 compare favorably. This might be expected since N_2 is nearly spherical. However, the experimental CO_2 values are greater at the highest temperature and drop to a

value somewhat lower than that calculated. This may possibly be explained by hindered rotation.

Consider that at the lower temperature CO_2 is more likely to be flat on the surface. If one then views the CO_2 molecule in the Kihara or Corner sense as interacting along the length of the core, then the CO_2-CO_2 interactions should be stronger at the lower temperature where the cores are more likely to be in the same plane and the trends observed should in fact occur. At the higher temperatures, one would expect to approach a case similar to that observed for Ar and N_2 adsorption. That is, a depression of ε^*_{12}/k below the gas phase value due to the perturbation of the surface. If a value of approximately 170°K is assumed for ε^*_{12}/k, dq_{st}/dN_a is equal to 18.5×10^6 cal/(mole/g) at 300.91°K. This compares favorably with the experimental result. No doubt the higher relative errors in the higher temperature B_{2D} data represent a higher probability of deviation due to experimental error.

Non-Spherical Potential Model for CO_2 and N_2 Adsorption on P33

In order to evaluate the B_{2s} data in terms of the non-spherical model proposed in Chapter II, the parameters A' and B' defined by equations (34b) and (37b) respectively, must be determined.

A' is easily defined in terms of polarizabilities

listed in the literature.[40] These are listed in Table 9.

To arrive at B', the Kihara parameter[41,42] for CO_2 and N_2 are employed. The Kihara model allows for the asymmetry of the molecule in determining the distance of closest approach, but does not allow for a change in the potential function as one goes around the molecular core. Attempts to apply the Kihara model to surface adsorption were made by Bullock[42] without much success. However, for a lack of better data, it was decided to use the Kihara core parameters to determine B'.

The core parameters for the linear molecule are ρ_m and ℓ. A diagram of the Kihara model for the linear molecule is shown in Figure 15. ρ_m is the equilibrium distance of two cores from each other as one goes around the molecule. ℓ is the length of the core. Since the non-spherical model proposed here is based on the hard sphere and not equilibrium distances, ρ_m must be converted to an equivalent hard sphere value, ρ_o. For the (12,6) potential $\rho_o = \rho_m/2^{1/6}$ and for the (9,3) potential $\rho_o = \rho_m/3^{1/6}$. Both cases are considered here. In either instance the parallel value of z_o, $z_{o\parallel}$, is given by

$$z_{o\parallel} = \frac{1}{2}(\rho_o + \sigma_p) \tag{82}$$

and the perpendicular distance by

Table 9. Principal Polarizabilities[40] of Nitrogen, Carbon Dioxide and Benzene

Gas	$\alpha_{av} x10^{24}$ cm^3	$\alpha_1 x10^{24}$ cm^3	$\alpha_2 x10^{24}$ cm^3	$\alpha_3 x10^{24}$ cm^3
N_2[a,c]	1.76	2.38	1.45	1.45
CO_2[a,c]	2.65	4.01	1.97	1.97
C_6H_6[b,c]	10.32	6.35	12.31	12.31

[a] α_1 symmetry axis

[b] $\alpha_1 \perp$ to plane of ring

[c] For N_2 and CO_2, $\alpha_\perp$ is taken as α_1 and $\alpha_{||}$ as α_2 for the calculation of A'. For benzene, the designations are reversed. The use of the principal polarizabilities for $\alpha_{||}$ and $\alpha_\perp$ is not exact, but is within the limitations of the model.

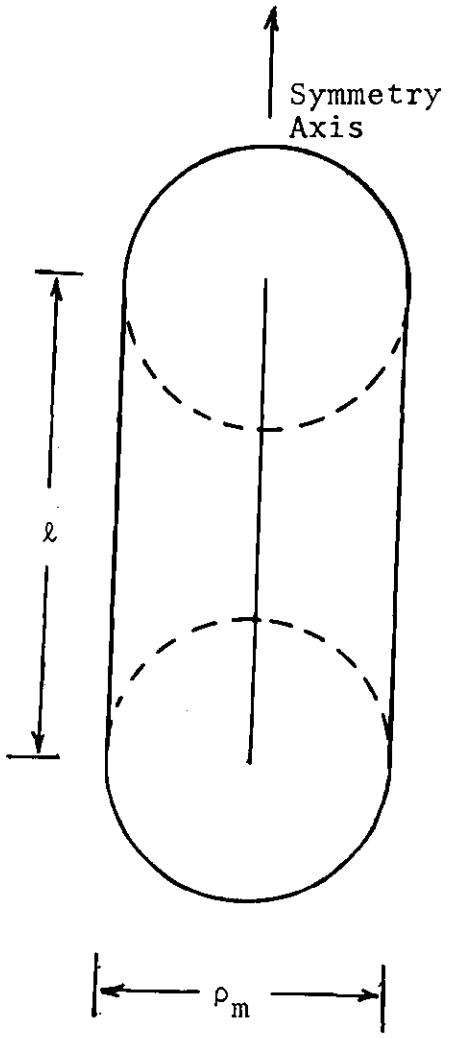

Figure 15. Kihara Model for a Linear Molecule (ℓ corresponds to the N-N distance in N_2 and the 0-0 distance in CO_2)

$$z_{o\perp} = \frac{1}{2}\,(\rho_o + \sigma_p + \ell)\ . \tag{83}$$

Diagrams of the two configurations are given in Figure 3. The Kihara parameters for N_2 and CO_2 are given in Table 10 along with $z_{o\parallel}$, $z_{o\perp}$ and A' for both the (12,6) and (9,3) potentials.

The results of the B_{2s} analysis by the above method is given in Table 11. Keeping in mind that a value of 8.45 m^2/g was obtained for the surface area from Ar-P33 data[5-8] using the Crowell model[33] for z_o, it is clear that the (9,3) model for ρ_o gives the better agreement: 8.41 m^2/g for N_2-P33 and 8.51 m^2/g for CO_2-P33. Both potential models give improvement over the spherical analysis results of Table 5, 7.88 m^2/g for N_2-P33 and 5.80 m^2/g for CO_2-P33. Also listed in Table 11 are the values of $\varepsilon^*_{1s\perp}/k$ which are calculated by setting θ equal to zero and taking the appropriate derivatives. It is interesting to note that $\varepsilon^*_{1s\parallel}/k$ and $\varepsilon^*_{1s\perp}/k$ are not very different for N_2-P33 reflecting the nearly spherical behavior of the N_2 molecules. On the other hand, the value of ε^*_{1s}/k differs markedly for CO_2-P33 in the two opposite configurations. The actual minimum in the θ dependent potential function is of course a function of temperature.

Plots of the potential function averaged over θ by the Boltzman factor are shown in Figures 16 and 17. Two points

Table 10. Parallel and Perpendicular Distances of N_2 and CO_2 Centers from the P33 (2700°) Surface at Zero Potential

Molecule	N_2	CO_2
Spherical System		
σ (nm)	0.3698[a]	0.4486[a]
z_o (nm)	0.2975	0.3369
Non-Spherical System		
-Kihara Parameters[41,42]		
ρ_m (nm)	0.347	0.336
ℓ (nm)	0.1094	0.230
ρ_o (nm)	0.3091[c], 0.2889[e]	0.2993[c], 0.2798[e]
$z_{o\parallel}$ (nm)[b]	0.2672[c], 0.2571[e]	0.2623[c], 0.2525[e]
$z_{o\perp}$ (nm)[d]	0.3219[c], 0.3118[e]	0.3773[c], 0.3675[e]
B'	0.2048[c], 0.2128[e]	0.4384[c], 0.4555[e]

[a]Reference 35.

[b]Calculated by equation (82).

[c]$\rho_o = \rho_m/2^{1/6}$, (12,6) potential.

[d]Calculated by equation (83).

[e]$\rho_o = \rho_m/3^{1/6}$, (9,3) potential.

Table 11. B_{2s} Surface Parameters for the N_2-P33 (2700°) and CO_2-P33 (2700°) Systems Using the Non-Spherical (9,3) Potential Model (Angle Averaging at 0.25° Increments)

	N_2	CO_2
$z_{o\parallel}$ (nm)	0.2672[a], 0.2571[b]	0.2623[a], 0.2525[b]
B'	0.2048 , 0.2128	0.4384 , 0.4555
A'	0.6414 , 0.6414	1.0355 , 1.0355
$\varepsilon^*_{1s\parallel}/k$ (°K)	1191 , 1201	1844 , 1841
$Az_{o\parallel} \times 10^3$ (cm^3/g)	2.156 , 2.154	2.078 , 2.149
$\sigma(\ln Az_{o\parallel})$	0.0033 , 0.0034	0.0046 , 0.0045
A (m^2/g)	8.07 , 8.41	7.92 , 8.51
$\varepsilon^*_{1s\perp}/k$ (°K)	1118 , 1105	1261 , 1215

[a]Calculated using $\rho_o = \rho_m/2^{1/6}$, (12,6 potential).

[b]Calculated using $\rho_o = \rho_m/3^{1/6}$, (9,3 potential).

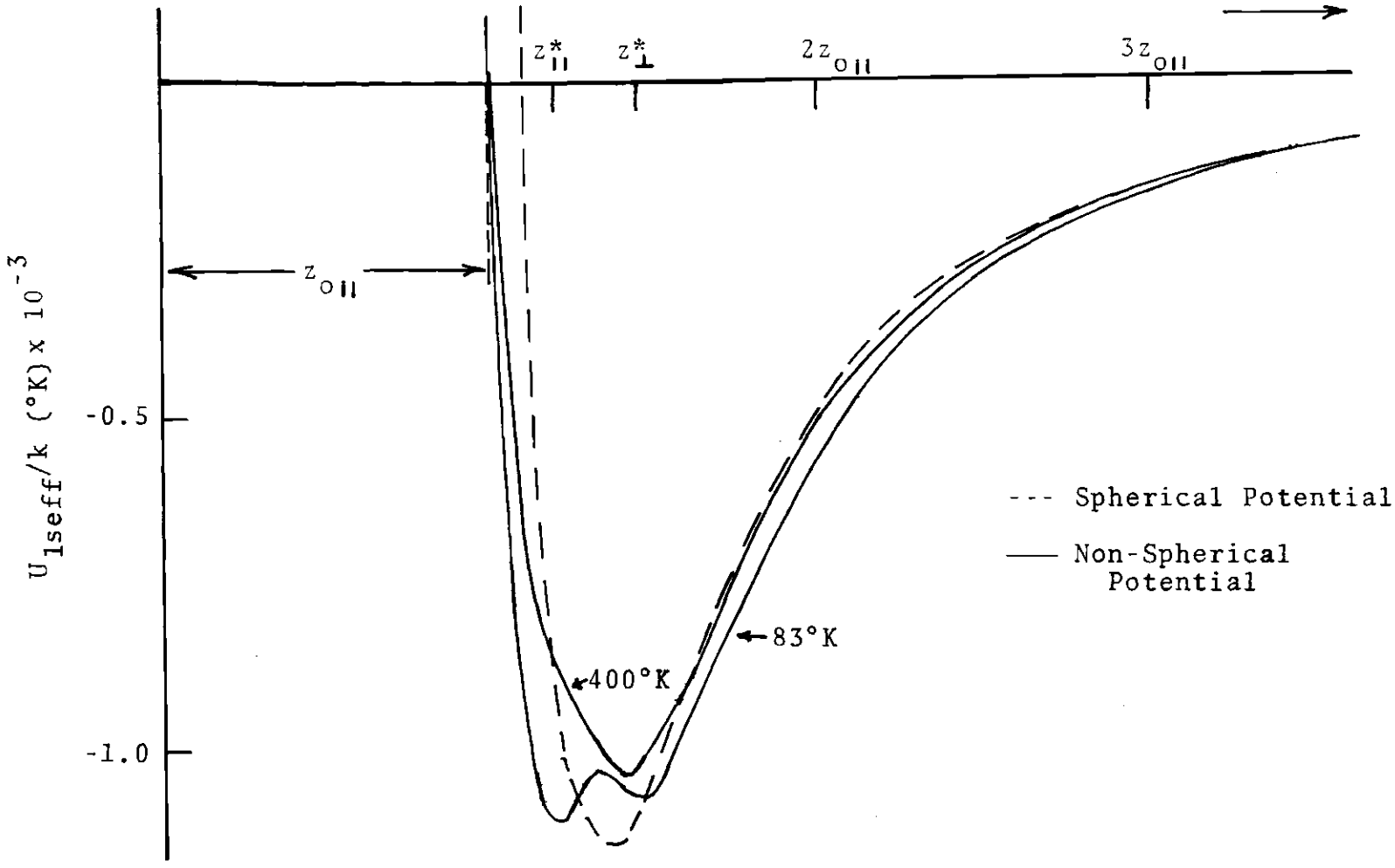

Figure 16. Angle Averaged Non-Spherical Potential Function at Various Temperatures: N_2-P33

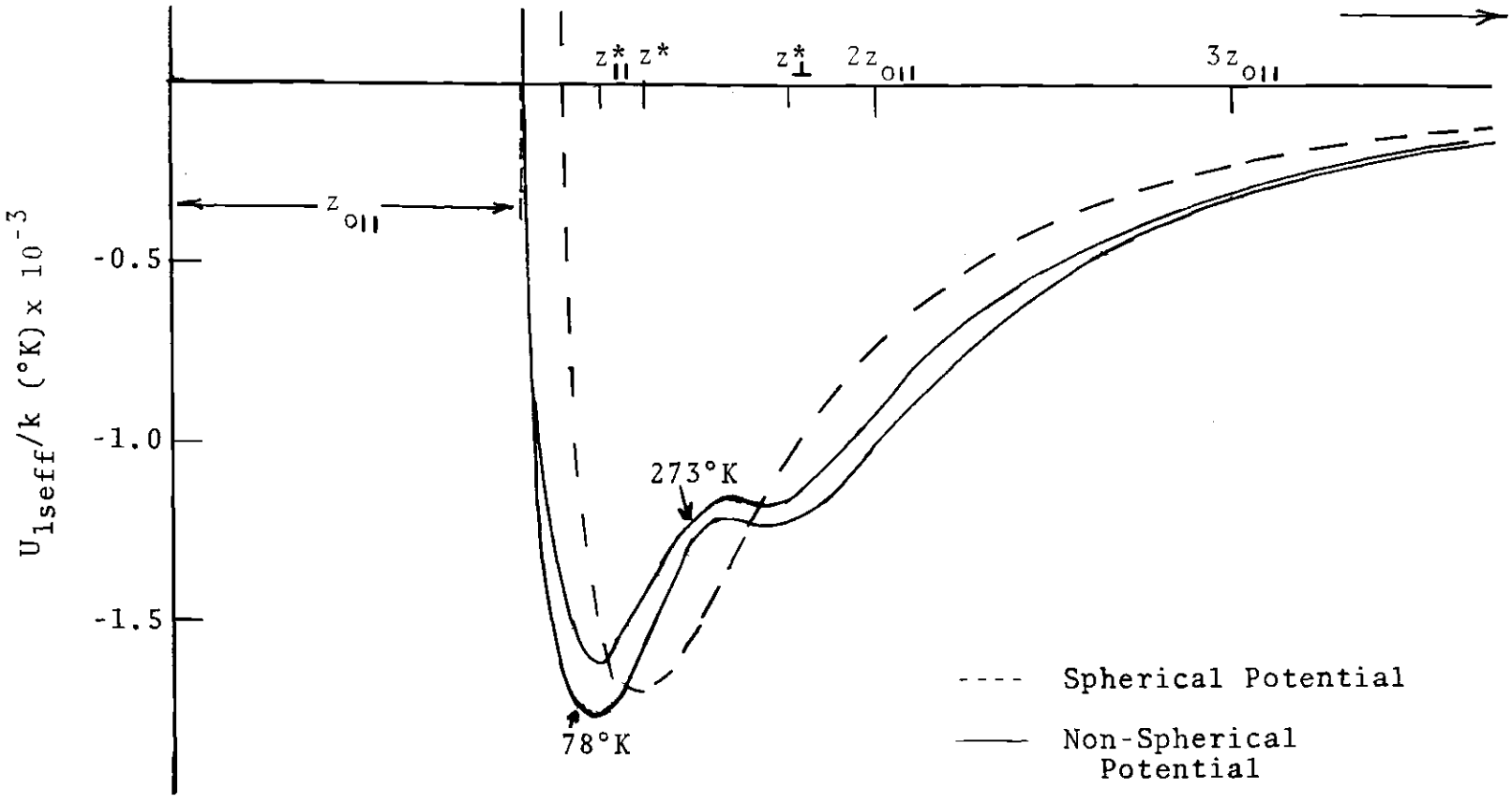

Figure 17. Angle Averaged Non-Spherical Potential Function at Various Temperatures: CO_3-P33

are evident from their examination. The first is the occurrence of the double potential minima which are accentuated at the lower temperatures. The minima are at the approximate positions of the equilibrium positions for the parallel and perpendicular conformations, but are not equal in value to $\varepsilon^*_{1s\parallel}/k$ and $\varepsilon^*_{1s\perp}/k$ since all values of θ are weighted. The second observation is that the spherical and non-spherical potential functions overlap for the most part and that a larger spherical potential at some center separations is compensated for by smaller potentials at other separations. It is for this reason that both functions as indicated by $\sigma \ln Az_o$ and $\sigma \ln Az_{o\parallel}$ appear to give reasonable degrees of fit. The goodness of fit for N_2 is essentially the same, but is measurably better in the non-spherical case for CO_2. The goodness of fit in the latter case for the spherical potential is, however, not poor.

Non-Spherical Potential Model for Benzene Adsorption on P33

The potential model for benzene is given by equation (38a). The value of A' is determined as before from polarizabilities given in Table 9. The value of $z_{o\parallel}$ is determined from the equilibrium separation of benzene molecules in the crystal lattice, 0.344 nm, and the previously determined value of σ for P33 given in Table 2. The value of σ for benzene in the flat position is then found by dividing by

$3^{1/6}$. The increase in the distance of the benzene center from the surface when the molecule is on end with ψ equal to 0° is 0.187 nm. The values of A' amd B' determined from the above are given in Table 12.

As previously discussed ψ varies from 0° to 30° and therefore $z_{o\perp}$ does not change greatly as the molecule rotates about the perpendicular to the center of benzene plane. Minimal error is introduced by integrating over ψ before conducting the potential angle averaging over θ required by equation (39). This greatly reduces the number of computer operations required. A plot of the angle averaged potential function analogous to those for N_2 and CO_2 is given in Figure 18.

The results of the analysis of B_{2s} data are given in Table 12. The value of $\sigma \ln Az_{o\parallel}$ is not appreciably improved over the spherical treatment reported in Table 5. In fact there is a broad range for $\varepsilon^*_{1s\parallel}/k$ over which $\sigma \ln Az_{o\parallel}$ does not change appreciably. Considering the large value of $\sigma \ln Az_{o\parallel}$, this is to be expected. The optimized value of A attained from the above treatment is a factor of four higher than the spherical value but still falls short of the 8.45 m^2/g from the Ar-P33 treatment. A value of 11.7 m^2/g is reported by Pierotti[9] using the harmonic approximation in combination with the potential function of Kiselev.[44] In the harmonic approximation the force constant $k_z\{\theta\}$ is allowed to change as the orientation of the benzene molecular plane

Table 12. Analysis of B_{2s} Data for the Adsorption of Benzene on P33 Using the (9,3) Non-Spherical Potential Model (Angle Averaging at 0.1° Increment)

$z_{o\parallel}$ (nm)	0.256
$z_{o\perp}$ (nm) (ψ = 90°)	0.443
A'	0.9386
B'	0.730
$\varepsilon^*_{1s\parallel}/k$ (°K)	5090±110 (5510)[a]
$Az_{o\parallel} \times 10^3$ (cm^3/g)	$0.35\pm^{0.15}_{0.17}$
$\sigma(\ln Az_o)$	0.068-0.072
A (m^2/g)	$1.4\pm^{0.6}_{0.7}$ (11.7)[a]
$\sigma \ln A$	-- (0.077)[a]
$\varepsilon^*_{1s\perp}/k$ (°K)	2009

[a]Reference 9 (harmonic potential model).

[b]Range of values for ±110°K range in ε^*_{1s}/k.

[c]The result of the integration using the method of reference 9 is B_{2s}/A. Therefore, the standard deviation of the fit to the data for reference 9 is reported in terms of $\sigma \ln A$ instead of $\sigma \ln Az_o$.

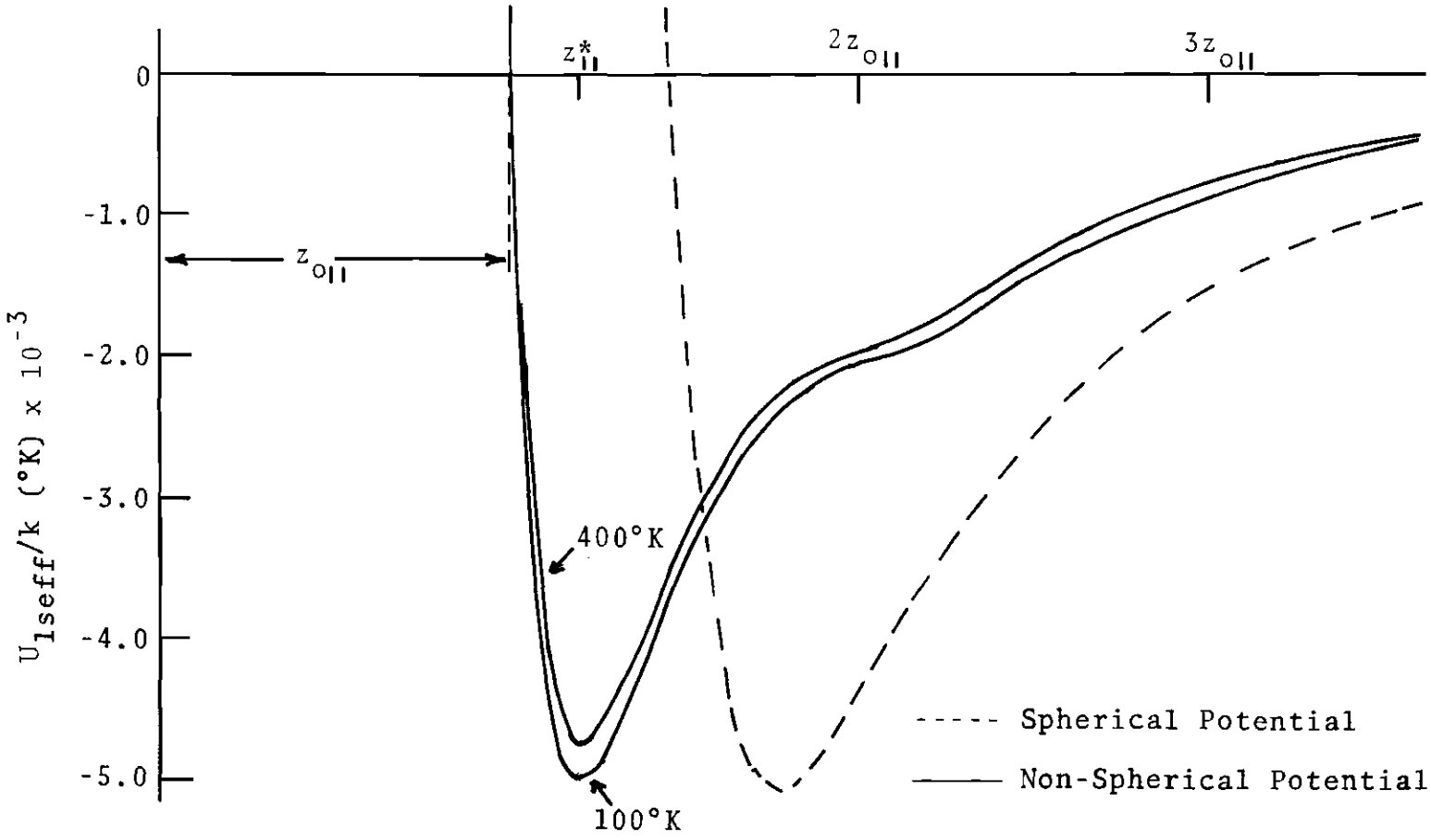

Figure 18. Angle Averaged Non-Spherical Potential Function at Various Temperatures: Benzene-P33

with the surface changes. The Kiselev lattice summation is described in the next section.

One would expect the B_{2s} values calculated from a harmonic potential to be more temperature dependent than those calculated from a (9,3) potential. Since the data requires this, the harmonic potential does appear to give a better result than the (9,3) non-spherical potential, although somewhat overestimating A based on the B_{2s} analysis value.

The one disturbing point is the large $\sigma \ln Az_{o\parallel}$ and $\sigma \ln A$ shown in Table 12 for the two non-spherical treatments. As previously discussed, there is a high degree of uncertainty in the B_{2s} values obtained from the benzene adsorption data. For this reason, it is necessary to obtain more accurate B_{2s} data before a more conclusive judgement of the nature of benzene adsorption on P33 can be made.

Lattice Summation Technique of Kiselev for Non-Spherical Molecules

A lattice summation technique for determining the potential function for the adsorption of spherical and non-spherical molecules has been developed by Kiselev and Poskhus[44-46] and applied to rare gas, N_2, H_2 and benzene adsorption on graphite. However, before the results are discussed, a comparison of this method with that of Crowell[33] as applied to Ar-P33 is in order. The reason is that the

results of this paper are tied to the work of Crowell through the values of $z_{o\parallel}$ and $z_{o\perp}$ which use the value of σ_{P33} derived from Crowell's Ar-P33 lattice summation.

Both methods conduct summation with the aid of the generalized Riemann zeta function. The base function for Crowell is the Lennard-Jones (12,6) potential for the interaction of two molecular centers.

The form of the Kiselev potential[44] used in the lattice summation is

$$\phi_{ij} = -C_1 r_{ij}^{-6} - C_2 r_{ij}^{-8} + B_{ij} \exp(-r_{ij}/\rho_{ij})$$

for the pair interaction and

$$\phi_i = \sum_j \phi_{ij}$$

for the summation. The constants C_1 and C_2 are calculated from the Kirkwood-Mueller formulas using the mean values of the polarizabilities and magnetic susceptibilities of the adsorbate and effective values for the graphite lattice. The screening constant, ρ_{ij}, is taken as 0.28 and B_{ij} is defined by the restraint

$$\left(\frac{\partial \phi_i}{\partial z_i}\right)_{z_i = z^*} = 0 \ .$$

In both methods, the proper choice of z* is most important in determining the nature of the potential function.

The value of z* from Poskhus[44] for Ar adsorption on graphite is 0.361 nm computed as the sum of the van der Waals radius of Ar and one-half the interplanar spacing in graphite. The value of z* from Crowell[31] is 0.340 nm; a value somewhat less than that of Poskhus. The Crowell result is appropriate since the adsorbate is interacting with all sites in the adsorbent which effectively increases the attractive long range term and has little effect on the repulsive term as it is short range. This effectively decreases the equilibrium separation relative to the adsorbate interacting with only one surface site.

The effect of the above on the Ar-P33 ε^*_{1s}/k should be to give a larger value from Crowell's treatment. Table 13 shows this to be the case. The values of C_{ij} from Poskhus is also slightly larger than from Crowell which would further separate the two results.

For a non-spherical molecule, z_i is at the center of mass. The molecule is, however, sub-divided into groups such as N for N_2 and CH for benzene. The distances of the individual groups from the surface for a given z_i and orientation are calculated and the summation conducted with the aid of the generalized Riemann zeta function. See references 44 and 47 for details.

Table 13. Comparison of $\varepsilon^*_{1s\parallel}/k$, z* and V_o/k for N_2-P33 and Benzene-P33 Systems by Equation (38) and Lattice Summation

Adsorbate	Z*(nm)		$\varepsilon^*_{1s\parallel}/k$(°K)		V_o/k (°K)	
	Eq. (38)	Ref. 44	Eq. (38)	Ref. 44	Eq. (38)	Ref. 44
N_2	0.309 0.321	0.345	1201 1191	1087	96	247
C_6H_6	0.307	0.355(0.343)[a]	5090	4952(5510)[a]	3081	2466(3120)[a]
Ar[b]	0.340	0.361	1107	1082	--	--

[a]Reference 9.

[b]Equation (38) with A' = B' = 0, n = 9 and m = 3 gives the spherical (9,3) potential function.

Several differences other than the form of the repulsive term exist between this potential function and that given by equation (38). They are:

1. No dependence of adsorbate polarizability on adsorbate orientation with respect to the surface in the Kiselev case,
2. Interaction of sub-groups rather than the center of mass with the adsorbent, and
3. Choice of z*.

If one compares the value of $\varepsilon^*_{1s\parallel}/k$ obtained for N_2 and benzene adsorption by both methods, one would expect condition #1 above to give a larger $\varepsilon^*_{1s\parallel}/k$ for the Kiselev form; condition #3 to give a reduced value as previously discussed; and condition #2 to effect the barrier to rotation perpendicular to the surface at a given z_i.

Comparison of N_2-P33 and benzene-P33 systems as analyzed by both methods are given in Table 13. Also listed is the result of Pierotti[9] for benzene adsorption. Pierotti used the general form of the Kiselev potential[47] obtained from a direct lattice summation, but adjusted $\varepsilon^*_{1s\parallel}$ and $z^*_{\parallel}$ to give the best fit to experimental data; discussed in the previous section. The result is a higher value than obtained from the theoretical lattice summation. This supports the observation that the experimental $\varepsilon^*_{1s\parallel}/k$ for N_2-P33 by equation (38) is higher than predicted by the lattice summation.

The last column of Table 13 contains V_o/k, the difference between $\varepsilon^*_{1s\parallel}/k$ and $\varepsilon^*_{1s\perp}/k$, for the adsorption of N_2 and benzene on P33. The smaller V_o for N_2-P33 from this work reflects the increased N_2 polarizability in the perpendicular orientation which is not taken into account by the Kiselev potential. The benzene V_o is smaller for the Poshkus analysis due to the summation over the CH centers rather than the molecular center. This would tend to more than offset the effect of not considering the polarizability change with orientation.

CHAPTER VI

ADSORPTION OF RARE GASES ON HEXAGONAL BORON NITRIDE

The single surface values of B_{2s} and B_{3s} for the adsorption of Ar, Kr and Xe on Boron Nitride are given in Tables 14 and 15. The B_{2s} values at the ice point agree well with Ramsey's results[2,3] for Ar adsorption but differ by about one to 1.5 percent for Xe and Kr adsorption.

The result of the single surface B_{2s} analysis is shown in Table 16. Several points are of interest. The first is the extremely low value of the surface area relative to the 4.98 m^2/g BET area. The second is the poor fits obtained relative to the gas-P33 systems, especially with Xe and Kr, as evidenced by $\sigma \ln Az_o$. Both properties also appear to accentuate as the adsorbate becomes more polarizable. All of the above is symptomatic of some sort of surface heterogeniety which might be expected since electron micrographs indicate 5 to 10% edge sites.

Since the data of Ramsey[1] did not contain the very low coverage points necessary to accurately determine B_{2s}^b and B_{2s}^e by a two-surface virial approach, Thomas, Ramsey and Pierotti[3] developed a two-surface approach where the Argon isotherm curvature was attributed to the edge and was fitted

Table 14. Best Fit Value of B_{2s} for the Adsorption of Xe, Kr and Ar on Hexagonal Boron Nitride

Adsorbate	Temperature (°K)	Single Surface $B_{2s}x10^2$ (cm^3/g)	Two Surface $B_{2s}^b x10^2$ (cm^3/g)	Two Surface $B_{2s}^e x10^2$ (cm^3/g)
Xe	273.150	25.70[a](25.4)[d]	9.70	16.00
	337.412	6.081[a]	3.531	2.581
	358.954	4.363[b]	2.735	1.632
	368.034	3.868[b]	2.478	1.368
Kr	273.150	4.820[a](4.88)[d]	2.946	1.847
	296.215	3.138[a]	2.131	1.041
	333.460	1.889[b]	1.387	0.493
Ar	273.150	1.541[b](1.534)[d]	1.168	0.368
	295.284	1.139[c]	0.908	0.241
	310.027	0.9754[c]	0.781	0.188

[a]From fit to $N_a = a_o+a_1P+a_2P^2+a_3P^3$ with (0,0) weighted by a factor of ten.

[b]From fit to $N_a=a_o+a_1P+a_2P^2$ with (0,0) weighted as in (a).

[c]From fit to $N_a = a_o+a_1P$ with (0,0) weighted as in (a).

[d]References 2 and 3.

Table 15. Parameters for the Adsorption of Xe, Kr and Ar on Hexagonal Boron Nitride from B_{3s} Data

Adsorbate	Temperature (°K)	B_{3s} (cm^6/g-mole)	$B_{2D} \times 10^{-7}$ (cm^2/mole)	ε^*_{12}/k
Xe	273.150	-19969	33.3[a]	139
	337.412	- 597	36.5[a]	167
	358.954	b	--	--
	368.034	b	--	--
Kr	273.150	- 489	56.4[a]	94
	296.215	- 91.3	31.5[a]	143
	333.460	b	--	--
Ar	273.150	- 23.8	54.5[a]	82
	295.284	b	--	--
	310.027	b	--	--

[a]Computed using two surface values of A and X listed in Table 16.

[b]Computation not meaningful due to the large experimental uncertainty in B_{3s} at this temperature.

Table 16. Best Fit Parameters for the Adsorption of Xe, Kr and Ar on Hexagonal BN from B_{2s} Data

Single Surface	Xe	Kr	Ar
ε^*_{1s}/k (°K)	2232	1610	1211 (1212)[a]
$Az_o x10^4 (cm^3/g)$	3.14	4.58	5.29 (5.27)[a]
$\sigma \ln Az_o$	0.0162	0.0138	0.0083 (0.0075)[a]
A (m^2/g)	0.99	1.55	1.87

Two Surface	Xe	Kr	Ar
ε^{*b}_{1s}/k (°K)	1650±15	1305±20	1038±8 (1083)[a]
ε^{*e}_{1s}/k (°K)	2810[b]	2200[b]	1735[b] (1573)[a]
$Az_o x10^4 (cm^3/g)$	8.443	7.770	7.230 (6.39)[a]
$\sigma \ln Az_o$	0.0045	0.0093	0.0077 (0.008)[a]
A	2.66[b]	2.63[b]	2.56[b] (2.36)[a]
% edge	3.25	3.25	3.25 (5)[a]

Average Values from Two-Surface Fit

$A = 2.62 \pm 0.05\ m^2/g$ $\qquad$ $\varepsilon^{*e}_{1s}/\varepsilon^{*b}_{1s} = 1.687 \pm 0.016$

[a]References 2 and 3.

[b]Values of ε^{*e}_{1s}/k and A required to minimize $\sigma \ln Az_o$ for the above ε^{*b}_{1s}/k.

by the Langmuir isotherm. The value of B_{2s}^{e} for the edge was then subtracted off the single surface result to give B_{2s}^{b}. Each of the two sets were then treated in the conventional manner to obtain ε_{1s}^{*}/k, Az_o and $\sigma \ln Az_o$ for each of the two surfaces. The sum of Az_o for the two surfaces was divided by z_o to arrive at the total surface area. The results are shown in Table 16.

An obvious shortcoming of this approach is that as one goes lower in temperature, the contributions of the basal plane interactions to the isotherm curvature becomes more important and cannot be ignored. There is also a degree of uncertainty in N_m^e, the Langmuir monolayer volume, which also contributes to the B_{2s} error.

The resultant analysis using a Langmuir fit for the edge surface does not give an improvement in $\sigma \ln Az_o$ for the basal plane over the single surface value and A is only about 50% of the BET area. The Ar-P33 system gives an A about 70% of the BET area.

The isotherm data in this work contains the low coverage points necessary to do the two-surface virial treatment described in Chapter II. In addition the isotherms are at the ice point and above so as to minimize the coverage at a given pressure relative to low temperature isotherms.

Unfortunately, the data contains only three isotherms each for Ar and Kr adsorption and four isotherms for Xe-BN. Since there are now additional parameters involved, a number

of combinations of choices of ε_{1s}^{*e}/k, ε_{1s}^{*b}/k, X and Az_o give approximately the same goodness of fit for a given system as evidenced by $\sigma \ln Az_o$. However if the requirements are made that

- X,
- A and
- $\varepsilon_{1s}^{*e}/\varepsilon_{1s}^{*b}$

be the same for the three systems, than a unique set of parameters may be found.

The first two requirements are reasonable in that the absolute value and make-up of the surface should be independent of the adsorbate.

The last restraint follows from the convention that the potential at equilibrium separation for two different type molecules, A and B, can be expressed as

$$\varepsilon_{AB} = \sqrt{\varepsilon_{AA}\ \varepsilon_{BB}}$$

where ε_{AA} and ε_{BB} are the equilibrium separations of molecules A and B interacting with like molecules. Therefore, for the interaction of a rare gas molecule, the ratio of the edge to basal plane interaction is

$$\varepsilon_{1s}^{*e}/\varepsilon_{1s}^{*b} = \sqrt{\varepsilon_{BN-BN}^{e}\ \varepsilon_{G-G}} \Big/ \sqrt{\varepsilon_{BN-BN}^{b}\ \varepsilon_{G-G}}$$

$$= \sqrt{\varepsilon_{BN-BN}^{e}} \Big/ \sqrt{\varepsilon_{BN-BN}^{b}} \qquad (84)$$

which is independent of the type of adsorbate.

The actual analysis is performed graphically. First, a value of X is assumed and then a set of ε_{1s}^{*e}/k and ε_{1s}^{*b}/k values are computed by the two-surface virial analysis method for each gas-BN system. The optimum value of ε_{1s}^{*e}/k for each choice of ε_{1s}^{*b}/k is obtained by minimizing with respect to $\sigma \ln Az_o$. This necessarily generates a value of A for each choice of ε_{1s}^{*b}/k. Plots of $\varepsilon_{1s}^{*b}/\varepsilon_{1s}^{*b}$ versus A are then made for each system on the same set of coordinates for the given choice of X. If the proper choice of X is made, the plots of the three systems converge at a common point thereby giving a unique set of A,X and $\varepsilon_{1s}^{*e}/\varepsilon_{1s}^{*b}$ values from which the corresponding ε_{1s}^{*e}/k and ε_{1s}^{*b}/k can be extracted by going back to the original data used to construct the plot. The plot is shown in Figure 19.

Although the plot at X = 0.0325 does not have one common point, the closeness of the three individual intersections defines a unique set of parameters within the experimental accuracy of the experiment. Since each gas-BN curve is intersected twice, two values of ε_{1s}^{*b}/k, ε_{1s}^{*e}/k and A are produced for each system. The average of the two values of ε_{1s}^{*b}/k and the average deviation is reported for each system in Table 16. The values of ε_{1s}^{*e}/k and A reported here are those required to minimize $\sigma \ln Az_o$ using the previously determined ε_{1s}^{*b}/k. At the bottom of Table 16 are the averages and standard deviations from the averages of A and

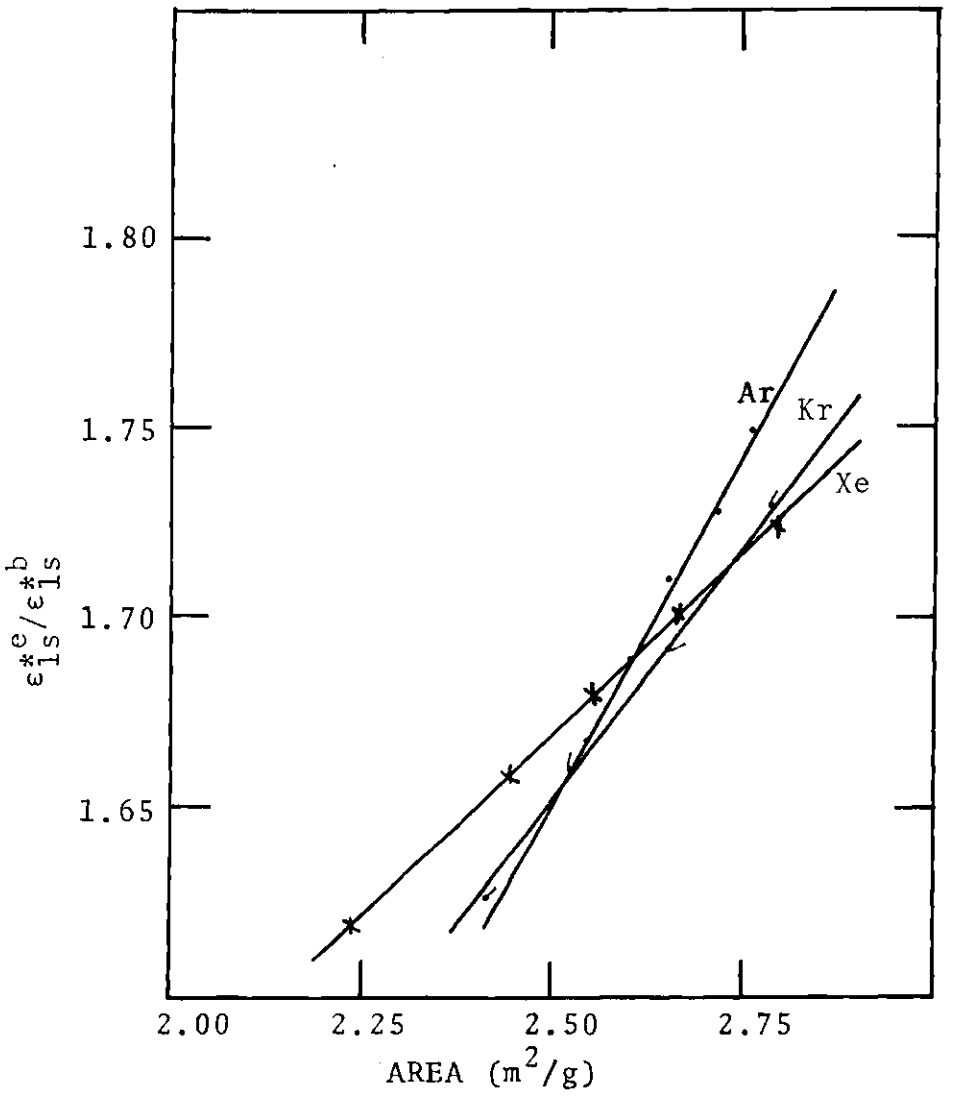

Figure 19. Plot of $\varepsilon^{*e}_{1s}/\varepsilon^{*b}_{1s}$ Versus Area for Ar, Kr and Xe Adsorbed on BN Containing 3.25% Edge Sites

$\varepsilon_{1s}^{*e}/\varepsilon_{1s}^{*b}$.

The values of $\sigma \ln Az_o$ given in Table 16 show an improvement in data fit for the two-surface analysis relative to the single surface treatment for all systems. The value of 3.25% edge surface is slightly smaller than Ramsey's[3] and the surface area is larger. The larger surface area is in the right direction, but is still smaller than might be expected based on the 4.98 m^2/g BET area.

The values of ε_{1s}^{*b}/k for the three systems are compared with those reported in the literature in Table 17. In general, the results for Ar-BN and Kr-BN fall within the general range of calculated results. The value for Xe-BN is slightly smaller. B_{2s}^b and B_{2s}^e back calculated from the results of the two-surface fit are reported in Table 14.

An attempt was also made to include the three highest temperature B_{2s} values of Ramsey[1-3] in the previous analysis. This proved unsatisfactory as it gave values of ε_{1s}^{*b}/k which appeared low and had wide variability: Ar-BN, 928 ± 53°K; Kr-BN, 1208 ± 108°K; and Xe-BN, 1638 ± 38°K at 2.75% edge surface. Considering the uncertainty in B_{2s} at 231.252°K and 248.467°K due to extrapolation errors this might be expected. It was for this very reason that the close-in points were measured in this work to avoid uncertainty in B_{2s}.

The results of the two-surface analysis of B_{3s} data via equations (48) through (50) and (44) are given in Table

Table 17. Various Values of ε^*_{1s}/k (°K) for the Adsorption of Inert Gases on the Basal Plane of Boron Nitride

Adsorbate	This Work	Ref. 3	Ref. 34	Ref. 48	Ref. 4	Ref. 49	Ref. 50
Ar	1038	1083	1123	1047	--	956	1007
Kr	1305	1414	1312	1409	1321	--	--
Xe	1650	1847	1783	1855	--	--	--

15. The values of A^b and A^e are obtained from X and A reported in Table 16. The most reliable of the B_{2D} data is from the ice point isotherm of each adsorbate as they contained the most points. The values of ε^*_{12}/k reported for each adsorbate shows the same trend as observed on graphite with Ar and N_2; a depression due to a perturbation of the pair interaction by the surface.[21] The value of σ used for each adsorbate is taken from Table 2.

CHAPTER VII

CONCLUSIONS

Assessment of Results

Graphitized P33 Adsorbent

On the basis of results using the N_2 and CO_2 data, a primary conclusion must be that the virial analysis technique pioneered by Halsey and his co-workers is applicable to the adsorption of simple, non-linear molecules. In particular, the non-spherical function put forth in equation (38) properly takes into account changes in the attractive and repulsive forces as a function of the adsorbate orientation with the surface. This is done by using an orientation dependent polarizability for the adsorbate and an orientation dependent z_o for the system.

The value of ε^*_{12}/k found for N_2 adsorption supports the proposed theory[21] of additional repulsion between adsorbate molecules due to perturbation of the pair interaction by the surface field.

The effect of hindered rotation of non-spherical molecules by the surface can be seen in the reduction of the surface area as determined using the spherical (9,3) potential and reduction of σ_{12} for N_2 and CO_2 as determined from the (12,6) B_{2D} analysis. By use of the non-spherical potential,

a surface area consistent with Ar-P33 is obtained.

The non-spherical potential model as extended to benzene gives a more realistic value for the surface area than for a spherical potential, but still underestimates A. The non-spherical harmonic approximation model of Pierotti[9] gives a surface area consistent with the BET area. The fit of both models to the B_{2s} data is poor relative to the Ar-P33, N_2-P33 and CO_2-P33 results. This may be due to large errors introduced by necessary extrapolation of high coverage data to determine the B_{2s}'s or the models may be simply insufficient to treat such a complex system.

Hexagonal Boron Nitride Adsorbent

The two-surface virial approach used for Ar, Kr and Xe adsorbates appears valid in that it gives a reasonable value of the surface area and an improvement in the fit to the B_{2s} data over the single surface approach. Both of these are shortcomings of the two-surface approach using the Langmuir model for the high energy surface.

The result of the analysis requiring A, X and $\varepsilon_{1s}^{*e}/\varepsilon_{1s}^{*b}$ to be the same for all gas-BN systems investigated gives reasonable values for ε_{1s}^{*b} and % edge, but still gives a value for the surface area which appears low.

A very important conclusion based on ε_{12}^{*}/k results again is that there is a reduction in ε_{12}^{*}/k due to perturbation of the adsorbate-adsorbate interaction by the surface. This is important in that a recent paper by Morrison and

Ross[39] has cast doubt on this predicted phenomena.[21]

Recommendations for Further Study

An obvious shortcoming of the non-spherical potential function proposed here is that it cannot be evaluated without the use of a high-powered computer. For this reason, it is recommended that a more analytical form of the potential be sought which might be interpreted directly.

Further experimentation of more complex systems such as CCl_4-P33 should be undertaken and the potential models developed for data treatment.

In order to obtain a better understanding of benzene adsorption, more data in the very low coverage region should be obtained. It might be necessary to go to higher temperatures to accomplish this.

Another logical extension of this work would be to the adsorption of non-spherical molecules on heterogeneous surfaces.

The observed effect of an increase in ε^*_{12}/k for CO_2 should be investigated further, possibly using other adsorbates, to determine the nature of the forces involved.

APPENDICES

APPENDIX A

ADDITIONAL LITERATURE REVIEW

The purpose of this section is to summarize some of the more recent work done in the area of surface adsorption. The papers discussed are applicable to the general area of study undertaken here, but not to the specific cases experimentally investigated.

One of the more interesting experimental papers is that of Putnam and Fort.[31] Their section on the heterogeniety of P33(2700°-3700°) has been previously discussed. A second section of this paper deals with a change in packing of Kr adsorbed on P33 near monolayer coverage. The change involves a shift from an in-registry to an out-of-registry conformation. This conclusion is supported by an irregular change in the curvature near monolayer coverage.

A second experimental paper[51] deals with B_{2s} data obtained by gas chromatographic techniques for n-pentane, methane and benzene adsorbed on a number of different graphitized carbon blacks. The benzene data is from higher temperatures than measured by Smallwood.[37] However, a graphically extrapolated value of B_{2s} at 323°K compares favorably with that given by Pierotti[9] based on Smallwood's data.

Two papers on theoretical calculation of various molecules adsorbed on a graphite surface are of interest. The first[52] deals with calculated adsorptive potentials using a three parameter (6,exp) function for the rare gas-graphite systems. The potentials are calculated at different positions on the graphite lattice. The results do not agree well with experiment.

The second paper in this area[53] calculates the equilibrium conformations of a number of hydrocarbons on the graphite surface. The Lennard-Jones (12,6) potential function is used in the pair-wise additive approximation in conjunction with a potential expansion technique.

One of the more interesting papers is that of Morrison and Ross.[39] Their main contention is that the curvature of a series of isotherms can be fit by the two-dimensional virial equation of state as transformed by the Gibbs adsorption isotherm by simply using the experimental Henry's law constants and best fit surface area in conjunction with the two dimensional virial coefficients as computed from the gas phase parameters. That is, there is no need to determine ε_{12}^{*}/k from experimental data as there is no depression of ε_{12}^{*}/k due to perturbation of the adsorbate pair interaction by the surface field. However, the fit given by Morrison and Ross to the Ar-P33 data of Sams[54] is poor in the range where B_{2D} is most important and is good only in the higher coverage range where hard disk approximations are used for the higher

two-dimensional virial coefficients. This would seem to contradict the papers conclusions.

Another two-dimensional equation of state and corresponding isotherm equation is proposed by Bergman.[55] The long range portion of the adsorbate pair potential is taken as the sum of attractive sixth power term and a repulsive inverse third power term. The repulsive term is added to account for the perturbation of the pair interaction by the surface. The short range portion is the familiar constant r.[12]

The final paper[56] proposes a model for adsorption on a substrate containing a gaussian distribution of adsorptive potentials. The effect of the distribution parameters on the second and third two-dimensional virial coefficients is discussed.

APPENDIX B

DERIVATION OF THE VIRIAL TREATMENT OF LOW COVERAGE SURFACE ADSORPTION

The general virial equation of state may be derived from the statistical mechanical treatment of the grand canonical ensemble.[22,57] The procedure for surface adsorption is to express adsorption in terms of the excess number of moles of gas, N_a, in a geometric volume, V_{geo}, when the gas is allowed to interact with a solid surface or

$$N_a = N^* - N^o \tag{85}$$

where N^* is the total number of moles of gas in the system in the presence of the solid's external field and N^o is the number of moles of imperfect gas in V_{geo} in the absence of the field. Therefore, to obtain N_a, one must first determine the form of N^* and N^o.

The grand canonical ensemble consists of an ensemble of representative systems each with the same volume, V; temperature, T; and chemical potential, μ. The partition function is then

$$\Xi(\mu,V,T) = \sum_{N\geq 0} Q(N,V,T)\ e^{N\mu/kT} \tag{86}$$

where $Q(N,V,T)$ is the canonical partition function for N molecules. For simplicity, $Q(N,V,T)$ is denoted as Q_N and $e^{\mu/kT}$, the absolute activity, by λ in all the following equations.

The characteristic equation of the grand canonical emsemble is

$$PV = kT\ln\Xi \tag{87}$$

Another useful relationship is

$$\bar{N} = \left[\frac{\partial \ \ell n \ \Xi}{\partial\lambda}\right]_{V,T} \tag{88}$$

where $\bar{N}$ is the average number of molecules in a system in the ensemble.

Now equation (86) may be rewritten

$$\Xi = 1 + Q(1,V,T)\lambda + Q(2,V,T)\lambda^2 + \ldots \tag{89}$$

for the low density region of adsorption. Note that $Q(0,V,T)$ is unity.

Next a Taylor series expansion of $\ell n\ \Xi$ about unity yields

$$\ell n\ \Xi = (\ell n\ \Xi)_{\Xi=1} + \left(\frac{\partial\ \ell n\ \Xi}{\partial \Xi}\right)_{\Xi=1} (\Xi - 1)$$

$$+ \left(\frac{\partial^2\ \ell n\ \Xi}{\partial \Xi^2}\right)_{\Xi=1} \frac{1}{2!} (\Xi-1)^2 + \ldots \tag{90}$$

$$= (\Xi-1) - \frac{1}{2} (\Xi-1)^2 + 1/3\ (\Xi-1)^3 + \ldots$$

or

$$\ell n\ \Xi = Q_1\lambda + Q_2\lambda^2 + Q_3\lambda^3 - \frac{1}{2} (Q_1\lambda+Q_2\lambda^2+Q_3\lambda^3 + \ldots)^2 \tag{91}$$

$$+ 1/3\ (Q_1\lambda + Q_2\lambda^2 + Q_3\lambda^3 + \ldots)^3$$

Collecting terms of like power of λ, one obtains

$$\ell n\ \Xi = Q_1\lambda + (Q_2 - \frac{1}{2} Q_1^2) + (Q_3-Q_1Q_2 + 1/3\ Q_1^3)\lambda^3 + \ldots \tag{92}$$

which may be substituted into equation (87) to give

$$\frac{PV}{kT} = Q_1\lambda + (Q_2 - 1/2\ Q_1^2)\lambda^2 + (Q_3-Q_1Q_2 + 1/3\ Q_1^3)\lambda^3 + \ldots \tag{93}$$

Recall that for a real gas

$$\mu = \mu^o\{T\} + kT\ \ell n\ f \tag{94}$$

where f is the fugacity.

This leads to

$$\lambda = e^{\mu/kT} = fe^{\mu^{o}\{T\}/kT} = \frac{\Lambda^3 f}{kT} \tag{95}$$

for a monatomic gas where Λ is the thermal de Broglie wavelength defined as

$$\Lambda = \left(\frac{h^2}{2\pi mkT}\right)^{1/2} . \tag{96}$$

Also for a monatomic gas

$$Q(N,V,T) = \frac{Z(N,V,T)}{\Lambda^{3N} N!} \tag{97}$$

where Z(N,V,T) is the configurational integral of the canonical partition function. Substitution of equation (95) and (97) into (93) gives

$$\frac{PV}{kT} = \ln \Xi = Z_1 f/kT + \frac{1}{2}(Z_2 - Z_1^{\,2})\left(\frac{f}{kT}\right)^2 + \frac{1}{3!}(Z_3 - 3Z_1Z_2 + 2Z_1^{\,3})$$

$$\left(\frac{f}{kT}\right)^3 + \ldots \tag{98}$$

This can be written as the sum

$$\ln \Xi = \sum_{i \geq 1} \beta_i (f/kT)^i \tag{99a}$$

or

$$\frac{P}{kT} = \sum_{i \geq 1} b_i (f/kT)^i \tag{99b}$$

where

$$b_1 V = \beta_1 = Z_1, \tag{100a}$$

$$b_2 V = \beta_2 = \frac{1}{2!} (Z_2 - Z_1{}^2) \tag{100b}$$

and

$$b_3 V = \beta_3 = \frac{1}{3!} (Z_3 - 3Z_1 Z_2 + 2Z_1{}^3). \tag{100c}$$

Now by taking the appropriate derivative of equation (99a) required by equation (88), it follows that

$$\bar{N} = \sum_i i \, \beta_i \, (f/kT)^i \tag{101}$$

and in terms of number density,

$$\bar{\rho} = \frac{\bar{N}}{V} = \sum_i b_i (f/kT)^i.$$

Now recall equation (85) and (101) and obtain for the gas in the presence of the solid

$$N_a = \sum_i i\ (\beta_i - \beta_i^o)\ (f/kT)^i$$

$$= (Z_1 - Z_1^o) f/kT + (Z_2 - Z_2^o - Z_1^2 + (Z_1^o)^2) f/kT)^2 + \ldots$$

$$= \sum_i B_{i+1,s} f/kT)^i \tag{102}$$

where the notation is such that $\bar{N}$ in equation (101) corresponds to N^* in equation (85),

$$B_{2s} = (Z_1 - Z_1^o) \tag{103a}$$

and

$$B_{3s} = (Z_2 - Z_2^o - Z_1^2 + (Z_1^o)^2)\,. \tag{103b}$$

β_i now corresponds to the system in the presence of the solid and β_i^o to the imperfect gas in the absence of the solid. The $B_{i+1,s}$ values are the gas-solid virial coefficients.

Experimentally one measures the pressure and not the fugacity. Therefore, it is necessary to obtain an expression for the fugacity in terms of pressure. This can be done by a series of manipulations involving the inversion of equation (99b) and (101) to give

$$f/kT = \bar{\rho} - 2b_2\bar{\rho}^2 + (8b_2^2 - 3b_3)\bar{\rho}^3 + \ldots \tag{104}$$

and

$$f/kT = \frac{P}{kT} - b_2 \left(\frac{P}{kT}\right)^2 + (2b_2^2 - b_3)(P/kT)^3 + \ldots \qquad (105)$$

Note that $b_1 = 1$ since $f/P \to 1$ as $P \to 0$ and therefore does not appear in equations (104) and (105).

Next, equation (104) is substituted into (99b) and terms gathered to give

$$P/kT = \bar{\rho} + \sum_{i \geq 2} B_i \bar{\rho}^i \qquad (106)$$

where

$$B_2 = -b_2 = -1/2 \ (Z_2 - Z_1^2)/V \qquad (107a)$$

and

$$B_3 = 4b_2^2 - 2b_3. \qquad (107b)$$

The B's are the virial coefficients.

Based on the above definition, equation (105) is rewritten

$$f/kT = P/kT + B_2(P/kT)^2 + 1/2 \ (B_3 - B_2^2) \ (P/kT)^3 + \ldots \qquad (108)$$

Finally the desired results are obtained by substitution of equation (108) into (102) to give

$$N_a = \sum_{i \geq 1}^{\infty} C_{i+1,s} \, (P/kT)^i \tag{109}$$

where

$$C_{2s} = B_{2s}, \tag{110a}$$

$$C_{3s} = B_{3s} + B_{2s} \, B_2 \tag{110b}$$

and

$$C_{4s} = B_{4s} + 2B_{3s}B_2 + (1/2)B_{2s}(B_3+B_2^2) \tag{110c}$$

APPENDIX C

TWO DIMENSIONAL VIRIAL DERIVATION

Since physical adsorption occurs on a surface, a common convention is to develop a two dimensional equation of state via the canonical partition function with the spreading pressure, π, replacing the experimentally measurable pressure and the area, A, replacing the volume. Of course, a two dimensional system is an idealization which does not actually exist. This must be kept in mind when using the relationships developed in this section.

Pierotti and Thomas[21,51] have shown that if the partition function in the presence of the field is treated in accordance with the McMillan-Mayer theory of solutions that one obtains a function which as applied to adsorption yields

$$\pi A = kT \ln (\Xi'/\Xi^*) \tag{111}$$

where Ξ' and Ξ^* are the semi-grand partition functions in the presence and absence of the external field respectively.

In a manner similar to that used in Appendix B one obtains

$$\pi A = \sum_{i \geq 1} \left(\frac{B_{i+1,s}}{i}\right) \left(\frac{f}{kT}\right)^i \tag{112}$$

The next step is to invert equation (102) to give

$$f = \frac{N_a kT}{B_{2s}} \left[1 - \left(\frac{B_{3s}}{B_{2s}}\right) N_a - \left(\frac{B_{2s}B_{4s} - 2B_{3s}^{\ 2}}{B_{2s}^4}\right) N_a^{\ 2} + \ldots \right] \tag{113}$$

which when substituted into equation (112) gives

$$\frac{\pi A}{kT\ N_a} = 1 - \frac{B_{3s}}{2B_{2s}^{\ 2}} N_a + \left(\frac{B_{3s}^{\ 2}}{B_{2s}^{\ 4}} - \frac{2B_{4s}}{3B_{2s}^{\ 3}}\right) N_a^{\ 2} + \ldots \tag{114}$$

Now the two dimensional equation of state analogous to equation (106) is

$$\frac{\pi A}{kT\ N_a} = 1 + \left(\frac{B_{2D}}{A}\right) N_a + \left(\frac{C_{2D}}{A^2}\right) N_a^{\ 2} + \ldots \tag{115}$$

Here N_a/A is analogous to $\bar{\rho}$ in equation (106).

Comparison of (114) and (115) then leads to the conclusion that

$$\frac{B_{2D}}{A} = - \frac{B_{3s}}{2B_{2s}^{\ 2}} \tag{116}$$

and

$$\frac{C_{2D}}{A^2} = \left[\frac{B_{3s}^{\ 2}}{B_{2s}^{\ 4}} - \frac{2B_{4s}}{3B_{2s}^{\ 3}} \right] . \tag{117}$$

APPENDIX D

ERROR ANALYSIS

The experimental error may be broken down into two categories: calibration errors and errors in pressure and temperature measurements associated with adsorption data.

The only calibration error of great significance is in the value of the sample cell volume, V_{13}, which amounts to ± 0.010 cm^3. Since this is a volume error, it contributes directly to a B_{2s} error. On a per gram of adsorbent basis this is an error of ± 0.00043 cm^3/g for graphite adsorption and 0.00012 cm^2/g for BN adsorption.

The experimental error associated with each adsorption point comes from the error in the pressure measurement. Temperature measurement error is not significant. Four measurements must be made for each pressure determination; two on the meter bar and one each on each manometer. The error in each reading is approximately ± 0.0005 cm of Hg. Therefore the expected error in the pressure is

$$\Delta P = \sqrt{4(0.0005)^2} = 0.0010 \text{ cm Hg.}$$

Since the pressure error is spread over the entire system volume, it is advantageous to minimize the volume of

the system in making measurements. It is for this reason that use of the largest pipet volume was avoided. The error in the value of N_a for a given pressure is

$$\Delta N = \frac{\Delta PV}{RT} . \tag{118}$$

Since a dose measurement must be made in addition to the adsorption measurement, the error enters twice. The dose volume most frequently used was approximately 140 cm^3 and the average volume for the adsorption measurement was 130 cm^3.

By use of equation (118), the dose error at the ice point is $\pm 0.82 \times 10^{-7}$ moles and the average error from the adsorption portion is $\pm 0.76 \times 10^{-7}$ moles.

The expected error in the number of moles adsorbed is then

$$\Delta N = (10^{-7}) \sqrt{(0.82)^2 + (0.76)^2} = \pm 1.12 \times 10^{-7} \text{ moles.}$$

On a per gram basis this is $\pm 0.048 \times 10^{-7}$ moles/g for the P33 system and $\pm 0.013 \times 10^{-7}$ moles/g for the BN system.

If the average adsorption pressure is 25 cm Hg, the above error in N_a corresponds to a B_{2s} error of ± 0.00033 cm^3/g for P33 and ± 0.00009 cm^3/g for BN.

Combining this pressure error with the calibration volume error, the expected error in B_{2s} is

for P33

$$\Delta B_{2s} = \sqrt{(.00033)^2 + (.00043)^2} = \pm 0.00054 \text{ cm}^3/\text{g}$$

and

$$\Delta B_{2s} = \sqrt{(.00009)^2 + (.00012)^2} = \pm 0.00015 \text{ cm}^3/\text{g}$$

for BN.

Comparison of this with the experimental values of B_{2s} shows that the % B_{2s} error varies from 0.06% at 227.322°K to 0.59% at 342.041°K for N_a adsorption. If one computes the average error for the B_{2s} values used in the determination of $Az_{o||}$, one obtains 0.78% for N_2 adsorption and 0.23% for CO_2 adsorption. Both average percent values compare favorably with the respective values of $\sigma \ln Az_{o||}$; 0.0034 for N_2-P33 and 0.0045 for CO_2-P33.

The average error in B_{2s} values used in the rare gas-BN systems, based on 0.00015 cm^3/g for any given B_{2s}, are 1.28% for Ar-BN, 0.53% for Kr-BN and 0.26% for Xe-BN. This again compares favorably with the $\sigma \ln Az_o$ results for the two surface virial analysis: 0.0083 for Ar-BN, 0.0093 for Kr-BN and 0.0045 for Xe-BN.

The B_{3s} error comes almost entirely from the pressure measurement error as the volume calibration error should reflect mainly in B_{2s} with no significant effect on B_{3s}.

The B_{3s} error can be approximated by

$$\Delta B_{3s} = \Delta N_a \left(\frac{RT}{P}\right)^2 .$$

Again using the ice point as a reference, since it was the temperature used to determine ΔN_a, and a pressure of 25 cm of Hg,

$$\Delta B_{3s} = \pm 22.2 \text{ cm}^6/\text{g-mole}$$

for the P33 adsorption.

Once again a comparison of ΔB_{3s} with experimental B_{3s} data is made. It shows a range of 0.6% error at 156.166°K to 11.6% at 214.015°K for N_2-P33 and 0.1% at 227.322°K to 18.5% at 300.910°K for CO_2-P33. This clearly points out why the B_{3s} data above 214.015°K for N_2-P33 and 300.410°K for CO_2-P33 was not used in the two dimensional analysis.

The average % errors of the B_{3s} values used into two dimensional analysis are 5.0% and 5.7% for the N_2-P33 and CO_2-P33 systems, respectively. The percent error in $\pi\sigma_{12}^2$ as computed from the standard deviation in σ_{12}, Table 5, are 3.3% and 5.9% for the N_2-P33 and CO_2-P33 systems, respectively. This compares favorably with average percent errors expected in B_{3s}.

APPENDIX E

ISOTHERM DATA

All pressures are reported in both standard centimeters of mercury and kN/m^2. The temperatures have been corrected to the 1968 IPTS temperature scale.[58]

Table 18. N_2-P33 (2700°) Adsorption Data

T = 156.155°K

P (kN/m^2)	P (cm Hg)	N_ax10^7 (moles/g)
6.1436	4.6081	40.897
9.3871	7.0409	61.477
12.0975	9.0739	78.332
13.3894	10.0429	86.456
14.8161	11.1130	95.186
16.8150	12.6123	107.318

T = 214.015°K

P (kN/m^2)	P (cm Hg)	N_ax10^7 (moles/g)
23.2666	17.4514	19.345
28.3426	21.2587	23.453
32.4032	24.3044	26.696
37.3037	27.9801	30.833
43.1683	32.3789	35.416
52.3381	39.2568	42.561

T = 177.096°K

P (kN/m^2)	P (cm Hg)	N_ax10^7 (moles/g)
12.6566	9.4932	33.694
14.2218	10.6672	37.612
16.0355	12.0276	42.346
18.1137	13.5864	47.545
21.1648	15.8749	55.400

T = 234.200°K

P (kN/m^2)	P (cm Hg)	N_ax10^7 (moles/g)
19.5012	14.6271	10.017
23.9620	17.9730	12.254
27.5821	20.6883	14.102
32.0256	24.0212	16.337
46.1277	34.5986	23.417

T = 197.434°K

P (kN/m^2)	P (cm Hg)	N_ax10^7 (moles/g)
15.4043	11.5542	20.691
18.6075	13.9568	24.767
21.1332	15.8512	27.917
24.1285	18.0979	31.928
33.0355	24.7787	43.271

Table 19. N_2-P33 (2700°) Adsorption Data

T = 273.150°K

P (kN/m^2)	P (cm Hg)	N_ax10^7 (moles/g)
7.7564	5.8178	1.831[b]
9.1250	6.8443	2.227[b]
13.7391	10.3052	3.255[b]
27.1791	20.3860	6.535[c]
39.3772	29.5353	9.460[c]
54.5255	40.8975	13.175[a]
55.0855	41.3175	13.172[c]
69.7308	52.3024	16.851[c]
76.2731	57.2095	18.315[a]
96.5558	72.4228	23.358[a]

T = 296.424°K

P (kN/m^2)	P (cm Hg)	N_ax10^7 (moles/g)
23.4533	17.5914	3.966
34.3890	25.7939	5.672
48.8562	36.6452	8.045
62.7572	47.0718	10.531

T = 311.466°K

P (kN/m^2)	P (cm Hg)	N_ax10^7 (moles/g)
39.3389	29.5066	5.281
56.4066	42.3084	7.557
73.1168	54.8421	9.975

T = 329.299°K

P (kN/m^2)	P (cm Hg)	N_ax10^7 (moles/g)
26.5237	19.8944	2.862
36.7916	27.5960	4.219
57.1668	42.8786	6.095
74.8786	56.1636	7.954

T = 347.358°K

P (kN/m^2)	P (cm Hg)	N_ax10^7 (moles/g)
25.0118	18.7604	2.328
37.4821	28.1139	3.159
54.8475	41.1390	4.472
72.5507	54.4175	6.035

[a]Run 1.

[b]Run 2.

[c]Run 3.

Table 20. CO_2-P33 (2700°) Adsorption Data

T = 227.322°K

P (kN/m^2)	P (cm Hg)	N_ax10^7 (moles/g)
15.2750	11.4572	79.370
20.5244	15.3946	110.911
23.1473	17.3619	127.971[a]
26.1468	19.6117	147.656
30.4690	22.8536	178.068

T = 300.910°K

P (kN/m^2)	P (cm Hg)	N_ax10^7 (moles/g)
18.7085	14.0325	12.329
27.2939	20.4721	18.300
32.2551	24.1933	21.607
38.5442	28.9105	25.809
49.2398	36.9329	33.013

T = 250.072°K

P (kN/m^2)	P (cm Hg)	N_ax10^7 (moles/g)
16.7898	12.5934	38.792
23.4862	17.6161	55.212
27.0999	20.3266	64.242[a]
31.4261	23.5715	75.377
38.2013	28.6533	93.210

T = 317.392°K

P (kN/m^2)	P (cm Hg)	N_ax10^7 (moles/g)
19.0723	14.3054	9.170
28.0846	21.0652	13.636
40.1412	30.1084	19.456
51.8759	38.9101	25.245

T = 273.150°K

P (kN/m^2)	P (cm Hg)	N_ax10^7 (moles/g)
21.3196	15.9910	26.116
30.5240	22.8949	37.631[a]
30.5278	22.8977	37.549
35.6713	26.7557	44.319[a]
42.0504	31.5404	52.299
52.4637	39.3510	66.108

T = 342.041°K

P (kN/m^2)	P (cm Hg)	N_ax10^7 (moles/g)
19.5361	14.6533	6.219
24.6934	18.5216	7.876
29.0945	21.8227	9.211
34.8159	26.1141	11.149
42.2681	31.7037	13.404
55.4965	41.6258	17.627

[a]Desorption.

Table 21. N_2-P33 (2700°) BET Plot Data

T = 82.792°K A = 11.84[a] m^2/g

P (kN/m^2)	P (cm Hg)	$N_a x10^5$ (moles/g)	P/P_o	$P/(P-P_o)RN_a$
0.0440	0.0330	3.9849	0.000243	b
0.1541	0.1156	8.4736	0.000852	b
2.2771	1.7080	11.5450	0.12589	b
6.5152	4.8868	12.5834	0.036020	3.6188
8.7883	6.5918	12.8144	0.048587	4.8567
16.1221	12.0926	13.3526	0.089132	8.9311
22.0075	16.5070	13.7892	0.12167	12.2427
27.6663	20.7514	14.2738	0.15296	15.4173
37.8297	28.3746	15.3788	0.20914	20.9563
49.4951	37.1244	17.3361	0.27364	b

[a]Based on a N_2 area of 16.2 $Å^2$/molecule and P_o = 135.67 cm Hg or 180.88 kN/m^2.

[b]Not used in BET area determination.

Table 22. Ar-P33 (2700°) and Ar-BN Adsorption Data at the Ice Point

Ar-P33 (2700°)

Constabaris[32]			This Work		
P		$N_a x10^7$	P		$N_a x10^7$
(kN/m^2)	(cm Hg)	(moles/g)	(kN/m^2)	(cm Hg)	(moles/g)
31.30	23.48	6.826	32.2671	24.2023	7.041
37.02	27.77	8.030	55.0355	41.2800	11.903
45.40	34.05	9.860			
55.66	41.75	12.046			
58.38	43.79	12.760			
66.83	50.13	14.723			

Ar-BN[a]

Ramsey[2]		
P		$N_a x10^7$
(kN/m^2)	(cm Hg)	(moles/g)
39.0953	29.3239	2.569
48.5231	36.3953	3.214
61.9532	46.4687	4.067
89.5513	67.1690	5.842
29.7112	22.2852	2.010
51.1383	38.3569	3.388
65.2885	48.9704	4.294
76.6473	57.4902	5.009
94.3776	70.7890	6.170

[a]See Table 23 for the Ar-BN data from this work.

Table 23. Ar-BN Adsorption Data

T = 273.150°K

P (kN/m^2)	P (cm Hg)	N_ax10^7 (moles/g)
27.2062	20.4063	1.810[a]
41.6675	31.2532	2.733[a]
50.6840	38.0161	3.328[a]
23.1878	17.3923	1.578[b]
35.5179	26.6406	2.358[b]
53.6237	40.2211	3.526[b]
9.9433	7.4581	0.680[c]
15.0120	11.2599	1.014[c]
41.2269	30.9227	2.682[d]

T = 310.027°K

P (kN/m^2)	P (cm Hg)	N_ax10^7 (moles/g)
18.3577	13.7694	0.718
28.5728	21.4314	1.074
44.1841	33.1408	1.666
62.0465	46.5387	2.531

T = 295.284°K

P (kN/m^2)	P (cm Hg)	N_ax10^7 (moles/g)
18.1648	13.6247	0.832
23.4244	17.5698	1.088
28.0954	21.0733	1.317
34.3906	25.7951	1.618
43.0614	32.2987	1.975

[a]Run 1.

[b]Run 2.

[c]Run 3.

[d]Check point at conclusion of BN studies.

Table 24. Kr-BN Adsorption Data

T = 273.150°K

P (kN/m^2)	P (cm Hg)	N_ax10^7 (moles/g)
24.8386	18.6305	4.860[a]
37.7850	28.3411	7.261[a]
45.7733	34.3328	8.734[a]
14.4919	10.8698	2.919[b]
26.2177	19.6649	5.073[b]
39.8865	29.9173	7.582[b]
3.5020	2.6267	0.723[c]
6.2234	4.6679	1.277[c]

T = 333.460°K

P (kN/m^2)	P (cm Hg)	N_ax10^7 (moles/g)
17.7823	13.3378	1.221
27.8402	20.8819	1.892
43.4571	32.5955	2.933
61.6912	46.2722	4.178

T = 296.215°K

P (kN/m^2)	P (cm Hg)	N_ax10^7 (moles/g)
14.4099	10.8083	1.805
21.0635	15.7989	2.631
26.2800	19.7116	3.258
36.2902	27.2199	4.472

[a]Run 1.

[b]Run 2.

[c]Run 3.

Table 25. Xe-BN Adsorption Data

T = 273.150°K

P (kN/m^2)	P (cm Hg)	N_ax10^7 (moles/g)
2.4919	1.8691	2.615[a]
3.6556	2.7419	3.710[a]
5.2272	3.9207	5.037[a]
6.7680	5.0764	6.303[a]
4.5384	3.4041	4.464[b]
6.6962	5.0226	6.216[b]
9.6009	7.2013	8.537[b]
12.4740	9.3563	10.728[b]

T = 358.954°K

P (kN/m^2)	P (cm Hg)	N_ax10^7 (moles/g)
12.5155	9.3874	1.859
14.2530	10.6906	2.059
16.2735	12.2061	2.353
19.6580	14.7447	2.836
24.2888	18.2181	3.529
30.8168	23.1145	4.456

T = 337.412°K

P (kN/m^2)	P (cm Hg)	N_ax10^7 (moles/g)
8.3420	6.2570	1.763
20.0292	15.0231	4.147
28.0869	21.0669	5.795

T = 368.034°K

P (kN/m^2)	P (cm Hg)	N_ax10^7 (moles/g)
8.5480	6.4115	1.090
13.4720	10.1048	1.700
21.2424	15.9331	2.685
30.5167	22.8894	3.880

[a]Run 1.

[b]Run 2.

BIBLIOGRAPHY

1. R. N. Ramsey, Ph.D. Thesis, Georgia Institute of Technology, 1970.

2. R. N. Ramsey, H. E. Thomas, and R. A. Pierotti, J. Phys. Chem., 76, 317(1972).

3. H. E. Thomas, R. N. Ramsey, and R. A. Pierotti, J. Chem. Phys., 59, 6163(1973).

4. A. C. Levy, M. S. Thesis, Georgia Institute of Technology, 1966.

5. G. Constabaris, J. H. Singleton, and G. D. Halsey, Jr., J. Phys. Chem., 63, 1350(1959).

6. J. R. Sams, Jr., G. Constabaris, and G. D. Halsey, Jr., J. Phys. Chem., 64, 1689(1960).

7. G. Constabaris, J. R. Sams, Jr., and G. D. Halsey, Jr., J. Phys. Chem., 65, 367(1961).

8. J. R. Sams, Jr., G. Constabaris, and G. D. Halsey, Jr., J. Chem. Phys., 36, 1334(1962).

9. R. A. Pierotti, Chemical Physics Letters, 2, 420(1968).

10. I. Langmuir, J. Am. Chem. Soc., 38, 2269(1916); Ibid, 40, 1361(1918); Phys. Rev., 8, 149(1916).

11. R. H. Fowler and E. A. Guggenheim, "Statistical Thermodynamics," Cambridge University Press, Cambridge, Mass., 1949, p. 431.

12. J. H. de Boer, "The Dynamical Character of Adsorption," Clarendon Press, Oxford, 1953, p. 17.

13. J. J. McAlpin and R. A. Pierotti, J. Chem. Phys., 41, 68(1964).

14. J. J. McAlpin and R. A. Pierotti, J. Chem. Phys., 42, 1842(1965).

15. H. Eyring, T. Ree and N. Hirai, Proc. Natl. Acad. Sci. U. S., 44, 683(1958).

16. T. L. Hill, "Statistical Mechanics," McGraw-Hill Book Co., Inc., New York, 1956, p. 424.

17. S. Brunauer, P. H. Emmett and E. Teller, J. Am. Chem. Soc., 60, 309(1938).

18. F. London, Z. Physik, 63, 245(1930).

19. J. E. Lennard-Jones, Proc. Roy. Soc. (London), A106, 441, 463(1924).

20. J. O. Hirschfelder, C. F. Curtiss and R. B. Bird, "Molecular Theory of Gases and Liquids," Wiley, New York, 1967, p. 948.

21. R. A. Pierotti and H. E. Thomas, "Surface and Colloid Science," edited by E. Matijevic, Wiley-Interscience, New York, 1971, Vol. 4, pp. 93-259.

22. O. Sinanoğlu and K. S. Pitzer, J. Chem. Phys., 32, 1279(1960).

23. W. G. Bronbacher, D. P. Johnson and J. L. Cross, "Mercury Barometers and Manometers," NBS Monograph 8, 1960.

24. A. A. Giardini, "Boron Nitride," Bureau of Mines Information Circular 7664, U. S. Department of Interior (1953).

25. Clarence J. West, Ed., "International Critical Tables of Numerical Data," McGraw-Hill Book Co., Inc., New York, Vol. 2, 1927, p. 459.

26. P. L. Walker, Jr., H. A. McKinstry and C. C. Wright, Ind. Eng. Chem., 45, 1711(1953).

27. R. S. Pease, Acta Crystallographica, 5, 356(1952).

28. M. H. Polley, W. D. Shaeffer and W. R. Smith, J. Phys. Chem., 57, 469(1953).

29. D. Graham and W. S. Kay, J. Colloid Science, 16, 182 (1961).

30. D. Graham, J. Phys. Chem., 61, 1310(1957).

31. F. A. Putnam and T. Fort, Jr., J. Phys. Chem., 79, 459(1975).

32. G. Constabaris, Ph.D. Thesis, University of Washington, 1957.

33. A. D. Crowell and R. B. Steele, J. Chem. Phys., 34, 1347(1961).

34. A. D. Crowell and C. O. Chang, J. Chem. Phys., 43, 4364(1965).

35. J. O. Hirschfelder, C. F. Curtiss and R. B. Bird, "Molecular Theory of Gases and Liquids," Wiley, New York, 1967, pp. 1110-1111, 1212-1213.

36. A. L. Myers and J. M. Prausnitz, Trans. Faraday Soc., 61, 755(1965).

37. R. E. Smallwood, M. S. Thesis, Georgia Institute of Technology, 1967.

38. S. Ross and J. P. Olivier, "On Physical Adsorption," Interscience Publishers, New York, 1964, pp. 150-153.

39. I. D. Morrison and S. Ross, Surface Science, 39, 21(1973).

40. S. Ross and J. P. Olivier,"On Physical Adsorption, Interscience Publishers, New York, 1964, p. 176.

41. T. Kihara, J. Phys. Soc. (Japan), 6, 289(1951).

42. T. Kihara, Rev. Mod. Phys., 25, 831(1953).

43. M. J. Bullock, Jr., M. S. Thesis, Georgia Institute of Technology, 1974.

44. D. P. Poshkus, Dis. Faraday Soc., 40, 188(1965).

45. A. V. Kiselev, D. P. Poshkus and A. Ya. Afreimovich, Russ. J. Phys. Chem., 39, 630(1965).

46. A. V. Kiselev and D. P. Poshkus, Russ. J. Phys. Chem., 39, 204(1965).

47. A. V. Kiselev and D. P. Poshkus, Trans. Faraday Soc., 59, 428(1963).

48. G. Curthoys and P. A. Elkington, J. Phys. Chem., 71, 1477(1967).

49. J. J. McAlpin, Ph.D. Thesis, Georgia Institute of Technology, 1966.

50. R. A. Pierotti and J. C. Petricciani, J. Phys. Chem., 64, 1596(1960).

51. C. Vidal-Madjar, M. Gonnord, M. Goedert and G. Giuochon, J. Phys. Chem., 79, 732(1975).

52. C. Pisani, F. Ricca and C. Roetti, J. Phys. Chem., 77, 657(1973).

53. L. Battezzati, C. Pisani and F. Ricca, J. Chem. Soc., Faraday Trans. II, 71, 1629(1975).

54. J. R. Sams, Ph.D. Thesis, University of Washington, 1962.

55. E. Bergman, J. Phys. Chem., 78, 405(1974).

56. P. Ripa and G. Zgrablich, J. Phys. Chem., 79, 2118(1975).

57. R. A. Pierotti and H. E. Thomas, J. Chem. Soc., Faraday Trans. I, 70, 1725(1974).

58. C. R. Barber and Anne Horsford, Metrologia, 1, 75(1965); C. R. Barber, Metrologia, 5, 35(1969).

VITA

Alvin Charles Levy was born June 6, 1942 in Norfolk, Virginia to Nettie Cohen Levy and Lewis Frank Levy. He was reared in Norfolk and graduated from Maury High School in June, 1960. He entered the Georgia Institute of Technology in September, 1960, and received a Bachelor of Science in Chemistry in June 1964, and a Master of Science in Chemistry in June, 1967. From February, 1966 to January, 1968 he served in the United States Navy. In March, 1968, he began work at E. I. du Pont de Nemours Co. in Richmond, Virginia, where he lived until August, 1973. In September 1973, he re-entered the Georgia Institute of Technology to study for the Doctor of Philosophy in the School of Chemistry.

On February 6, 1966 he was married to Joan Lynn Kottler. Their two children, Michael and Beth, were born on January 22, 1968 and May 13, 1970, respectively.